Thèse présentée pour obtenir le grade de

DOCTEUR DE L'ECOLE POLYTECHNIQUE

Spécialité : **Physique**

Par

ABDULLAH ATEF SHUKRI

Ab initio electronic stopping power in materials

Soutenue le 30 Novembre 2015 devant le jury composé de

Pr.	Silke Biermann	Présidente
Pr.	Arkady Krasheninnikov	Rapporteur
Dr.	Valerio Olevano	Rapporteur
Dr.	Elena Cannuccia	Examinatrice
Dr.	Lucia Reining	Directrice de thèse
Dr.	Fabien Bruneval	Encadrant

This thesis is dedicated to my parents, my brothers and my sisters, who have always loved me unconditionally.

This thesis is also dedicated to all my friends especially Mohammad Farhat, Mohammad Alshorman, Morad Khaled and Ahmad Al-Qawasmeh who have been a constant source of support and encouragement during the challenges of graduate school and life.

This thesis is also dedicated to my Mosque friends especially Ibrahim Mansy, Sami Shukri, Ahmed Tbeyshat and Mohammad Mestarihi whose good examples have taught me to work hard for the things that I aspire to achieve.

Acknowledgments

Foremost, I would like to express my profound gratitude to DEN, Service de Recherches de Métallurgie Physique, Université Paris-Saclay for giving me the opportunity to carry out my PhD thesis.

I am heartily thankful to my supervisors Dr. Fabien Bruneval and Dr. Lucia Reining for the unceasing support of my Ph.D study and research. I really appreciate their patience, motivation, enthusiasm, and immense knowledge. Their guidance always helped me to do my research in the right way.

Besides my supervisors, I would like to thank the rest of my thesis committee: Pr. Silke Biermann, Pr. Arkady Krasheninnikov, Dr. Valerio Olevano and Dr. Elena Cannuccia, for their encouragement and insightful comments.

I am grateful to my friends at the European Theoretical Spectroscopy Facility (ETSF) for their help and useful discussions during my visiting time at ETSF.

Finally, I would like to express my sincere gratitude to my friend Dr. Guido Petretto for his encouragement and inspirational guidance throughout this work. His encouragement have been a great motivation to me.

Contents

1 Motivations **12**

2 Introduction to the stopping power **15**
2.1 Historical review 15
2.2 Definition and classifications 17
2.3 Electronic stopping power of fast, light particles 17
2.3.1 Bohr formula 17
2.3.2 Bethe formula 18
2.4 Empirical models 20
2.5 Conclusion 23

3 Theoretical background **24**
3.1 Ground state density functional theory (DFT) 24
3.1.1 Hohenberg-Kohn theorem 25
3.1.2 Kohn Sham method 27
3.1.3 Local Density Approximation 28
3.1.4 Generalized Gradient Approximations 28
3.2 Time dependent density functional theory 29
3.2.1 Runge Gross theorem 30
3.2.2 Time-dependent Kohn Sham Equations 31
3.2.3 Adiabatic approximations 32
3.3 Conclusion 32

4 Linear response approach to TDDFT **33**
4.1 Linear response theory and Dyson-like equation 33
4.2 Dyson-like equation for a periodic lattice 36
4.3 Linear response function of the independent-particle system . . 37
4.4 Exchange-correlation Kernel 38
4.5 The dielectric function 39
4.6 Conclusion 40

5 Dielectric theory of the electronic stopping power of fast ions 41
5.1 Linear response electronic stopping power for the non-interacting homogeneous electron gas . . . 41
5.1.1 Lindhard's theory of stopping power . . . 42
5.1.2 Local density approximation to the stopping power . . . 44
5.2 Linear response electronic stopping power of a periodic crystal . 45
5.2.1 Position dependent of electronic stopping power . . . 46
5.2.2 Random electronic stopping power . . . 52
5.2.3 The Lindhard's formula as special case . . . 54
5.3 Conclusion . . . 55

6 Development and computational details 56
6.1 Practical implementation in a periodic plane-wave approach . . 56
6.1.1 Technicalities . . . 58
6.1.2 Assessment against previous calculations . . . 59
6.1.3 Convergence issues . . . 61
6.2 A method to achieve convergence at a lower cost . . . 64
6.2.1 Application to silicon . . . 67
6.3 Conclusion . . . 70

7 Stopping power of bulk materials 71
7.1 First principle against models based on the free-electrons gas . . 71
7.2 Physical approximations relevant for bulk materials . . . 73
7.2.1 RPA vs ALDA . . . 74
7.2.2 Core states contribution . . . 77
7.2.3 Effect of the higher order terms . . . 81
7.3 RESP for bulk materials . . . 82
7.3.1 How weak is the RESP anisotropy of anisotropic materials? 82
7.3.2 Is the Bragg's additivity rule valid? . . . 84
7.3.3 Is the structural phase effect vanishing? . . . 85
7.4 Conclusion . . . 86

8 Stopping power in organic systems 87
8.1 RESP of the H_2O molecule in two phases: The solid and gas phases . . . 87
8.2 RESP for polymers . . . 92
8.3 Conclusion . . . 96

9 Conclusions and perspectives 98

A Calculation parameters 101

Résumé

La perte d'énergie moyenne d'un ion par unité de longueur de longueur quand il se déplace à travers la matière est nommé pouvoir d'arrêt. La connaissance du pouvoir d'arrêt est essentielle pour de nombreuses applications modernes qui dépendent du transport des ions dans la matière, par exemple les techniques d'analyse par faisceau d'ions ou l'implantation d'ions. L'utilisation de faisceaux de protons ou d'ions plus lourds en radiothérapie nécessite également la connaissance du pouvoir d'arrêt dans les tissus. Mais, alors que les données expérimentales sont facilement disponibles pour les solides élémentaires, les données sont beaucoup plus rares pour les composés.

La réponse linéaire dans le formalisme diélectrique a été largement utilisée dans le passé pour étudier le pouvoir d'arrêt électronique. En particulier, les célèbres calculs pionniers de Lindhard évaluent le pouvoir d'arrêt électronique d'un gaz d'électrons libres. Dans cette thèse, nous développons un code ab initio entièrement basée sur la théorie de la fonctionnelle densité dépendant du temps dans sa version réponse linéaire afin de prédire le pouvoir d'arrêt électronique aléatoire (RESP en anglais), qui est la moyenne des pouvoirs d'arrêt pour les différents points d'impact. Le but est d'être capable de prédire le résultat d'expériences sans aucune connaissance du matériau cible en dehors de sa structure cristallographique.

Nos développements ont été réalisés au sein du code libre ab initio nommé ABINIT, dans lequel deux approximations sont maintenant disponibles : l'approximation de la phase aléatoire (RPA en anglais) et l'approximation de la densité locale adiabatique (ALDA en anglais). En outre, une nouvelle méthode nommée "méthode d'extrapolation" a été introduite pour surmonter les problèmes de convergence hardus que nous avons rencontrés. Ces questions de convergence ont empêché les études précédentes dans la littérature de permettre une comparaison directe à expérience.

Tout d'abord, nous démontrons l'importance de décrire la structure électronique réaliste en ab initio en comparant avec l'évaluation historique Lindhard du pouvoir d'arrêt. Bien que le pouvoir d'arrêt de Lindhard fournit une description acceptable au premier ordre qui permet capturer les caractéris-

tiques générales du pouvoir d'arrêt, les détails quantitatifs sont clairement au-delà du modèle de gaz d'électrons libres. De surcroît, nous montrons que le RESP ab initio se compare bien avec les données expérimentales pour les projectile proton pénétrant une large gamme de matériaux cibles. Dans la thèse, nous avons examiné des cibles métalliques (aluminium, lithium, graphite) et des cibles semi-conductrices (Si, diamant, SiC). Nous montrons aussi les résultats préliminaires pour les matériaux organiques. La description correcte du pouvoir d'arrêt nécessite un traitement attentif des électrons de coeur et de l'échange-corrélation pour les électrons de la cible. Nous avons également examiné la pertinence du formalisme de la réponse linéaire par rapport aux résultats de la littérature utilisant la propagation temporelle des fonctions d'onde, qui va au-delà de la théorie de la réponse linéaire que nous utilisons. Étonnamment, nous avons trouvé un très bon accord entre ses deux théories et avons évalué une limite supérieure pour les effets non-linéaires de 5 % dans la cible d'aluminium.

En outre, certaines règles empiriques rapides qui sont couramment utilisées pour l'interprétation ou la prédiction d'expériences avec les codes empiriques ont été évaluées. L'anisotropie du RESP dans des matériaux anisotropes peut être complétement ignoré par exemple. Toutefois, la règle d'additivité de Bragg et l'insensibilité de phase ne peuvent pas être considérés comme acquis en général. Nous avons découvert que, bien que le silicium, le diamant, et SiC possèdent une structure cristallographique très similaire et une structure électronique très similaire, l'erreur de la loi de Bragg est non négligeable lorsque l'on compare SiC à la somme du silicium et du carbone (diamant).

Enfin, nous avons exploré la possibilité d'utiliser notre code basé sur une base d'ondes planes pour calculer les systèmes isolés dans la phase gazeuse. Notre approche en utilisant des ondes planes n'est pas vraiment adaptée à ce type d'application, à moins que des efforts énormes de calcul soient consentis. Les développements futurs de code peuvent déverrouiller ce goulot d'étranglement et pourraient permettre d'aborder le sujet de la comparaison entre les systèmes isolés et de la matière condensée. Dans les expériences publiées, des différences notables ont été identifiées entre la phase solide de l'eau (glace) et sa vapeur. Ce serait une voie très intéressante à suivre à l'avenir.

Summary

The average energy loss of an ion per unit path length when it is moving through the matter is named the stopping power. The knowledge of the stopping power is essential for a variety of contemporary applications which depend on the transport of ions in matter, especially ion beam analysis techniques and ion implantation. Most noticeably, the use of proton or heavier ion beams in radiotherapy requires the knowledge of the stopping power. Whereas experimental data are readily available for elemental solids, the data are much more scarce for compounds.

The linear response dielectric formalism has been widely used in the past to study the electronic stopping power. In particular, the famous pioneering calculations due to Lindhard evaluate the electronic stopping power of a free electron gas. In this thesis, we develop a fully *ab initio* scheme based on linear response time-dependent density functional theory to predict the impact parameter averaged quantity named the random electronic stopping power (RESP) of materials without any empirical fitting. The purpose is to be capable of predicting the outcome of experiments without any knowledge of target material besides its crystallographic structure.

Our developments have been done within the open-source *ab initio* code named ABINIT, where two approximations are now available: the Random-Phase Approximation (RPA) and the Adiabatic Local Density Approximation (ALDA). Furthermore, a new method named "extrapolation scheme" have been introduced to overcome the stringent convergence issues we have encountered. These convergence issues have prevented the previous studies in literature from offering a direct comparison to experiment.

First of all, we demonstrate the importance of describing the realistic *ab initio* electronic structure by comparing with the historical Lindhard stopping power evaluation. Whereas the Lindhard stopping power provides a first-order description that captures the general features of the stopping power, the quantitative details are cleary beyond the free-electron gas model. Moreover, we show that the *ab initio* RESP compares well with experimental data for the proton projectile impinging a wide range of materials. In the thesis, we

considered metallic targets (aluminum, lithium, graphite) and semiconductors (Si, diamond, SiC). We also show preliminary results for organic materials. The correct description of the stopping power requires a carefully treatment of the core states and of the exchange-correlation for the electrons of the target. We have also examined the adequacy of the linear response formalism against published time-propagation results that go beyond the linear-response theory. Amazingly we have found a very good match between the two frameworks and have evaluated an upper bound for the non-linear effects of 5 % in aluminum target.

In addition, some empirical rules of thumbs that are commonly employed for the experimental interpretation or for the prediction with empirical codes have been checked. The anisotropy of the RESP in anisotropic materials can be safely ignored. However, the Bragg's additivity rule and the phase insensitivity cannot be taken for granted in general. We have found that, even though silicon, diamond, and SiC have a very similar crystallographic structure and a very similar electronic structure, the Bragg's law error is non negligible when comparing SiC to the sum of silicon and carbon (diamond).

Finally, we have explored the possibility of using our code within the plane-waves to calculate isolated systems in the gas phase. Our framework using plane-waves is not really suitable to this type of application, unless huge computational efforts are achieved. Future code developments may unlock this bottleneck and allow one to address the topic of the comparison between isolated systems and condensed matter. In the experimental reports, noticeable differences have been acknowledged between the solid phase of water (ice) and its vapour. This would be a valuable route to follow in the future.

Acronyms

Table 1: List of acronyms that will be used in this manuscript.

ALDA	Adiabatic local density approximation
BZ	Brillouin Zone
DFT	Density functional theory
EELS	Electron energy loss spectroscopy
ELF	Energy loss function
FEG	Free electron gas
GOS	Generalized oscillator strength
HK	Hohenberg-Kohn
IXSS	Inelastic X-ray scattering
KS	Kohn-Sham
LDA	Local density approximation
LFC	Local field correction
LPDA	Local plasma density approximation
LR	Linear response
MELF	Mermin energy loss function
RESP	Random electronic stopping power
RPA	Random phase approximation
TDDFT	Time-dependent density function theory
PE	Polyethylene
PA	Polyacetylene
PW	Plane wave
rprim	Real space Primitive translations
xred	The atom positions in reduced coordinates.
xcart	The atom positions in Cartesian coordinates

Chapter 1

Motivations

The stopping power of an irradiating ion in condensed matter is defined as the kinetic energy loss per unit of path length:

$$S = -\frac{dE}{dx}. \tag{1.1}$$

This quantity is central to the many technological fields, which involve particle irradiation. Besides materials in nuclear or space environments, the stopping power is highly relevant for the depth of implantation of dopants in electronics and for the accurate prediction of damage in the proton therapy used in nuclear medicine. Due to its importance, the stopping power of ions has been the subject of intense research for the last 80 years.

The stopping power consists of two components: the nuclear stopping power S_n, which involves energy losses due to collisions with the nuclei of the target and the electronic stopping power S_e, which arises from the excitation of the electrons of the target. As soon as the kinetic energy of the impinging ion is larger than a few tens of keV/amu, the electronic part becomes the vastly dominating contribution.

Historically, the electronic stopping power has been first evaluated with model scattering formulas [79]. Then came the calculations based on the free-electron gas, pioneered by Lindhard [47]. The electron gas modelling and its further refinements have been continuoulsy used since then [40, 93, 1, 4]. More recently, with the advent of density functional theory and its time-dependent version (TDDFT) [63], the fully *ab initio* evaluation of the electronic stopping power has become within reach [20, 21, 64, 65, 67, 54, 77].

Among the recent applications of TDDFT to the calculation of stopping power, two frameworks have emerged: either in the linear response regime, in which the response functions are expressed in terms of the frequency; or in the time-propagation approach, in which the time-dependent Kohn-Sham

(KS) equations have to be solved. Both approaches have pros and cons. Time-propagation incorporates the response to all orders and this is expected to yield important contributions at low velocity. However, the time discretization can be technical and supercells have to be employed. All this leads to very cumbersome calculations. The linear-response framework is conceptually simpler, however still requires a carefully monitoring of the convergence. Moreover, the limitation to the linear terms might be questionable for the low ion velocities.

In this thesis, we aim at developing an *ab initio* code that predicts the electronic stopping power of any material within the linear response dielectric formalism. We aim at producing a linear response electronic stopping power code within two options the Random Phase Approximation (RPA) and Time Dependent Adiabatic Local-Density Approximation (TD-ALDA). However, as we will show the absolute convergence is difficult to be obtained since the convergence factors have different origins. Therefore, we will introduce a new method (extrapolation method) to overcome this problem.

In this thesis, we propose to push the linear-response approach to its limit and appreciate his range of validity to evaluate the random electronic stopping power (RESP). We aim at exploring the power of the calculations to predict experimental results, since the experimental data are scarce for non-elemental crystals. Due to the slow convergence of the practical calculations, we produce, to the best of our knowledge, the first fully converged *ab initio* electronic stopping power within linear-response theory. The comparison against time-propagation results is surprisingly good as we will show. We furthermore evaluate the validity of a few rule of thumbs empirically used in practice, such as the Bragg's additivity rule or the bond effect. In addition, to have a deep understanding of the RESP results, we will answer the following two questions: Can we take the phase insensitivity for granted? Also, can we safely ignore the anisotropy of anisotropic materials?

At the end of this thesis, we will check if the linear response RESP code within the plane wave (PW) framework is suitable to study more complex targets, such as water (in solid and gas phase) and polymer materials. These organic materials are highly interesting since their stopping power strongly depends on the phase in water and strongly depends on the bond type in polymers.

The thesis is organized as follows: Chapter 1 (the present Chapter) announces the motivations and the purpose of this thesis. Also, Chapter 2 presents a brief summary of the history of the most closely related stopping power theories to our framework here. Furthermore, Chapter 3 reviews the fundamental basis of the work, namely the *ab initio* methods (DFT and TD-DFT). Chapter 4 gives a brief overview of the basic linear response formalism of TDDFT. However, this chapter is very important for this work, since we are

going to study the electronic stopping power from the linear response point of view.

Then, the remaining parts of the thesis is devoted the electronic stopping power theory , given as follows: In Chapter 5, the first section reviews the Lindhard theory of stopping power. Also, the second section shows the full derivation with extensive details of the linear-response in periodic solids for both the position dependent electronic stopping power and the RESP. Then, to make the story complete, the last part shows how to derive the Lindhard's theory of (FEG) as a special case from RESP of real solid (periodic solid). Chapter 6 presents the details of the practical implementation in a plane-waves and proposes a working approach to achieve convergence. In Chapter 7, the first part evaluates the validity of the simpler models (based on FEG) that are often used for real targets, the second part tests the effect of the physical approximations on the RESP and the last one examines the validity of some commonly stated rules of thumbs concerning the RESP. The Chapter 8 shows our first steps in understanding and in investigating the stopping power in organic systems such as: water (in solid and gas phase) and polymers (PE and PA as isolated chain form). Finally, the thesis is concluded in Chapter 9.

Appendix A summarized all the convergence parameters we use for the practical calculations.

The atomic units will be used throughout the text ($\hbar = e = a_0 = 1$), unless otherwise stated.

Chapter 2

Introduction to the stopping power

In this chapter, we present an overview of the existing stopping power theories. In particular, we focus on reviewing the earliest theories, such as the Bohr and Bethe theories. Finally, we will also sketch the main ideas of some widely used empirical models for the electronic stopping power.

2.1 Historical review

For many years, the stopping of energetic ions in matter has been a subject of great interest to theoretical and experimental physicists. Bohr [12, 14, 13], Bethe [8], and Bloch [10, 11] were the pioneering theoretical investigators of the charged particles stopping in matter. In his first papers [12, 14, 13], Bohr suggested a formula for the stopping power based on the assumption that the atoms of the target are classical oscillators. Later, in Ref. [8], Bethe carried out a consistent quantum mechanical study and obtained a fundamental equation to describe the stopping of the fast charged particles moving in a quantized medium. Then, Bloch [10, 11] constructed a bridging formulation between the classical Bohr impact parameter approach and the quantum Bethe approach. His work introduced a modified Bethe formula named "Bethe-Bloch equation". This equation reduces to Bohr formula at low velocity and to Bethe formula at high velocity. Furthermore, Moller [51] and Bethe [9] improved the Bethe's stopping theory by adding the relativistic corrections. However, Bohr's and Bethe's theories are only valid for the swift particles. Anyway, both theories are still used up to the present day for the large velocities.

On the other hand, for slow particles, the stopping power theory of the condensed matter was developed further by Fermi and Teller [30]. They treated the target medium as a free electron gas and derived an electronic stopping power formula which is proportional to the projectile velocity.

A more general treatment of the electronic stopping was later developed by Lindhard [47]. Lindhard introduced the first linear dielectric formulation of stopping theory for a charged particle penetrating a free electron gas. The Lindhard formula captures many important features of the electronic stopping power. However, it still misses an important point: since it is derived for an homogeneous electron gas, it is inadequate to describe the directional dependence of the stopping power.

Furthermore, Lindhard theory has two correct limits for low and high velocities. For low velocities, the Lindhard theory can be replaced with the Fermi-Teller theory (the linear dependence). For the high but non-relativistic velocities, the Lindhard theory can be replaced with Bethe theory [68, 47].

Then, the so called local plasma density approximation [45, 41] was introduced in order to better treat the solid targets. This model has been widely used for long time for two reasons: it is simple and it is rather accurate [41].

Also, a semi-empirical scheme was proposed by Ritchie and Howie to treat realistic materials [70]. They suggested to use the experimental optical data to find a fitted formula in the optical limit for the energy loss function (ELF), then the extrapolated to finite momemta with a dispersion relation such as the "extended Drude model" to incorporate the momentum $\mathbf{q}$ dependence of the energy loss function. Similar work have been done using different extended models for the ELF, such as the Penn model [62] and MELF-GOS model [1]. For more details, see Ref. [24].

Finally, the first results to describe the stopping power in a periodic crystal using ab initio linear response theory were due to Saslow and Reiter [76]. Later, Campillo et al. [20, 64] obtained equations for both random electronic stopping power (RESP) and position dependent stopping electronic power using the linear response theory within the time-dependent DFT framework. Several attempts were conducted to include the effect of the crystal structure of the target into the electronic stopping power calculations. For instance, Campillo et al. [20] and Pitarke and Campillo [64] compared the calculated stopping power values in Al and Si targets with an equivalent calculations in a free-electron gas target considered at the same average density as bulk Al and Si. According to their results, the crystal effect must be included in the stopping power calculations to obtain high quality results.

More details about the electronic stopping power in a periodic crystal will be described in Chapter 5 of the present work. The main task of this work is to study the random electronic stopping power for proton moves in a periodic crystal within the linear response dielectric formalism. The study of electronic stopping for the heavy particle with all velocities range is out the scope of this thesis.

2.2 Definition and classifications

The stopping power of an irradiating ion in condensed matter is defined as the kinetic energy loss E per unit of path length x:

$$S = -\frac{dE}{dx}. \tag{2.1}$$

Note that the stopping power has a force dimension, which is why it is also referred to as the stopping force.

The stopping power consists of two components: the nuclear stopping power S_n, which involves energy losses due to collisions with the nuclei of the target, and the electronic stopping power S_e, which arises from the excitation of the electrons of the target. As soon as the kinetic energy of the impinging ions is larger than a few tens of keV/amu, the electronic part becomes the vastly dominating contribution.[86] The total stopping power is given as the sum of the two stopping types:

$$S = S_n + S_e, \tag{2.2}$$

In this thesis, we will only study the electronic part of the stopping power of the proton when it moves through the solid target.

Next, we present a brief summary about the most successful electronic stopping power theories.

2.3 Electronic stopping power of fast, light particles

In the beginning of 20th century, Bohr [12] and Bethe [8] proposed the first reliable and acceptable theories to study the stopping power phenomena. In fact, they managed to solve several limitations and problems corresponding to in the earlier works done by Thomson and Darwin [81, 23].

The work of both Bohr and Bethe are still used in many applications, since a nice result compared to the experimental data can be achieved in the case of the swift particles only. More details can be found in [79].

2.3.1 Bohr formula

Bohr theory of electronic stopping considers the energy transfer from a point charge projectile to classical electrons harmonically bound to the atoms of the target with a resonance angular frequencies, say ω_j.

Bohr obtained within a classical perturbation treatment the following formula of the electronic stopping power cross section

$$S(Z, \mathbf{v}) = \frac{4\pi Z^2 e^4}{m_e v^2} L_{Bohr}, \tag{2.3}$$

with the Bohr stopping number

$$L_{Bohr} = \sum_j f_j \ln\left(\frac{C m_e v^3}{Z e^2 \omega_j}\right), \tag{2.4}$$

where $C = 1.1229$, f_j values represent the relative contributions of different ω_j values subject to $\sum_j f_j = 1$.

In fact, Bohr theory can be used for the weak interactions only, since he derived the stopping formula under a classical perturbation assumption. In addition, Bohr considered two approximations in order to simplify the problem: First, the dipole approximation; the interaction of the projectile with the electrons is treated under the assumption that the strength of the Coulomb interaction does not vary significantly over the range of motion of the electron; Second, the momentum approximation, in which the projectile path is not changed and the target electrons remain at rest throughout the collision.

In Bohr approach, the impact parameter between the particle's trajectory and the target nucleus is limited to the maximum and minimum values, $\mathbf{b}_{max}$ and $\mathbf{b}_{min}$. More details, see [68, 12].

2.3.2 Bethe formula

An alternative stopping power formula has been derived by Bethe [8]. Unlike Bohr, in views of the quantum mechanics, Bethe derived a stopping formula for the case of the high velocity projectile.

The classical expression Bethe stopping formula for a free electron gas target can be written as [56]

$$S(Z, v) = \left(\frac{Ze\omega_p}{v}\right)^2 \ln \frac{2 m_e M_p v^2}{(m_e + M_p)\omega_p \hbar}, \tag{2.5}$$

where v, Ze and M_p indicate to the projectile velocity, charge, and mass. ω_p refers to the classical plasma frequency that is obtained with the relation $\omega_p = \sqrt{\frac{4\pi n e^2}{m_e}}$, where n is number density of electrons and m_e is the electron mass.

Furthermore, for heavy projectile $M_p \gg m_e$ the stopping power in Eq. (2.5) reduces to

$$S(Z, v) = \left(\frac{Ze\omega_p}{v}\right)^2 \ln \frac{2m_e v^2}{\omega_p \hbar}. \tag{2.6}$$

In this derivation, two assumptions have been used: The stopping resulted from Coulomb excitation and ionization of the target electrons. In addition, the interaction is considered within the first Born approximation.

Hence, the stopping number L_{Bethe} reads

$$L_{Bethe} = \sum_j f_j \ln \left(\frac{2m_e v^2}{\hbar\omega_j}\right), \tag{2.7}$$

where $\hbar\omega_j$ is the energy corresponding to the j^{th} excitation of electrons in the target atom and f_j is a generalized oscillator strength (GOS).

In practice, it is very hard to calculate the j^{th} electronic excitation, instead we can calculate the average excitation energy. The average excitation energy is defined as

$$\ln I = \sum_j f_j \ln (\hbar\omega_j). \tag{2.8}$$

Empirically, it can be approximated using a commonly used scaling relation [11]:

$$I \approx Z_2 \times 10 \ \text{ eV} \tag{2.9}$$

In order to judge the accuracy of using both Both theory and Bethe theory in predicting the electronic stopping power, we present the results of electronic stopping power of proton moving through Si target.

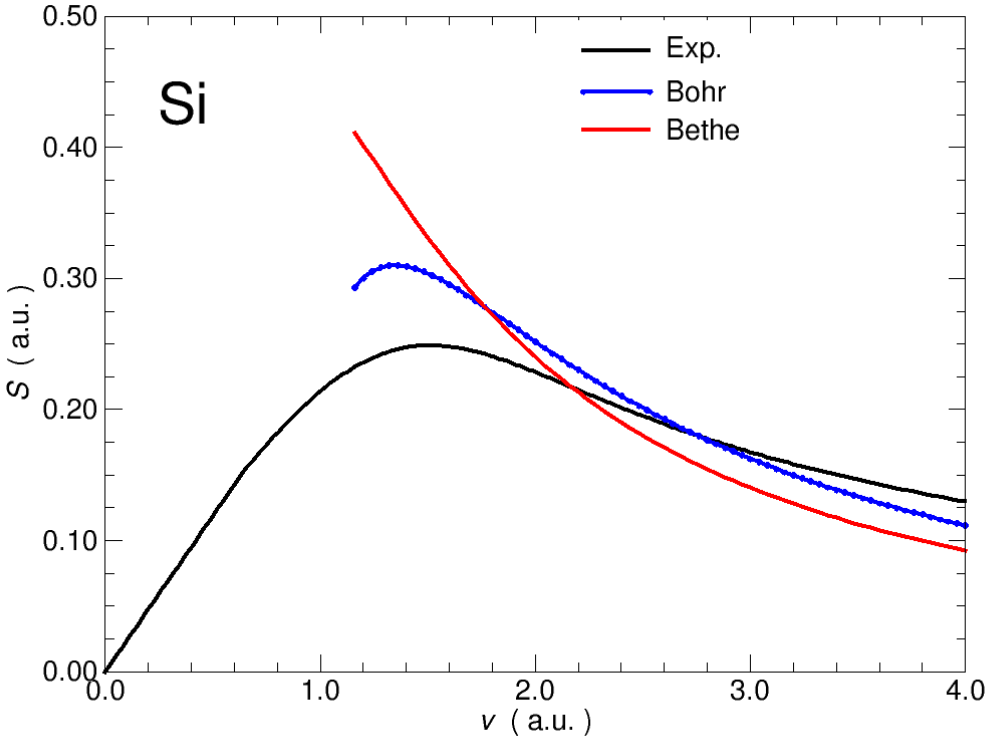


Figure 2.1: Electronic stopping power as a function of the projectile velocity calculated using both Bohr's formula (blue line) and Bethe's formula (red line). Experiment from the PSTAR database [7] (black line) is given as a reference.

Figure 2.1 shows that both Bohr formula and Bethe formula are valid only for large velocity.

2.4 Empirical models

Predicting the stopping of any projectile in any stopping target medium is the main purpose in modeling electronic stopping powers. For many applications, one needs only the stopping power data as an input values for other calculations. For this, we should use the most direct method "the empirical method" which provides us with the desired stopping data.

The possibility of success of the empirical models can be seen from Figure 2.2. This figure points to the useful scaling relations for the behavior of the experimental data. Therefore, it is possible to produce a fitting electronic

stopping curve as a function of the projectile velocity or other variables like the atomic number of the target or the atomic number of the energetic particles. As shown in Figure 2.2, by simple transformations, the experimental data of different targets and projectiles can be superimposed.

For instance, the most popular fitting schemes is called the stopping and range of ions in matter "SRIM" code [91] by Ziegler et al [93]. The approach of Ziegler et al. is based on scaling proton stopping powers, $S(Z_1 = 1, Z_2, v)$, by an effective charge fraction γ such that

$$S(Z_1, Z_2, v) = Z_1^2 \gamma^2 S(Z_1 = 1, Z_2, v). \tag{2.10}$$

The proton stopping powers are calculated using the local density approximation of the Lindhard an Sharff [45]. The Lindhard-Sharff theory is described in details in Chapter 5.

Another successful empirical approach "MSTAR" is found in literature by Paul and Schinner [59, 61]. In their approach, they have considered the helium stopping data as an experimental data reference instead of the proton stopping data.

Using a large experimental electronic stopping power dataset for H and He ions in elemental targets in conjunction with program JUDGE, Paul and Schinner [60] compared these data to the theoretical programs and semi-empirical programs. They showed that the average accuracy of SRIM is about $7-8\%$ for solid and $3-4\%$ for gaseous targets. Anyway, in their results, the experimental accuracy of the measurements for gases is about twice as good as for solid.

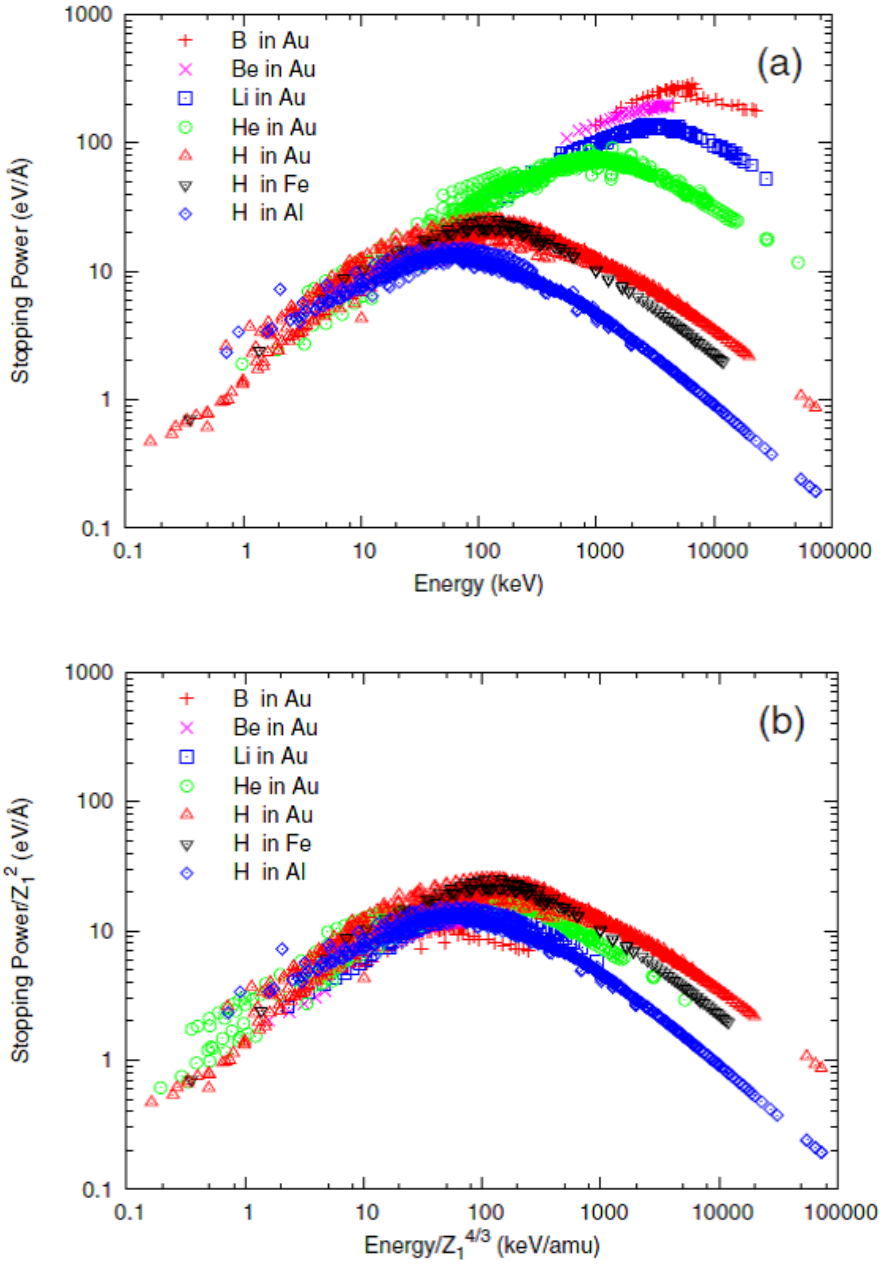


Figure 2.2: A demonstration of how simple scaling relationships (b) can capture much of the behaviour of the electronic stopping power (a) for a variety of projectile and target combinations. The scaling of stopping power by $1/{Z_1}^2$ is informed by the prefactor in the fast particle stopping theories [79], [27] and [53] and the normalization of the particle velocity by $1/{Z_1}^{2/3}$ is suggested by the Thomas-Fermi scaling of electronic velocities. Data are from the database of Paul[58])

2.5 Conclusion

In this chapter, we have presented an overview of the stopping power theories. Also, we have presented a brief summary of the history of the most famous stopping power theories. Furthermore, we have focused on reviewing the earliest theories such as the Bohr and Bethe theories. Finally, we have introduced the idea of the most used empirical methods of the electronic stopping power found in the literature.

Chapter 3

Theoretical background

Ab initio methods are used to predict the properties of materials by solving the equations of quantum mechanics without using any adjustable variables. Most prominently among the available ab initio methods, the ground state density functional theory (DFT), based on the Hohenberg-Kohn theorem [38], has simplified the electronic structure calculations by focusing on the density of the electronic system instead its wave function.

The most popular approach to DFT is the Kohn-Sham (KS) auxiliary system, which introduces non interacting electrons having the same density as the interacting system. In practice, DFT calculations are relatively light and provide an access to a large systems. DFT gives new tools to study and understand the results of the calculations. This is why DFT is today the most used approach to the theoretical prediction of physical and chemical properties.

Later, the extension of the ground state theory to the time-dependent case has provided us with a new method, namely the time-dependent density functional theory (TDDFT), which can access excited state properties. Based on the Runge-Gross theorem [73] and sometimes combined with linear-response theory, TDDFT allows us to study the time dependent phenomena of the electronic excitations [63]. In this chapter, we will discuss and review the ab initio methods that are to be used in our work, namely DFT in the first section and TDDFT in the second one.

3.1 Ground state density functional theory (DFT)

In solid state physics and quantum chemistry, several approaches, such as Configuration Interaction or Quantum Monte Carlo, have been proposed in order to solve the time-independent non-relativistic Schrödinger equation. Unfortunately, these approaches use the ground state wave function, Ψ_0, of the

N-electron system as the main quantity. In practice calculating this quantity is very hard and is usually limited to very small systems.

Therefore, one has to implement a new strategy to deal with the many body problem. First, Thomas and Fermi (TF) [29, 80] introduced the first density functional theory, in which they managed to use the density as a basic variable of the total energy. Based on the uniform electron gas, they completely expressed the total energy of the electrons in terms of the ground state density, as follows:

$$E^{TF}(\rho(\mathbf{r})) = \frac{3}{10}(3\pi^2)^{2/3}\int d\mathbf{r}\ \rho^{5/3}(\mathbf{r}) + \int d\mathbf{r}\ \rho(\mathbf{r})v_{ext}(\mathbf{r}) + \frac{1}{2}\int d\mathbf{r}d\mathbf{r}'\ \frac{\rho(\mathbf{r})\rho(\mathbf{r}')}{|\mathbf{r}-\mathbf{r}'|}, \tag{3.1}$$

where the first term is the Thomas-Fermi kinetic energy T^{TF} of the non interacting homogeneous electron gas, the second one is the energy due to the external potential v_{ext} and the last term is the electrostatic electron electron interaction, the Hartree energy E_H.

Thomas-Fermi model can not be used as it for real systems because of two main limitations:

- In general, it is not possible to express T^{TF} in terms of the sole density;
- The electron electron interaction is only treated with an electrostatic term and there is no account for exchange or correlation.

For instance, the Thomas-Fermi model is not able to describe important features, such as electronic shells in atoms or chemical bounds.

Here after, we review the modern DFT as first introduced by Hohenberg-Kohn with their celebrated theorem.

3.1.1 Hohenberg-Kohn theorem

In 1960's, a rigourous proof for the validity of the DFT approach was introduced by Hohenberg and Kohn. For a system N interacting electrons subjected to an external potential v_{ext}, the exact Hamiltonian is given by

$$H = T + v_{ee} + v_{ext}, \tag{3.2}$$

where the kinetic energy is the first term and electron-electron interaction is a second term.

The Hohenberg-Kohn theorem (HK) states that there exists a one-to-one mapping between the density and the external potential. This statement has very interesting consequences, such as

- The total energy is a functional of the electron density $\rho(\mathbf{r})$ only.

- The ground state expectation value of any observable is a unique functional of the electron density $\rho(\mathbf{r})$:

$$\left\langle \Psi^0 | O | \Psi^0 \right\rangle = O(\rho(\mathbf{r})), \tag{3.3}$$

  where Ψ^0 is the many-body ground state wave function.

- Thanks to the variational principle, the total energy functional $E[\rho(\mathbf{r})]$ has a minimum, the ground state energy E_0, if and only if the input density is the true ground state density ρ_0.

The total energy functional $E[\rho]$ is defined as

$$E[\rho] = F[\rho] + \int d\mathbf{r} v_{ext}(\mathbf{r})\rho(\mathbf{r}). \tag{3.4}$$

If one assumes further that the system has a non-degenerate ground-state Ψ_0 with a corresponding $\rho(\mathbf{r})$, one can define the functional $F[\rho]$ by

$$F[\rho] = \left\langle \Psi^0 | T + v_{ee} | \Psi^0 \right\rangle \tag{3.5}$$

which is a unique functional of $\rho(\mathbf{r})$.

F is also called the universal functional, since it does not depend on the external potential, then it does not on the system under study. For the moment, $F[\rho(\mathbf{r})]$ is left not determined by the HK theorem. HK theorem is only telling us about the existence of such a universal functional. In other words, the ground state density and also all the desired physics or chemistry ground state properties can not yet been determined by using only HK theorem.

The problem is to find an expression for the functional $F[\rho]$ which could be formally split into three different parts:

$$F[\rho] = T_s[\rho] + E_H[\rho(\mathbf{r})] + E_{xc}[\rho(\mathbf{r})], \tag{3.6}$$

where

- $T_s[\rho]$ is the kinetic energy of non-interacting electrons,
- $E_H[\rho]$ is the classical electrostatic (Hartree) energy,
- $E_{xc}[\rho]$ is the exchange-correlation energy.

While the two first terms can be given an analytical expression by using an auxiliary system of non-interacting electrons as we will see in the next section, the last term is not known analytically. It contains the non-classical electron-electron interaction energy, the so-called exchange and correlation energy, and the difference between the kinetic energies of the interacting and the non-interacting systems.

3.1.2 Kohn Sham method

Kohn and Sham (KS) suggested to study a non-interacting electron system, that has the same electronic density as the interacting electron system. Introducing non-interacting electron orbitals $\phi_i(\mathbf{r})$ is particularly helpful to write down an analytical expression for the main part of the kinetic energy:

$$T_s[\rho] = \sum_i^{N_e} \langle \phi_i | -\frac{\nabla^2}{2} | \phi_i \rangle. \tag{3.7}$$

According to KS, the total energy of the interacting electron system within an external potential v_{ext} is given as

$$E[\rho] = T_s[\rho] + \int v_{ext}\rho(\mathbf{r})d\mathbf{r} + \frac{1}{2}\int \frac{\rho(\mathbf{r})\rho(\mathbf{r}')}{|\mathbf{r}-\mathbf{r}'|} d\mathbf{r}d\mathbf{r}' + E_{xc}[\rho]. \tag{3.8}$$

Minimizing the total energy with respect to the density indeed corresponds to solving an effective Hamiltonian eigenvalue problem, the so-called KS equation:

$$H_{KS}\phi_i(\mathbf{r}) = [-\frac{1}{2}\nabla^2 + v_{KS}(\mathbf{r})]\phi_i(\mathbf{r}) = \epsilon_i^{KS}\phi_i(\mathbf{r}), \tag{3.9}$$

where the potential v_{KS} is the functional derivative of the the last three terms in the total energy equation:

$$v_{KS}(\mathbf{r}) = v_{ext}(\mathbf{r}) + v_H[\rho](\mathbf{r}) + v_{xc}[\rho](\mathbf{r}). \tag{3.10}$$

The Hartree potential v_H reads

$$v_H[\rho](\mathbf{r}) = \int \frac{\rho(\mathbf{r}')}{|\mathbf{r}-\mathbf{r}'|} d\mathbf{r}' \tag{3.11}$$

and the exchange-correlation potential reads

$$v_{xc}[\rho](\mathbf{r}) = \frac{\delta E_{xc}[\rho(\mathbf{r})]}{\delta\rho(\mathbf{r})}. \tag{3.12}$$

In order to find the ground-state density $\rho_0(\mathbf{r})$, Eq. (3.9) needs to be solved self-consistently with

$$\rho(\mathbf{r}) = \sum_{i=1}^{N_e} |\phi_i(\mathbf{r})|^2 \tag{3.13}$$

where ϕ_i are the single particle orbitals obtained from the diagonalization of H_{KS}.

In practice, from the solution of the Kohn-Sham equation, we can evaluate the energy via the eigenvalues as

$$E[\rho(\mathbf{r}] = \sum_{i}^{N_e} \epsilon_i - \int \rho(\mathbf{r}) v_{xc}(\mathbf{r}) d\mathbf{r} - E_H[\rho(\mathbf{r})] + E_{xc}[\rho(\mathbf{r})]. \tag{3.14}$$

So far the only unknown part in the last equation is $E_{xc}[\rho]$. Finally, the total energy can be evaluated by including the ion-ion interaction. The missing term E_{xc} can be efficiently approximated using the very simple expressions given by the local density approximation (LDA) or by the generalized gradient approximation (GGA).

3.1.3 Local Density Approximation

The simplest approximation for calculating the term of exchange and correlation is the local density approximation or LDA. This approximation assumes that the density varies very slowly. It replaces the exchange and correlation energy in each point in space by that of a uniform interacting electron gas with the same density. The LDA for the exchange correlation energy is:

$$E_{xc}^{LDA}[\rho] = \int \rho(\mathbf{r}) \varepsilon_{xc}^{heg}(\rho(\mathbf{r})) d\mathbf{r}, \tag{3.15}$$

where $\varepsilon_{xc}^{heg}[\rho(\mathbf{r})]$ is the exchange-correlation energy per electron of a homogeneous electron gas of density $\rho(\mathbf{r})$.

In practice, LDA can be regarded as an accurate approximation, even when the density fluctuates noticeably. However, whereas this method usually gives fairly reasonable molecular structures, it leads to overestimated binding energy, which can result in too short atomic distances. Thus, the parameters of lattice in solids are often underestimated [43].

3.1.4 Generalized Gradient Approximations

The most natural way to improve the LDA is to consider inhomogeneity of the electron density by introducing the exchange and correlation terms which further dependend on the density gradient $\nabla\rho$. This improvement is called the Generalized Gradient Approximation or GGA. Within this approximation, the term E_{xc} is written as a function of the electron density and its gradient as follows [90]

$$E_{xc}^{GGA}[\rho] = \int \rho(\mathbf{r}) f_{xc}[\rho(\mathbf{r}), \nabla\rho(\mathbf{r})] d\mathbf{r}, \tag{3.16}$$

where $f_{xc}[\rho(\mathbf{r}), \nabla\rho(\mathbf{r})]$ is a function of the local density and the local density gradient.

In practice, the GGA works generally better than LDA and improves the LDA results concerning the binding energies of molecules. However the lattice constants of solids are still not as accurate as one would have expected: GGA generally yields slightly overestimated lattice constants [32, 94].

3.2 Time dependent density functional theory

To study the phenomena related to the excited states of a system, DFT is not sufficient. DFT gives only access to ground state properties. But one may be interested in excited state phenomena: for example the photo-absorption spectra, a photo-dissociation induced by an intense laser, or the phenomenon we are interested in here, the electronic stopping power, in which the energy loss of the impinging ion is due to the electronic excitation of the target electrons. In years 1984-85, Runge, Gross and Kohn [73, 35] have extended DFT to the general situation of the systems subjected to a time dependent external field. This extension is named the time dependent-density functional theory (TDDFT). In this section, we give a brief introduction into the TDDFT: the time dependent equivalent of HK theorem "the Runge-Gross theorem" will be presented, then the KS time dependent system will be discussed. More details about the TDDFT can be found in Ref. [85].

The time dependent Schrödinger describes a system of N interacting electrons system exposed to a time dependent external potential $v_{ext}(\mathbf{r}, t)$ is given by

$$H(t)\Psi(\mathbf{r}_1, ..\mathbf{r}_N, t) = i\partial_t\Psi(\mathbf{r}_1, ..\mathbf{r}_N, t), \tag{3.17}$$

where $\Psi(\mathbf{r}_1, ..\mathbf{r}_N, t)$ is the time dependent wave function of the interacting electrons. It is fully determined from the specified initial state $\Psi(\mathbf{r}_1, ..\mathbf{r}_N, t_0)$ at initial time t_0 and from the Hamiltonian $H(t)$.

The Hamiltonian $H(t)$ can be written in the form

$$H(t) = \sum_{i=1}^{N}(-\frac{\nabla_i^2}{2} + v_{ext}(\mathbf{r}_i, t)) + \frac{1}{2}\sum_{i,k=1,i\neq k}^{N}\frac{1}{|\mathbf{r}_i - \mathbf{r}_k|}, \tag{3.18}$$

where the first term is the kinetic energy of the electrons and the last term is the electron electron interaction.

Again, as in DFT, TDDFT aims to replace the hard task of calculating the many-electron wavefunction $\Psi(\mathbf{r}_1, ..\mathbf{r}_N, t)$ by solving the (3.17) with the easier task of calculating the time dependent density $\rho(\mathbf{r}, t)$. The electron density

$\rho(\mathbf{r},t)$ is obtained from

$$\rho(\mathbf{r},t) = N \int d\mathbf{r}_2 ... d\mathbf{r}_N |\Psi(\mathbf{r},\mathbf{r}_2,..\mathbf{r}_N,t)|^2 \tag{3.19}$$

Now the following question is in our mind: Can the density $\rho(\mathbf{r},t)$ be used to determine all the properties of the system exposed to an external potential $v_{ext}(\mathbf{r}_i,t)$? Therefore we would need a time dependent version of the HK theorem in order to establish a one to one correspondence between the $v_{ext}(\mathbf{r},t)$ and $\rho(\mathbf{r},t)$. Next we review the Runge Gross theorem which gives the answer of this question.

3.2.1 Runge Gross theorem

The Runge Gross theorem (RG) consists of two parts.

Existence of a one-to-one mapping between densities and potentials The RG theorem states that:

For two densities $\rho(\mathbf{r},t)$ and $\rho'(\mathbf{r},t)$ evolving from a common initial state $\Psi(\mathbf{r}_1,..\mathbf{r}_N,t_0)$ under the influence of two potentials $v_{ext}(\mathbf{r},t)$ and $v'_{ext}(\mathbf{r},t)$ which are both Taylor-expandable about the initial time t_0, then $\rho(\mathbf{r},t)$ would differ from $\rho'(\mathbf{r},t)$ if and only if the potentials differ by more than a purely time dependent function, i.e. if and only if $v_{ext}(\mathbf{r},t) - v'_{ext}(\mathbf{r},t) \neq c(t)$.

Therefore, these two potentials can not produce the same $\rho(\mathbf{r},t)$, i.e.

$$v_{ext}(\mathbf{r},t) - v'_{ext}(\mathbf{r},t) \neq c(t) \Rightarrow \rho(\mathbf{r},t) \neq \rho'(\mathbf{r},t), \tag{3.20}$$

According to the last statement the existence of a one-to-one correspondence between the potential $v_{ext}(\mathbf{r},t)$ and the density $\rho(\mathbf{r},t)$ (up to purely time-dependent function $c(t)$) has been demonstrated.

Therefore, as well the potential $v_{ext}(\mathbf{r},t)$ is a functional of the density $\rho(\mathbf{r},t)$, the many-body Hamiltonian $H(t)$ and the many-body wavefunction $\Psi(\mathbf{r}_1,..\mathbf{r}_N,t)$ are also functional of $\rho(\mathbf{r},t)$ (for a given fixed initial state Ψ_0):

$$\begin{aligned} v_{ext}(\mathbf{r},t) = v_{ext}[\rho,\Psi_0](\mathbf{r},t) &\Rightarrow H(\mathbf{r},t) = H[\rho,\Psi_0](\mathbf{r},t) \\ &\Rightarrow \Psi(\mathbf{r}_1,..\mathbf{r}_N,t) = \Psi[\rho,\Psi_0](\mathbf{r}_1,..\mathbf{r}_N,t), \end{aligned} \tag{3.21}$$

As a consequence, the expectation value of any physical observable $O(t)$ is also a unique functional of the density $\rho(\mathbf{r},t)$

$$O(t) = O[\rho,\Psi_0](t) = \langle \Psi[\rho,\Psi_0]|O(t)|\Psi[\rho,\Psi_0]\rangle \tag{3.22}$$

In a few words, a proof of the RG theorem can be obtained in two steps, in which they considered two systems primed and unprimed evolving from a common initial state $\Psi(\mathbf{r}_1,..\mathbf{r}_N,t_0)$, for more details see [73, 35, 85]:

- Proof of the one-to-one correspondence between the potential $v_{ext}(\mathbf{r}, t)$ and the current density $\mathbf{J}(\mathbf{r}, t)$
- Then using the continuity equation

$$\frac{\partial \rho(\mathbf{r}, t)}{\partial t} = -\nabla \mathbf{J}(\mathbf{r}, t) \tag{3.23}$$

  to relate the current density to the density itself.

Extremum of the quantum-mechanical action Since the minimization principle for the total energy can not be used in the time dependent theory, we have to replace it by the stationary principle of the quantum mechanical action A.

Remember that the time dependent Schrödinger equation is equivalent to the stationary principle for A with appropriate initial condition, such as the knowledge of the initial many-body wavefunction Ψ_0.

Due to the first part of RG theorem, this action is also density functional $A[\rho]$. According to the stationary principle, we then have that

$$A[\rho] = \int_{t_0}^{t_1} dt \, \langle \Psi[\rho, \Psi_0] | i\partial_t - H(t) | \Psi[\rho, \Psi_0] \rangle \tag{3.24}$$

has stationary point at the correct time dependent density. In other words, the solution of $\dfrac{\delta A[\rho]}{\delta \rho(\mathbf{r}, t)} = 0$ with appropriate condition will give the correct time dependent density. Similarly to ground-state DFT, Eq. (3.24) can also be written as

$$A[\rho] = A_0[\rho] - \int_{t_0}^{t_1} dt \int d\mathbf{r} \rho(\mathbf{r}, t) v_{ext}(\mathbf{r}, t), \tag{3.25}$$

where $A_0[\rho]$ is the universal function

$$A_0[\rho] = \int_{t_0}^{t_1} dt \, \langle \Psi[\rho, \Psi_0] | i\partial_t - T - v_{ee} | \Psi[\rho, \Psi_0] \rangle \tag{3.26}$$

And similar to DFT we will use an auxiliary system in order to approximate the unknown action functional $A[\rho]$.

3.2.2 Time-dependent Kohn Sham Equations

One can construct a time dependent KS system, in which the time KS orbitals $\phi_j(\mathbf{r}, t)$ will obey the one-particle time dependent Schrödinger equation:

$$i\partial_t \phi_j(\mathbf{r}, t) = \left[-\frac{\nabla^2}{2} + v_{KS}(\mathbf{r}, t) \right] \phi_j(\mathbf{r}, t). \tag{3.27}$$

Here, $v_{KS}(\mathbf{r},t)$ is the time dependent Kohn-Sham potential. Simply, the correct time dependent density $\rho(\mathbf{r},t)$ is given by the following

$$\rho(\mathbf{r},t) = \sum_j |\phi_j(\mathbf{r},t)|^2. \tag{3.28}$$

Again, as for static DFT, the $v_{KS}(\mathbf{r},t)$ can be decomposed into three parts:

$$v_{KS}(\mathbf{r},t) = v_{ext}(\mathbf{r},t) + v_H(\mathbf{r},t) + v_{xc}(\mathbf{r},t), \tag{3.29}$$

where the first term is the external potential, the Hartree potential is the second term and the third one is the exchange correlation potential. The $v_{xc}part$ need to be approximated and the simplest approximation again is called the adiabatic local density approximation (ALDA).

3.2.3 Adiabatic approximations

It is a very simple method which employ the xc functionals $v_{xc}[\rho](\mathbf{r})$ of static DFT to be used in the TDDFT by evaluating $v_{xc}[\rho](\mathbf{r})$ at each time with the density $\rho(\mathbf{r},t)$. The adiabatic time-dependent xc potential is written as

$$v_{xc}^{adiabatic}(\mathbf{r},t) = v_{xc}[\rho](\mathbf{r})|_{\rho=\rho(\mathbf{r},t)}. \tag{3.30}$$

In other words, the xc potential does not have memory: it only depends on the present density. This is of course a very strong assumption.

The so-called adiabatic local density approximation (ALDA) is the result of inserting the LDA functional in Eq. (3.30)

$$v_{xc}^{ALDA}(\mathbf{r},t) = v_{xc}^{HEG}[\rho]|_{\rho=\rho(\mathbf{r},t)} \tag{3.31}$$

The ALDA considers that the xc potential at the point $\mathbf{r}$ and time t is equal to the xc potential of a homogeneous-electron gas (HEG) of density $\rho(\mathbf{r},t)$.

Certainly, ALDA has all the drawbacks of the LDA applications combined with all the drawbacks of the adiabatic approximation. For more details see Ref. [85].

3.3 Conclusion

In conclusion, we have reviewed the static density functional theory and the time dependent density functional theory. In our study, we will use DFT to calculate the KS orbitals and its eigenenergies, as necessary quantities to obtain the KS linear response function χ^{KS} within TDDFT. The next chapter is about the linear response theory in details.

Chapter 4

Linear response approach to TDDFT

The dynamics of the electronic many body systems can be described exactly within TDDFT by solving a time-dependent Schrödinger equation for the time-dependent KS orbitals. In the case of a system which has small deviation from the ground state, the full solution of the time-dependent Schrödinger equation or TDKS can be much simplified and still capture the response of the electronic many body systems upon an external perturbation. This formalism is the the linear response theory that deals directly with this small deviation from the ground state. The density functional formalism is very well suited for the implementation of the linear response of a many-body system to an external potential [63]. The linear response theory is a very widely used method to describe the response to a weak perturbation, such as encountered in many types of spectroscopy for instance. In this chapter we give a brief overview of the basic linear response formalism.

4.1 Linear response theory and Dyson-like equation

The linear change in the density due to a change in the external potential can be written as [48, 85, 63]:

$$\delta\rho(\mathbf{r},t) = \int dt' \int d\mathbf{r}' \ \chi(\mathbf{r},\mathbf{r}',t-t')\delta v_{ext}(\mathbf{r}',t'). \tag{4.1}$$

If we make a small change in the external potential at point $\mathbf{r}'$ and time t' , χ tells us how the density will change at point $\mathbf{r}$ and later time t. Note that,

because of the causality condition, χ in this equation is non zero function only for $t > t'$

Alternatively the linear change in the density due to a change in the KS potential can be written as:

$$\delta\rho(\mathbf{r},t) = \int dt' \int d\mathbf{r}' \; \chi^{KS}(\mathbf{r},\mathbf{r}',t-t')\delta v_{KS}[\rho](\mathbf{r}',t'). \tag{4.2}$$

In the two previous equations, we have introduced the density-density response functions. $\chi(\mathbf{r},\mathbf{r}',t-t')$ describes the change $\delta\rho(\mathbf{r},t)$ in the electron density due to a change in the potential $\delta v_{ext}(\mathbf{r}',t')$

$$\chi(\mathbf{r},\mathbf{r}',t-t') = \frac{\delta\rho(\mathbf{r},t)}{\delta v_{ext}(\mathbf{r}',t')}, \tag{4.3}$$

and the Khon-Sham density-density response function $\chi^{KS}(\mathbf{r},\mathbf{r}',t-t')$, which is the response of the independent KS particle

$$\chi^{KS}(\mathbf{r},\mathbf{r}',t-t') = \frac{\delta\rho(\mathbf{r},t)}{\delta v_{KS}(\mathbf{r}',t')}. \tag{4.4}$$

By using the chain rule for derivatives, the response function $\chi(\mathbf{r},\mathbf{r}',t-t')$ for the true system can be written in term of the $\chi^{KS}(\mathbf{r},\mathbf{r}',t-t')$ for the Kohn-Sham system as follows

$$\begin{aligned}\chi(\mathbf{r},\mathbf{r}',t-t') &= \int dt'' \int d\mathbf{r}'' \; \frac{\delta\rho(\mathbf{r},t)}{\delta v_{KS}(\mathbf{r}'',t'')}\frac{\delta v_{KS}(\mathbf{r}'',t'')}{\delta v_{ext}(\mathbf{r}',t')} \\ &= \int dt'' \int d\mathbf{r}'' \; \chi^{KS}(\mathbf{r},\mathbf{r}'',t-t'')\frac{\delta v_{KS}(\mathbf{r}'',t'')}{\delta v_{ext}(\mathbf{r}',t')}\end{aligned} \tag{4.5}$$

The only unknown part in Eq. (4.5) is $\dfrac{\delta v_{KS}(\mathbf{r}'',t'')}{\delta v_{ext}(\mathbf{r}',t')}$. It can be further worked out along the following lines. First, using the definition of KS potential and taking the partial derivative of $v_{KS}(\mathbf{r}',t')$ with respect to $v_{ext}(\mathbf{r}',t')$

$$\frac{\delta v_{KS}(\mathbf{r}'',t'')}{\delta v_{ext}(\mathbf{r}',t')} = \frac{\delta}{\delta v_{ext}(\mathbf{r}',t')}\left\{v_{ext}(\mathbf{r}'',t'') + v_H(\mathbf{r}'',t'') + v_{xc}(\mathbf{r}'',t'')\right\}, \tag{4.6}$$

and using the definition of the Hartree potential $v_H(\mathbf{r}'',t'')$

$$\begin{aligned}v_H(\mathbf{r}'',t'') &= \int d\mathbf{r}''' \frac{\rho(\mathbf{r}''',t'')}{|\mathbf{r}''-\mathbf{r}'''|} \\ &= \int dt''' \int d\mathbf{r}''' \frac{\delta(t''-t''')\rho(\mathbf{r}''',t''')}{|\mathbf{r}''-\mathbf{r}'''|},\end{aligned} \tag{4.7}$$

Eq. (4.6) now reads

$$\frac{\delta v_{KS}(\mathbf{r}'',t'')}{\delta v_{ext}(\mathbf{r}',t')} = \delta(\mathbf{r}'-\mathbf{r}'')\delta(t'-t'') + \int dt''' \int d\mathbf{r}''' \frac{\delta(t''-t''')}{|\mathbf{r}''-\mathbf{r}'''|} \frac{\delta\rho(\mathbf{r}''',t''')}{\delta v_{ext}(\mathbf{r}',t')} + \frac{\delta v_{xc}(\mathbf{r}'',t'')}{\delta v_{ext}(\mathbf{r}',t')}. \tag{4.8}$$

The chain rule via density $\rho(\mathbf{r}''',t''')$ can be used in the last term of (4.8)

$$\begin{aligned}\frac{\delta v_{KS}(\mathbf{r}'',t'')}{\delta v_{ext}(\mathbf{r}',t')} = \delta(\mathbf{r}'-\mathbf{r}'')\delta(t'-t'') &+ \int dt''' \int d\mathbf{r}''' \frac{\delta(t''-t''')}{|\mathbf{r}''-\mathbf{r}'''|} \frac{\delta\rho(\mathbf{r}''',t''')}{\delta v_{ext}(\mathbf{r}',t')} \\ &+ \frac{\delta v_{xc}(\mathbf{r}'',t'')}{\delta\rho(\mathbf{r}''',t''')} \frac{\delta\rho(\mathbf{r}''',t''')}{\delta v_{ext}(\mathbf{r}',t')}.\end{aligned} \tag{4.9}$$

Then the definition of the exchange-correlation kernel f_{xc}

$$f_{xc}(\mathbf{r},\mathbf{r}',t-t') = \frac{\delta v_{xc}(\mathbf{r},t)}{\delta\rho(\mathbf{r}',t')}, \tag{4.10}$$

can be used in Eq. (4.9):

$$\begin{aligned}\frac{\delta v_{KS}(\mathbf{r}'',t'')}{\delta v_{ext}(\mathbf{r}',t')} &= \delta(\mathbf{r}'-\mathbf{r}'')\delta(t'-t'') \\ &+ \left\{ \int dt''' \int d\mathbf{r}''' \frac{\delta(t''-t''')}{|\mathbf{r}''-\mathbf{r}'''|} + f^{xc}(\mathbf{r}'',\mathbf{r}''',t''-t''') \right\} \frac{\delta\rho(\mathbf{r}''',t''')}{\delta v_{ext}(\mathbf{r}',t')}.\end{aligned} \tag{4.11}$$

If we use the expression found in Eq. (4.11) in Eq. (4.5), we obtain the so-called Dyson-like equation for χ of an interacting system:

$$\begin{aligned}\chi(\mathbf{r},\mathbf{r}',t-t') &= \chi^{KS}(\mathbf{r},\mathbf{r}',t-t') \\ &+ \int dt'' \int d\mathbf{r}'' \int dt''' \int d\mathbf{r}''' \; \chi^{KS}(\mathbf{r},\mathbf{r}'',t-t'') \\ &\quad \times [v(\mathbf{r}'',\mathbf{r}''',t''-t''') + f_{xc}(\mathbf{r}'',\mathbf{r}''',t''-t''')] \\ &\quad \times \chi(\mathbf{r}''',\mathbf{r}',t'''-t'),\end{aligned} \tag{4.12}$$

here, v is the usual Coulomb potential.

If the Fourier transform of the Dyson-like equation is taken with respect to the different pairs of t, one obtains the Dyson-like equation in frequency space:

$$\begin{aligned}\chi(\mathbf{r},\mathbf{r}',\omega) &= \chi^{KS}(\mathbf{r},\mathbf{r}',\omega) \\ &+ \int d\mathbf{r}'' \int d\mathbf{r}''' \; \chi^{KS}(\mathbf{r},\mathbf{r}'',\omega) \left[v(\mathbf{r}'',\mathbf{r}''') + f_{xc}(\mathbf{r}'',\mathbf{r}''',\omega)\right] \\ &\times \chi(\mathbf{r}''',\mathbf{r}',\omega),\end{aligned} \tag{4.13}$$

The exchange-correlation kernel f_{xc} is the key quantity of linear response TDDFT. Eq. (4.13) gives an exact solution of the interacting system, the $\chi(\mathbf{r}, \mathbf{r}', \omega)$ can be found from a series summation of this equation or alternatively from an inversion.

For periodic crystal system, it would be practical to write the Dyson-like equation in the reciprocal an frequency space.

4.2 Dyson-like equation for a periodic lattice

By definition, the Fourier transformation of a periodic two-index quantity $f(\mathbf{r}, \mathbf{r}')$ is given as

$$f(\mathbf{r}, \mathbf{r}') = \frac{1}{\Omega^2} \sum_{\mathbf{q}_1, \mathbf{q}_2}^{BZ} \sum_{\mathbf{G}, \mathbf{G}'} e^{i(\mathbf{q}_1 + \mathbf{G}).\mathbf{r}} e^{-i(\mathbf{q}_2 + \mathbf{G}').\mathbf{r}'} f(\mathbf{q}_1 + \mathbf{G}, \mathbf{q}_2 + \mathbf{G}'), \tag{4.14}$$

where $\mathbf{q}_1$ and $\mathbf{q}_2$ are restricted to the first Brillouin zone, $\mathbf{G}, \mathbf{G}'$ are the reciprocal lattice vectors and Ω is the solid volume. This can be simplified by using the invariance by a translation of the crystal. Thus, for any vector $\mathbf{R}$ of the direct lattice, $f(\mathbf{r}', \mathbf{r}')$ must satisfy the following equation:

$$f(\mathbf{r}, \mathbf{r}') = f(\mathbf{r} + \mathbf{R}, \mathbf{r}' + \mathbf{R}). \tag{4.15}$$

When inserting the Fourier transform in the left-hand and the right-hand sides, then one can show that the Fourier transform of Eq. (4.15) only needs one $\mathbf{q}$ vector in the first BZ. This proof uses the equality $e^{(i\mathbf{G}.\mathbf{R})} = 1$ and the fact that the only non-vanishing coefficient $e^{i(\mathbf{q}_1 - \mathbf{q}_2).\mathbf{R}}$ is obtained when $\mathbf{q}_1 - \mathbf{q}_2$ is a reciprocal lattice vector. As both $\mathbf{q}_1$ and $\mathbf{q}_2$ are located in the first BZ, then the only reciprocal lattice vector available is zero.

Therefore the expansion in Eq. (4.14) can be written as

$$f(\mathbf{r}_1, \mathbf{r}_2) = \frac{1}{\Omega} \sum_{\mathbf{q}}^{BZ} \sum_{\mathbf{G}, \mathbf{G}'} e^{i(\mathbf{q} + \mathbf{G}).\mathbf{r}} e^{-i(\mathbf{q} + \mathbf{G}').\mathbf{r}'} f_{\mathbf{G}, \mathbf{G}'}(\mathbf{q}), \tag{4.16}$$

Thus, due to (4.16), the Fourier expansion of density response function $\chi(\mathbf{r}, \mathbf{r}', \omega)$,

$$\chi(\mathbf{r}, \mathbf{r}', \omega) = \frac{1}{\Omega} \sum_{\mathbf{q}}^{BZ} \sum_{\mathbf{G}, \mathbf{G}'} e^{i(\mathbf{q} + \mathbf{G}).\mathbf{r}} e^{-i(\mathbf{q} + \mathbf{G}').\mathbf{r}'} \chi_{\mathbf{G}, \mathbf{G}'}(\mathbf{q}, \omega) \tag{4.17}$$

Using the definition of the Fourier transform of a two index function in a periodic lattice as explicited in Eq. (4.16), then one can write $\chi(\mathbf{r}, \mathbf{r}', \omega)$ in

reciprocal and frequency space:

$$\chi_{\mathbf{G},\mathbf{G}'}(\mathbf{q},\omega) = \chi^{KS}_{\mathbf{G},\mathbf{G}'}(\mathbf{q},\omega) + \sum_{\mathbf{G}''\mathbf{G}'''} \chi^{KS}_{\mathbf{G},\mathbf{G}''}(\mathbf{q},\omega)\left\{v_{\mathbf{G}'',\mathbf{G}'''}(\mathbf{q}) + f^{xc}_{\mathbf{G}'',\mathbf{G}'''}(\mathbf{q},\omega)\right\}\chi_{\mathbf{G}''',\mathbf{G}'}(\mathbf{q},\omega). \tag{4.18}$$

This is the Dyson-like equation in reciprocal and frequency space. The Fourier transform of the Coulomb interaction is well known to be

$$v_{\mathbf{G},\mathbf{G}'}(\mathbf{q}) = \frac{4\pi}{|\mathbf{q}+\mathbf{G}|^2}\delta_{\mathbf{G},\mathbf{G}'}. \tag{4.19}$$

4.3 Linear response function of the independent-particle system

The retarded density-density response function $\chi(\mathbf{r},\mathbf{r}',t-t')$ of the interacting particle system can be alternatively defined as

$$\chi(\mathbf{r},\mathbf{r}',t-t') = \frac{\delta\rho(\mathbf{r},t)}{\delta v_{ext}(\mathbf{r}',t')} = -i\theta(t-t')\,\langle\psi_I(t_0)|[\hat{\rho}_I(\mathbf{r},t),\hat{\rho}_I(\mathbf{r}',t')]|\psi_I(t_0)\rangle \tag{4.20}$$

For the derivation of the retarded $\chi(\mathbf{r},\mathbf{r}',t-t')$ see Ref. [31].

The wavefunctions and operators in the interaction picture differ from the wavefunctions and the operators in the Schrödinger picture by a unitary transformation:

$$\psi_I(t_0) = e^{iH_0(t-t_0)}\psi(t) \tag{4.21}$$

and

$$\hat{\rho}_I(\mathbf{r},t) = e^{iH_0(t-t_0)}\hat{\rho}(\mathbf{r})e^{-iH_0(t-t_0)}, \tag{4.22}$$

where H_0 is the time-independent Hamiltonian. Also the Heaviside function $\theta(t-t')$ is defined as:

$$\theta(t-t') = \begin{matrix}1 & t \geq t' \\ 0 & t \leq t'.\end{matrix}, \tag{4.23}$$

In case of non-interacting electrons system the initial and final states may be described by single Slater determinants. A Slater determinant is a product of single electron states, $\psi = A[\phi_1^{KS}...\phi_N^{KS}]$ (where A is the anti-symmetrization operator). Therefore the density-density response function $\chi^{KS}(\mathbf{r},\mathbf{r}',t-t')$ of the non interacting particle system is defined as

$$\chi^{KS}(\mathbf{r},\mathbf{r}',t-t') = -i\theta(t-t')\left\langle\phi_1^{KS}...\phi_N^{KS}|[\hat{\rho}(\mathbf{r},t),\hat{\rho}(\mathbf{r}',t')]|\phi_1^{KS}...\phi_N^{KS}\right\rangle \tag{4.24}$$

$\chi^{KS}(\mathbf{r},\mathbf{r}',t-t')$ has a well known formula [63]

$$\chi^{KS}(\mathbf{r},\mathbf{r}',\omega)=\sum_{ij}(f_i-f_j)\frac{\overset{*}{\phi_j^{KS}}(\mathbf{r}')\phi_i^{KS}(\mathbf{r}')\overset{*}{\phi_i^{KS}}(\mathbf{r})\phi_j^{KS}(\mathbf{r})}{\omega-(\epsilon_j-\epsilon_i)+i\eta}, \tag{4.25}$$

where f_i and f_j are the Fermi occupation numbers, ϵ_j and ϵ_i are KS eigenvalues and the sums run over all KS orbitals, and $\phi_i^{KS}(\mathbf{r}')$ and $\phi_j^{KS}(\mathbf{r}')$ are the ground state KS orbitals. $\epsilon_j-\epsilon_i$ are the excitation energy of the non interacting system and thus χ^{KS} has poles at the difference of KS energies.

In Fourier space, $\chi^{KS}(\mathbf{r},\mathbf{r}',\omega_0)$ can be written as [64]:

$$\begin{aligned}\chi^{KS}_{\mathbf{G},\mathbf{G}'}(\mathbf{q},\omega)=&\frac{1}{\Omega}\sum_{\mathbf{k}}^{BZ}\sum_{i,j}\frac{(f_{i,\mathbf{k}}-f_{j,\mathbf{k}+\mathbf{q}})}{\epsilon_{i,\mathbf{k}}-\epsilon_{j,\mathbf{k}+\mathbf{q}}+\omega+i\eta}\\&\times\left\langle\phi_{i,\mathbf{k}}\right|e^{-i(\mathbf{q}+\mathbf{G}).\mathbf{r}}\left|\phi_{j,\mathbf{k}+\mathbf{q}}\right\rangle\left\langle\phi_{j,\mathbf{k}+\mathbf{q}}\right|e^{+i(\mathbf{q}+\mathbf{G}').\mathbf{r}'}\left|\phi_{i,\mathbf{k}}\right\rangle,\end{aligned} \tag{4.26}$$

where the wave vector $\mathbf{q}$ and $\mathbf{k}$ are restricted to the first BZ, $\phi_{i,\mathbf{k}(\mathbf{r})}$ are single-particle Bloch states(important for periodic solid), and the broadening η must be infinitesimal small. The spin can be introduced in the previous equation.

In summary, in order to calculate the density response of the interacting system χ, the following step have to be done:

- **Ground state DFT calculation**: in which all the KS eigenstates $\phi_{i,\mathbf{k}}^{KS}$ (for occupied and empty states) and eigenvalues $\epsilon_{i,\mathbf{k}}^{KS}$ are calculated for a given v_{xc} potential;
- **Density response function of KS system** χ^{KS}: The matrix elements of $\chi^{KS}_{\mathbf{G},\mathbf{G}'}(\mathbf{q},\omega)$ can be evaluated by performing Eq. (4.26);
- **Dyson-like equation solution**: a solution of Eq. (4.18) through an inversion of the geometric series yields the response function χ.

4.4 Exchange-correlation Kernel

Unfortunately one piece of information is still missing at this stage: both the exchange-correlation potential or the kernel are unknown [48]. Within the adiabatic approximation, f_{xc} depends only on the density at present time as explained in the previous chapter. So that all the memory effects are not included, i.e. f_{xc} has $\delta(t-t')$ behavior.

The final expression of the adiabatic (LDA) kernel is given by

$$f_{xc}^{ALDA}(\mathbf{r},\mathbf{r}',t-t')=\left.\frac{dv_{xc}^{LDA}}{d\rho}\right|_{\rho(\mathbf{r},t)}\delta(\mathbf{r}-\mathbf{r}')\delta(t-t'). \tag{4.27}$$

Several other xc kernels could be introduced to improve the results [22, 84, 69]. If the kernel is simply neglected instead, the Dyson-like equation reduces to the random phase approximation (RPA).

In practice, the ALDA gives good results for finite systems, such as molecules [55]. In this work, we have found the using of ALDA for the random electronic stopping power(RESP) calculations will give good results for bulk targets especially for Aluminum and Silicon target materials. Also our results show the improvement using ALDA instead of RPA will be important only for low proton energy. Next section is devoted to the dielectric function, which is the quantity that allows us to link withexperiment. For instance, we need to use it to obtain the energy loss function, which it is the central task to obtain the RESP.

4.5 The dielectric function

The inverse dielectric function is used to calculate the electron energy loss spectra. The microscopic dielectric function is the basic quantity that gives information about the screening of the system in the linear response, given through the following relation:

$$v_{tot}(\mathbf{r},t) = \int dt' \int d\mathbf{r}' \varepsilon^{-1}(\mathbf{r},\mathbf{r}',t-t') v_{ext}(\mathbf{r}',t'), \tag{4.28}$$

The following relation represents the connection of inverse dielectric function with the density-density response function, given by

$$\varepsilon^{-1}(\mathbf{r},\mathbf{r}',\omega) = \delta(\mathbf{r}-\mathbf{r}') + \int d\mathbf{r}'' v(\mathbf{r}-\mathbf{r}'') \chi(\mathbf{r}'',\mathbf{r}',\omega). \tag{4.29}$$

For a periodic solid, ε^{-1} is given by

$$\varepsilon^{-1}_{\mathbf{G},\mathbf{G}'}(\mathbf{q},\omega) = \delta_{\mathbf{G},\mathbf{G}'} + \frac{4\pi}{|\mathbf{q}+\mathbf{G}|^2} \chi_{\mathbf{G},\mathbf{G}'}(\mathbf{q},\omega). \tag{4.30}$$

Therefore, one can use this equation to calculate the $\varepsilon^{-1}_{\mathbf{G},\mathbf{G}'}(\mathbf{q},\omega)$ if one knows the response function χ.

The energy loss function is defined as the imaginary part the inverse dielectric function $\mathrm{Im}[-\varepsilon^{-1}_{\mathbf{G},\mathbf{G}'}(\mathbf{q},\omega)]$.

$$\mathrm{Im}[-\varepsilon^{-1}_{\mathbf{G},\mathbf{G}'}(\mathbf{q},\omega)] = -\frac{4\pi}{|\mathbf{q}+\mathbf{G}|^2} \mathrm{Im}[\chi_{\mathbf{G},\mathbf{G}'}(\mathbf{q},\omega)], \tag{4.31}$$

The inversion of the dielectric matrix is computationally very demanding. At this point we are ready to calculate the RESP, in which the $\mathrm{Im}[\varepsilon^{-1}_{\mathbf{G},\mathbf{G}'}(\mathbf{q},\omega)]$ is needed.

4.6 Conclusion

We have presented a brief summary for the Linear response function. We have focused on the well known formula the Dyson like equation which is considered to be as the most important equation, because it allows us to evaluate the density-density response function χ from the KS density-density response function χ^{KS}. Finally we have introduced the link between the inverse dielectric matrix $\mathrm{Im}[\varepsilon^{-1}]$ and χ. Next chapter, we will study the electronic stopping power in details.

Chapter 5

Dielectric theory of the electronic stopping power of fast ions

In this chapter, the dielectric theory of the electronic stopping power is reviewed. Historically, the first evaluation of the electronic stopping power is due to Lindhard [47] in 1954. The calculation of Lindhard was based on the non-interacting homogeneous electron gas model (sometimes named jellium), which is the simplest model one can think of to represent electrons in solids: the electrons freely move without interacting in a positive charge background that ensures the overall charge neutrality. This model has been popular for many decades since many calculations can be performed analytically in this model and still the obtained electronic properties often capture the realistic features of experiments. The first section of the chapter is devoted to the Lindhard theory of stopping power. The second section will deal with the complete calculation of the electronic stopping power in linear response in periodic solids. The Lindhard results for the homogeneous electron gas can be understood as a limiting case of the complete theory.

5.1 Linear response electronic stopping power for the non-interacting homogeneous electron gas

The slowing down of the charged particle in a target material was an intense topic in the first half of the twentieth century with the advent of nuclear science. To evaluate the electronic contribution to the stopping power, Lindhard introduced the first dielectric formulation of stopping phenomenon [47]. He derived the dielectric formulation of the stopping effect for a free electron gas

(FEG) responding to a perturbation induced by a charged particle using perturbation theory [40, 92, 46]. The only parameter necessary to completely describe this model system is the average electron density ρ.

By performing the Lindhard calculation for different values of this parameter ρ, we can calculate the stopping power for a range of densities and then one apply a kind of local density approximation with Lindhard theory to evaluate the stopping value of the impinging ion in a real solids, as we will describe in the following. For many cases this approximation can produce a somewhat acceptable result compared to the experimental data [92].

5.1.1 Lindhard's theory of stopping power

We will not derive Lindhard's expressions here, but simply write them down. The Lindhard's formulas will be obtained later on as a special case of the complete periodic solid results. In this section, the atomic units (a.u.), with ($e = \hbar = m = 1$, etc) will not be used.

According to the Lindhard theory, the electronic stopping power within the dielectric formalism can be written as

$$-dE/dx = \frac{4\pi}{m}\left(\frac{Ze^2}{v}\right)^2 \rho L(\rho, v), \tag{5.1}$$

where the ion of charge Ze moving with velocity v in a medium of uniform density ρ, m is the electron mass and L is called the dimensionless stopping number.

In the dielectric formalism, L is written as

$$L = \frac{i}{\pi\omega_0^2}\int_0^\infty \frac{dk}{k}\int_{-kv}^{kv} \omega d\omega[\varepsilon^{-1}(k,\omega) - 1], \tag{5.2}$$

where the double integral cannot be evaluated analytically. In this last equation, the classical plasma frequency ω_0 is given by

$$\omega_0 = \sqrt{\frac{4\pi\rho e^2}{m}} \tag{5.3}$$

and $\varepsilon(k,\omega)$ is the wave number and frequency dependent longitudinal dielectric function.

Within the first order perturbation theory the dielectric function $\varepsilon(k,\omega)$

was obtained by Lindhard for free electron gas as the following equation

$$\varepsilon(k,\omega) = 1 + \frac{8\pi m e^2}{\hbar^2 k^2} \sum_n F(E_n) \left[\frac{1}{k^2 + 2\mathbf{k}.\mathbf{k}_n - (\frac{2m}{\hbar})(\omega + i\eta)} + \frac{1}{k^2 - 2\mathbf{k}.\mathbf{k}_n + (\frac{2m}{\hbar})(\omega + i\eta)} \right], \quad (5.4)$$

where the energy E_n and wave vector $\mathbf{k}_n$ are for an electron in the nth state and η is a small positive value.

For a free-electron gas at zero temperature, the occupation function F reduces to

$$\begin{aligned} F(E_n) =& 1 \quad E_n \leq E_f \\ & 0 \quad E_n \geq E_f, \end{aligned} \quad (5.5)$$

in terms of the gas density ρ the Fermi energy E_f can be written as

$$E_f = \frac{1}{2} m {v_f}^2 = \frac{\hbar^2 k_f^2}{2m} = \frac{\hbar^2}{2m} (3\pi^2 \rho)^{2/3}. \quad (5.6)$$

Using the reduced dimensionless variables $z = \dfrac{k}{2k_f}$ and $u = \dfrac{\omega}{k v_f}$ instead of k and ω, Eq. (5.4) can be also simplified into

$$\varepsilon(u,z) = 1 + \frac{\chi^2}{z^2} \left[f_1(u,z) + i f_2(u,z) \right], \quad (5.7)$$

where

$$\begin{aligned} f_1(u,z) =& \frac{1}{2} + \frac{1}{8z} \left[1 - (z-u)^2 \right] \left| \ln \frac{z-u+1}{z-u-1} \right| \\ & + \frac{1}{8z} \left[1 - (z+u)^2 \right] \left| \ln \frac{z+u+1}{z+u-1} \right|, \end{aligned} \quad (5.8a)$$

and

$$\begin{aligned} f_2(u,z) =& \frac{1}{2}\pi u, \quad \text{for } z+u<1 \\ =& \frac{\pi}{8z} \left[1 - (z-u)^2 \right] \quad \text{for } |z-u| < 1 < z+u \\ =& 0 \quad \text{for } |z-u| > 1. \end{aligned} \quad (5.8b)$$

Also, the dimensionless parameter χ in Eq. (5.7) is defined by

$$\chi^2 = \frac{v_0}{\pi v_f}, \tag{5.9}$$

where $v_0 = e^2/\hbar$ is the Bohr velocity, χ^2 is proportional to $\rho^{-1/3}$.

When the dielectric constant of Eq. (5.7) is substituted into Eq. (5.2), one obtains

$$L = \frac{6}{\pi} \int_0^{v/v_f} u \, du \int_0^{\infty} dz \frac{z^3 f_2(u,z)}{\left[z^2 + \chi^2 f_1(u,z)\right]^2 + \left[\chi^2 f_2(u,z)\right]^2}. \tag{5.10}$$

This expression for L in Eq. (5.10) is refered to as the Lindhard stopping number.

The double integral could be evaluated numerically in Eq. (5.10). Later Lindhard and Winther (L-W) [46] obtained an analytic form for the stopping power number in two limits: the high and the low projectile velocity with respect to the electron gas Fermi velocity. The main advantage of using the analytic forms of "the L-W expansions" of the stopping power number is to avoid the significant computational difficulties implied by the original Lindhard formula: it indeed presents singularities in the integrand [40, 41, 92].

In the following, we review in details the application of the local density approximation with the Lindhard's stopping theory for a realistic solid target.

5.1.2 Local density approximation to the stopping power

The simplest approximation is to assume that the solid can be treated locally as a uniform electron gas: the electronic stopping power at each point in a solid system is the same as that of a uniform electron gas of the same density. This local density approximation (LDA), also sometimes named local plasma density approximation (LPDA) was originally introduced by Lindhard and Scharff (L-S) [45, 41]. The electronic stopping power for a solid having an electronic density $\rho(r)$ is approximated by

$$-\frac{dE}{dx} = \frac{4\pi}{m} \left(\frac{Ze^2}{v}\right)^2 \int \rho(\mathbf{r}) L(\rho(\mathbf{r}), v) d\mathbf{r} \tag{5.11}$$

The LDA has been widely used to study the electronic stopping power of a solid target. This has been done by using different model that described the atomic charge distribution $\rho(r)$ of the target electrons, for an instance the Lenz-Jensen density model used by Bonderup [15], the Hartree-Fock-Slater (HFS) density model used by Rousseau et al. [72] and the spherically averaged solid state charge densities used by G. J. Iafrate *et al.* [41].

The importance of using the solid-state charge densities to study the stopping of impinging ion in solid target has been nicely understood by G. J. Iafrate *et al.*; they have compared the calculated value of stopping number for low energy (100 KeV/amu) and stopping number for high energy (10000 KeV/amu) of the impinging ion. It has been found for low energy of impinging ion the stopping number is caused by the valence electrons excitation, whereas for the high energy of impinging ion the stopping number is caused mainly by the core electrons excitation.[41]

In this work, we will use Eq. (5.11) to check the accuracy of using FEG model as compared the real target electrons in the electronic stopping power calculations, in which we used the density functional theory to calculate the charge density distribution for both valence and core electrons. This will be explained in details in chapter 7.

In the next section we review in details the theory of the electronic stopping power of a periodic crystal.

5.2 Linear response electronic stopping power of a periodic crystal

As we have just seen, a local density approximation to real solids can used based on the Lindhard stopping power of FEG system. However, a more realistic approach to the stopping power of solids is to consider the actual electronic wavefunctions in a periodic crystal potential, in which the electronic states are described by Bloch states and the spectrum of one-electron excitations splits into energy bands [21].

Among the first authors to describe the stopping in a periodic crystal using linear response theory were Saslow and Reiter [76]. They computed the energy loss of a high-energy charged particle, namely an electron, moving through a solid with a constant velocity v a long $\mathbf{r}_0 = \mathbf{v}t$ [76]. In fact the linear response dielectric formalism is valid for high ion velocities, i.e. ion velocity larger than the Fermi velocity of the electrons in the target ($v > v_f$). While at low ion velocities in metals, the nonlinear effects have to be included in principle. But it has been argued [65, 83] that the non-linear phenomena are less crucial in case of solids with a band gap.

For long time, simple models for the dielectric response function have been used to treat the stopping power in periodic crystal, however these attempts rely on rather unrealistic band structure calculations, which in turn might produce energy loss functions with a limited accuracy [16, 17, 25, 19].

Several attempts to introduce the full electronic band structure in the elec-

tronic stopping power calculations for low projectile velocities have been done. These attempts were carried out based on the linear combination of atomic orbitals (LCAO) framework [26] for instance or with a static treatment of the density-response of the solid for silicon target [83]. More recently, ab initio band structure calculations that are based on a full evaluation of the dynamical density response of the solid have been carried out by Campillo *et al.* for aluminum and silicon [21, 20, 64]. In the following we review and discuss the full derivation of the position dependent and of the random electronic stopping power for fast ions within the linear response theory.

5.2.1 Position dependent of electronic stopping power

Our calculations in this section will be based on classical electro-magnetism at the microscopic level. We would like to stress immediately that the electromagnetism language differs from the DFT language by a sign convention. Indeed, the electrons bear a negative charge and then their density in a solid $\rho(\mathbf{r})$ is a negative-valued function. In the DFT language, we use instead the electron density $n(\mathbf{r})$ which is a positive-valued function. The same statement holds when expressing the potentials. We will label ϕ the electrostatic potentials, whereas the electronic potential were labeled v in the previous chapters. However when expression the response functions the two sign conventions will luckily cancel out. Consider the density-density response functions χ which can alternatively be written as

$$\chi(\mathbf{r}, \mathbf{r}', t - t') = \frac{\delta n(\mathbf{r}t)}{\delta v_{ext}(\mathbf{r}'t')} \tag{5.12a}$$

or as

$$\chi(\mathbf{r}, \mathbf{r}', t - t') = \frac{\delta \rho(\mathbf{r}t)}{\delta \phi^{ext}(\mathbf{r}'t')}. \tag{5.12b}$$

In the following, we will compute the rate of the electronic energy loss, dE/dt, of a point particle as it moves through the solid. The electronic energy loss rate is given by the response of the system to the external potential.

Consider a classical point charge Ze passing through the solid, moving at a constant velocity along $\mathbf{r}_0 = \mathbf{b} + \mathbf{v}t$, where $\mathbf{b}$ is the impact parameter:

$$\begin{aligned} \rho^{ext}(\mathbf{r}, t) &= Z\delta(\mathbf{r} - \mathbf{r}_0) \\ &= Z\delta(\mathbf{r} - \mathbf{b} - \mathbf{v}t) \end{aligned} \tag{5.13}$$

ρ^{ext} denotes the external charge density.

The electronic energy loss rate is given by the real part of

$$\frac{dE}{dt} = \int d\mathbf{r}\ \rho^{ext}(\mathbf{r}, t)\ \mathbf{v}.\mathbf{E}^{ind}(\mathbf{r}, t), \tag{5.14}$$

where $\mathbf{E}^{ind}$ is the induced electric field in the target material.

The stopping power, $S = -dE/dx$, is given by

$$S(\mathbf{r}_0, \mathbf{v}) = -\frac{1}{v}\int d\mathbf{r}\ \rho^{ext}(\mathbf{r}, t)\ \mathbf{v}.\mathbf{E}^{ind}(\mathbf{r}, t). \tag{5.15}$$

In order to compute the dielectric formula of the electronic stopping power, one has to evaluate $\mathbf{E}^{ind}(\mathbf{r}, t) = -\nabla\phi^{ind}(\mathbf{r}, t)$. For periodic crystals a Fourier expansion of the induced electrostatic potential $\phi^{ind}(\mathbf{r}, \omega)$ is given by

$$\phi^{ind}(\mathbf{r}, \omega) = \frac{1}{\Omega}\sum_{\mathbf{q}}^{BZ}\sum_{\mathbf{G}} e^{i(\mathbf{q}+\mathbf{G}).\mathbf{r}}\phi^{ind}_{\mathbf{G}}(\mathbf{q}, \omega) \tag{5.16}$$

Using Eq. (5.16), one can write $\phi^{ind}(\mathbf{r}, t)$ as

$$\begin{aligned}\phi^{ind}(\mathbf{r}, t) &= \frac{1}{2\pi}\int d\omega\ e^{-i\omega t}\phi^{ind}(\mathbf{r}, \omega) \\ &= \frac{1}{\Omega}\sum_{\mathbf{q}}^{BZ}\sum_{\mathbf{G}}\ \frac{1}{2\pi}\int d\omega\ e^{i((\mathbf{q}+\mathbf{G}).\mathbf{r}-\omega t)}\phi^{ind}_{\mathbf{G}}(\mathbf{q}, \omega),\end{aligned} \tag{5.17}$$

where $\phi^{ind}_{\mathbf{G}}(\mathbf{q}, \omega)$ is the Fourier coefficients of the induced potential. Thus, $\mathbf{E}^{ind}(\mathbf{r}, t)$ is given by

$$\begin{aligned}\mathbf{E}^{ind}(r, t) &= -\nabla\phi^{ind}(\mathbf{r}, t) \\ &= -\nabla\frac{1}{\Omega}\sum_{\mathbf{q}}^{BZ}\sum_{\mathbf{G}}\ \frac{1}{2\pi}\int d\omega\ e^{i((\mathbf{q}+\mathbf{G}).\mathbf{r}-\omega t)}\phi^{ind}_{\mathbf{G}}(\mathbf{q}, \omega) \\ &= \frac{-i}{(2\pi)\Omega}\sum_{\mathbf{q}}^{BZ}\sum_{\mathbf{G}}\int d\omega\ e^{i((\mathbf{q}+\mathbf{G}).\mathbf{r}-\omega t)}\phi^{ind}_{\mathbf{G}}(\mathbf{q}, \omega)(\mathbf{q}+\mathbf{G}),\end{aligned} \tag{5.18}$$

where Ω is the solid volume, the first sum runs over $\mathbf{q}$ vectors within the first Brillouin zone (BZ), and $\mathbf{G}$ runs over the reciprocal lattice vectors.

In the following we are going to evaluate $\phi^{ind}_{\mathbf{G}}(\mathbf{q}, \omega)$ using the linear response theory:
The linear density response function $\chi(\mathbf{r}, \mathbf{r}', \omega)$ of an electron system is defined by equation

$$\rho^{ind}(\mathbf{r}, \omega) = \int d\mathbf{r}'\ \chi(\mathbf{r}, \mathbf{r}', \omega)\phi^{ext}(\mathbf{r}', \omega), \tag{5.19}$$

where $\rho^{ind}(\mathbf{r}, \omega)$ is the electron density induced by an external potential $\phi^{ext}(\mathbf{r}, \omega)$. According to Poisson's equation and with using (5.19) one can write the induced potential $\phi^{ind}(\mathbf{r}, \omega)$ as

$$\begin{aligned}\phi^{ind}(\mathbf{r},\omega) &= \int d\mathbf{r}' \ \frac{1}{|\mathbf{r}-\mathbf{r}'|}\rho^{ind}(\mathbf{r}',\omega) \\ &= \int d\mathbf{r}' \int d\mathbf{r}'' \ \frac{1}{|\mathbf{r}-\mathbf{r}'|}\chi(\mathbf{r}',\mathbf{r}'',\omega)\phi^{ext}(\mathbf{r}'',\omega).\end{aligned} \tag{5.20}$$

It is convenient to introduce the Fourier expansion of $\phi^{ext}(\mathbf{r},\omega)$, $\frac{1}{|\mathbf{r}-\mathbf{r}'|}$ and $\chi(\mathbf{r},\mathbf{r}',\omega)$ for periodic crystal,

$$\phi^{ext}(\mathbf{r}'',\omega) = \frac{1}{\Omega}\sum_{\mathbf{q}_1}^{BZ}\sum_{\mathbf{G}_1} e^{i(\mathbf{q}_1+\mathbf{G}_1).\mathbf{r}''}\phi^{ext}_{\mathbf{G}_1}(\mathbf{q}_1,\omega), \tag{5.21}$$

$$\frac{1}{|\mathbf{r}-\mathbf{r}'|} = \frac{1}{\Omega}\sum_{\mathbf{q}_2}^{BZ}\sum_{\mathbf{G}_2} e^{i(\mathbf{q}_2+\mathbf{G}_2).\mathbf{r}}e^{-i(\mathbf{q}_2+\mathbf{G}_2).\mathbf{r}'}\frac{4\pi}{|\mathbf{q}_2+\mathbf{G}_2|^2}, \tag{5.22}$$

$$\chi(\mathbf{r}',\mathbf{r}'',\omega) = \frac{1}{\Omega}\sum_{\mathbf{q}_0}^{BZ}\sum_{\mathbf{G}_0,\mathbf{G}_0'} e^{i(\mathbf{q}_0+\mathbf{G}_0).\mathbf{r}'}e^{-i(\mathbf{q}_0+\mathbf{G}_0').\mathbf{r}''}\chi_{\mathbf{G}_0,\mathbf{G}_0'}(\mathbf{q}_0,\omega), \tag{5.23}$$

where $\mathbf{q}$, $\mathbf{q}_0$, $\mathbf{q}_1$, and $\mathbf{q}_2$ are wave vectors within the first BZ, and $\mathbf{G}_0$, $\mathbf{G}_0'$, $\mathbf{G}_1$, and $\mathbf{G}_2$ are reciprocal lattice vectors. Then, substituting of Eq. (5.16), Eq. (5.21), Eq. (5.22) and Eq. (5.23) in Eq. (5.20) leads to the following equation:

$$\begin{aligned}\frac{1}{\Omega}\sum_{\mathbf{q}}^{BZ}\sum_{\mathbf{G}} e^{i(\mathbf{q}+\mathbf{G}).\mathbf{r}}\phi^{ind}_{\mathbf{G}}(\mathbf{q},\omega) = \int d\mathbf{r}' \int d\mathbf{r}'' \\ \frac{1}{\Omega}\sum_{\mathbf{q}_2}^{BZ}\sum_{\mathbf{G}_2} e^{i(\mathbf{q}_2+\mathbf{G}_2).\mathbf{r}}e^{-i(\mathbf{q}_2+\mathbf{G}_2).\mathbf{r}'}\frac{4\pi}{|\mathbf{q}_2+\mathbf{G}_2|^2} \\ \frac{1}{\Omega}\sum_{\mathbf{q}_0}^{BZ}\sum_{\mathbf{G}_0,\mathbf{G}_0'} e^{i(\mathbf{q}_0+\mathbf{G}_0).\mathbf{r}'}e^{-i(\mathbf{q}_0+\mathbf{G}_0').\mathbf{r}''}\chi_{\mathbf{G}_0,\mathbf{G}_0'}(\mathbf{q}_0,\omega) \\ \frac{1}{\Omega}\sum_{\mathbf{q}_1}^{BZ}\sum_{\mathbf{G}_1} e^{i(\mathbf{q}_1+\mathbf{G}_1).\mathbf{r}''}\phi^{ext}_{\mathbf{G}_1}(\mathbf{q}_1,\omega).\end{aligned} \tag{5.24}$$

Also the last equation can be written as

$$\frac{1}{\Omega}\sum_{\mathbf{q}}^{BZ}\sum_{\mathbf{G}} e^{i(\mathbf{q}+\mathbf{G}).\mathbf{r}}\phi^{ind}_{\mathbf{G}}(\mathbf{q},\omega) = \frac{1}{\Omega}\sum_{\mathbf{q}_2}^{BZ}\sum_{\mathbf{G}_2} e^{i(\mathbf{q}_2+\mathbf{G}_2).\mathbf{r}}\frac{4\pi}{|\mathbf{q}_2+\mathbf{G}_2|^2}$$
$$\frac{1}{\Omega}\sum_{\mathbf{q}_0}^{BZ}\sum_{\mathbf{G}_0,\mathbf{G}'_0}\int d\mathbf{r}'\ e^{i(\mathbf{q}_0+\mathbf{G}_0-\mathbf{q}_2-\mathbf{G}_2).\mathbf{r}'}\chi_{\mathbf{G}_0,\mathbf{G}'_0}(\mathbf{q}_0,\omega)$$
$$\frac{1}{\Omega}\sum_{\mathbf{q}_1}^{BZ}\sum_{\mathbf{G}_1}\int d\mathbf{r}''\ e^{i(\mathbf{q}_1+\mathbf{G}_1-\mathbf{q}_0-\mathbf{G}'_0).\mathbf{r}''}\phi^{ext}_{\mathbf{G}_1}(\mathbf{q}_1,\omega). \tag{5.25}$$

One now uses the following useful relation

$$\frac{1}{\Omega}\int_{\Omega} d\mathbf{r}\ e^{i(\mathbf{q}+\mathbf{G}-\mathbf{q}'-\mathbf{G}').\mathbf{r}} = \delta_{\mathbf{q},\mathbf{q}'}\delta_{\mathbf{G},\mathbf{G}'} \tag{5.26}$$

to simplify Eq. (5.25):

$$\frac{1}{\Omega}\sum_{\mathbf{q}}^{BZ}\sum_{\mathbf{G}} e^{i(\mathbf{q}+\mathbf{G}).\mathbf{r}}\phi^{ind}_{\mathbf{G}}(\mathbf{q},\omega) = \frac{1}{\Omega}\sum_{\mathbf{q}_2}^{BZ}\sum_{\mathbf{G}_2} e^{i(\mathbf{q}_2+\mathbf{G}_2).\mathbf{r}}\frac{4\pi}{|\mathbf{q}_2+\mathbf{G}_2|^2}$$
$$\sum_{\mathbf{G}'_0}\chi_{\mathbf{G}_2,\mathbf{G}'_0}(\mathbf{q}_2,\omega)\phi^{ext}_{\mathbf{G}'_0}(\mathbf{q}_2,\omega). \tag{5.27}$$

Again, by introducing $\int d\mathbf{r}\ e^{-i(\mathbf{q}_3+\mathbf{G}_3).\mathbf{r}}$ for the both side of the last equation as

$$\frac{1}{\Omega}\sum_{\mathbf{q}}^{BZ}\sum_{\mathbf{G}}\int d\mathbf{r}\ e^{i(\mathbf{q}+\mathbf{G}-\mathbf{q}_3-\mathbf{G}_3).\mathbf{r}}\ \phi^{ind}_{\mathbf{G}}(\mathbf{q},\omega) = \frac{1}{\Omega}\sum_{\mathbf{q}_2}^{BZ}\sum_{\mathbf{G}_2}\int d\mathbf{r}\ e^{i(\mathbf{q}_2+\mathbf{G}_2-\mathbf{q}_3-\mathbf{G}_3).\mathbf{r}}\ \frac{4\pi}{|\mathbf{q}_2+\mathbf{G}_2|^2}$$
$$\sum_{\mathbf{G}'_0}\chi_{\mathbf{G}_2,\mathbf{G}'_0}(\mathbf{q}_2,\omega)\phi^{ext}_{\mathbf{G}'_0}(\mathbf{q}_2,\omega), \tag{5.28}$$

and then using Eq. (5.26), this yields

$$\sum_{\mathbf{q}}^{BZ}\sum_{\mathbf{G}}\delta_{\mathbf{q},\mathbf{q}_3}\delta_{\mathbf{G},\mathbf{G}_3}\ \phi^{ind}_{\mathbf{G}}(\mathbf{q},\omega) = \sum_{\mathbf{q}_2}^{BZ}\sum_{\mathbf{G}_2}\delta_{\mathbf{q}_2,\mathbf{q}_3}\delta_{\mathbf{G}_2,\mathbf{G}_3}\frac{4\pi}{|\mathbf{q}_2+\mathbf{G}_2|^2}$$
$$\sum_{\mathbf{G}'_0}\chi_{\mathbf{G}_2,\mathbf{G}'_0}(\mathbf{q}_2,\omega)\phi^{ext}_{\mathbf{G}'_0}(\mathbf{q}_2,\omega). \tag{5.29}$$

Therefore, $\phi^{ind}_{\mathbf{G}}(\mathbf{q},\omega)$ has the following form

$$\phi^{ind}_{\mathbf{G}}(\mathbf{q},\omega) = \sum_{\mathbf{G}'} \frac{4\pi}{|\mathbf{q}+\mathbf{G}|^2}\ \chi_{\mathbf{G},\mathbf{G}'}(\mathbf{q},\omega)\phi^{ext}_{\mathbf{G}'}(\mathbf{q},\omega). \tag{5.30}$$

We now use the following formula for $\varepsilon^{-1}_{\mathbf{G},\mathbf{G}'}(\mathbf{q},\omega)$ which was derived by Martin and Schwinger [49],

$$\varepsilon^{-1}_{\mathbf{G},\mathbf{G}'}(\mathbf{q},\omega) = \left(\delta_{\mathbf{G},\mathbf{G}'} + \frac{4\pi}{|\mathbf{q}+\mathbf{G}|^2}\chi_{\mathbf{G},\mathbf{G}'}(\mathbf{q},\omega)\right). \tag{5.31}$$

We introduce it in Eq. (5.30) in order to write the $\phi^{ind}_{\mathbf{G}}(\mathbf{q},\omega)$ in terms of the dielectric matrix $\varepsilon^{-1}_{\mathbf{G},\mathbf{G}'}(\mathbf{q},\omega)$:

$$\phi^{ind}_{\mathbf{G}}(\mathbf{q},\omega) = \sum_{\mathbf{G}'}(\varepsilon^{-1}_{\mathbf{G},\mathbf{G}'}(\mathbf{q},\omega) - \delta_{\mathbf{G},\mathbf{G}'})\phi^{ext}_{\mathbf{G}'}(\mathbf{q},\omega) \tag{5.32}$$

From the Poisson equation one can show that

$$\phi^{ext}_{\mathbf{G}'}(\mathbf{q},\omega) = \frac{4\pi}{|\mathbf{q}+\mathbf{G}'|^2}\rho^{ext}_{\mathbf{G}'}(\mathbf{q},\omega), \tag{5.33}$$

where the Fourier components of $\rho^{ext}_{\mathbf{G}}(\mathbf{q},\omega)$ are given by

$$\begin{aligned}
\rho^{ext}_{\mathbf{G}}(\mathbf{q},\omega) &= \int_{\Omega} d\mathbf{r} \int dt\ \rho^{ext}(\mathbf{r},t)e^{-i((\mathbf{q}+\mathbf{G}).\mathbf{r}-\omega t)} \\
&= \int_{\Omega} d\mathbf{r} \int dt\ Z\delta(\mathbf{r}-\mathbf{b}-\mathbf{v}t)e^{-i((\mathbf{q}+\mathbf{G}).\mathbf{r}-\omega t)} \\
&= \int dt\ Ze^{+i(\omega-(\mathbf{q}+\mathbf{G}).\mathbf{v})t}\ e^{-i\mathbf{b}.(\mathbf{q}+\mathbf{G})} \\
&= 2\pi Z\delta(\omega-(\mathbf{q}+\mathbf{G}).\mathbf{v})e^{-i\mathbf{b}.(\mathbf{q}+\mathbf{G})}.
\end{aligned} \tag{5.34}$$

By substituting Eq. (5.33) into Eq. (5.32), the final expression of $\phi^{ind}_{\mathbf{G}}(\mathbf{q},\omega)$ can be written as

$$\phi^{ind}_{\mathbf{G}}(\mathbf{q},\omega) = \sum_{\mathbf{G}'}(\varepsilon^{-1}_{\mathbf{G},\mathbf{G}'}(\mathbf{q},\omega) - \delta_{\mathbf{G},\mathbf{G}'})\frac{8\pi^2 Z}{|\mathbf{q}+\mathbf{G}'|^2}\ \delta(\omega-(\mathbf{q}+\mathbf{G}').\mathbf{v})\ e^{-i\mathbf{b}.(\mathbf{q}+\mathbf{G}')} \tag{5.35}$$

Inserting Eq. (5.35) into Eq. (5.18) gives $\mathbf{E}^{ind}(r,t)$ as

$$\begin{aligned}\mathbf{E}^{ind}(\mathbf{r},t) &= \frac{-i}{(2\pi)\Omega}\sum_{\mathbf{q}}^{BZ}\sum_{\mathbf{G}}\int d\omega\ e^{+i((\mathbf{q}+\mathbf{G}).\mathbf{r}-\omega t)}\sum_{\mathbf{G}'}(\varepsilon^{-1}_{\mathbf{G},\mathbf{G}'}(\mathbf{q},\omega)-\delta_{\mathbf{G},\mathbf{G}'})\frac{8\pi^2 Z_1}{|\mathbf{q}+\mathbf{G}'|^2}\\ &\delta(\omega-(\mathbf{q}+\mathbf{G}').\mathbf{v})\ e^{-i\mathbf{b}.(\mathbf{q}+\mathbf{G}')}\ (\mathbf{q}+\mathbf{G})\\ &= \frac{-i4\pi Z_1}{\Omega}\sum_{\mathbf{q}}^{BZ}\sum_{\mathbf{G}}\int d\omega\ e^{+i((\mathbf{q}+\mathbf{G}).\mathbf{r}-\omega t)}\sum_{\mathbf{G}'}(\varepsilon^{-1}_{\mathbf{G},\mathbf{G}'}(\mathbf{q},\omega)-\delta_{\mathbf{G},\mathbf{G}'})\frac{(\mathbf{q}+\mathbf{G})}{|\mathbf{q}+\mathbf{G}'|^2}\\ &\delta(\omega-(\mathbf{q}+\mathbf{G}').\mathbf{v})\ e^{-i\mathbf{b}.(\mathbf{q}+\mathbf{G}')}.\end{aligned} \tag{5.36}$$

Finally, the electronic stopping power, $S(\mathbf{r}_0,\mathbf{v})$, can be obtained by substituting Eq. (5.13) and Eq. (5.36) in Eq. (5.15)

$$\begin{aligned}S(\mathbf{r}_0,\mathbf{v}) &= \frac{-Z_1}{v}\int d\mathbf{r}\ \delta(\mathbf{r}-\mathbf{b}-\mathbf{v}t)\ \mathbf{v}.\mathbf{E}^{ind}(\mathbf{r},t)\\ &= \frac{i4\pi Z_1^2}{\Omega\ v}\sum_{\mathbf{q}}^{BZ}\sum_{\mathbf{G}}\int d\omega\ e^{+i((\mathbf{q}+\mathbf{G}).\mathbf{v}-\omega)t}\sum_{\mathbf{G}'}(\varepsilon^{-1}_{\mathbf{G},\mathbf{G}'}(\mathbf{q},\omega)-\delta_{\mathbf{G},\mathbf{G}'})\frac{\mathbf{v}.(\mathbf{q}+\mathbf{G})}{|\mathbf{q}+\mathbf{G}'|^2}\\ &\delta(\omega-(\mathbf{q}+\mathbf{G}').\mathbf{v})\ e^{-i\mathbf{b}.(\mathbf{q}+\mathbf{G}')}\ e^{+i\mathbf{b}.(\mathbf{q}+\mathbf{G})}\\ &= \frac{i4\pi Z_1^2}{\Omega\ v}\sum_{\mathbf{q}}^{BZ}\sum_{\mathbf{G}}\sum_{\mathbf{G}'}(\varepsilon^{-1}_{\mathbf{G},\mathbf{G}'}(\mathbf{q},(\mathbf{q}+\mathbf{G}').\mathbf{v})-\delta_{\mathbf{G},\mathbf{G}'})\frac{\mathbf{v}.(\mathbf{q}+\mathbf{G})}{|\mathbf{q}+\mathbf{G}'|^2}\\ &e^{+i(\mathbf{G}-\mathbf{G}').\mathbf{v}t}\ e^{+i\mathbf{b}.(\mathbf{G}-\mathbf{G}')}\\ &= \frac{i4\pi Z_1^2}{\Omega\ v}\sum_{\mathbf{q}}^{BZ}\sum_{\mathbf{G}}\sum_{\mathbf{G}'}(\varepsilon^{-1}_{\mathbf{G},\mathbf{G}'}(\mathbf{q},(\mathbf{q}+\mathbf{G}').\mathbf{v})-\delta_{\mathbf{G},\mathbf{G}'})\frac{\mathbf{v}.(\mathbf{q}+\mathbf{G})}{|\mathbf{q}+\mathbf{G}'|^2}\\ &e^{+i(\mathbf{b}+\mathbf{v}t).(\mathbf{G}-\mathbf{G}')}\end{aligned} \tag{5.37}$$

By using $-\mathbf{J}=\mathbf{G}-\mathbf{G}'$ in Eq. (5.37) can be simplified to

$$S(\mathbf{r}_0,\mathbf{v}) = \frac{i4\pi Z_1^2}{\Omega\ v}\sum_{\mathbf{q}}^{BZ}\sum_{\mathbf{G}}\sum_{\mathbf{J}}(\varepsilon^{-1}_{\mathbf{G},\mathbf{G}+\mathbf{J}}(\mathbf{q},(\mathbf{q}+\mathbf{G}+\mathbf{J}).\mathbf{v})-\delta_{\mathbf{G},\mathbf{G}+\mathbf{J}})e^{-i\mathbf{J}.(\mathbf{b}+\mathbf{v}t)}\ \frac{\mathbf{v}.(\mathbf{q}+\mathbf{G})}{|\mathbf{q}+\mathbf{G}+\mathbf{J}|^2}. \tag{5.38}$$

This last equation contains an oscillating phase factor $e^{-i\mathbf{J}.\mathbf{v}t}=0$. The exponential factor $e^{-i\mathbf{J}.\mathbf{v}t}$ vanishes when averaging over time for any $\mathbf{J}$ vector which does not satisfy $\mathbf{J}.\mathbf{v}=0$. The only non vanishing contributions arise

from the vectors $\mathbf{J}_\perp$, i.e., the $\mathbf{J}$ vectors that are perpendicular to $\mathbf{v}$. Therefore the position dependent of the electronic stopping power is given by

$$\langle S(\mathbf{v},\mathbf{b})\rangle = \frac{i4\pi Z_1^2}{\Omega\ v}\sum_{\mathbf{q}}^{BZ}\sum_{\mathbf{G}}\sum_{\mathbf{J}_\perp}(\varepsilon^{-1}_{\mathbf{G},\mathbf{G}+\mathbf{J}_\perp}(\mathbf{q},(\mathbf{q}+\mathbf{G}).\mathbf{v})-\delta_{\mathbf{G},\mathbf{G}+\mathbf{J}_\perp})e^{-i\mathbf{J}_\perp.\mathbf{b}} \frac{\mathbf{v}.(\mathbf{q}+\mathbf{G})}{|\mathbf{q}+\mathbf{G}+\mathbf{J}_\perp|^2}. \tag{5.39}$$

This last equation has been averaged over time.

We have derived the position dependent electronic stopping power in periodic crystal as a general case. Then we will derive the averaged impact parameter electronic stopping power, named the "random electronic stopping power" in the next Section. Note that the position dependent electronic stopping power is not studied in the present work.

5.2.2 Random electronic stopping power

The random electronic stopping power (RESP) is "the average over impact parameters of the position-dependent electronic stopping power". The most important contribution in Eq. (5.39) is resulted by the term $\mathbf{J}=0$. Other contributions from other terms of $\mathbf{J}$ vectors depends on the velocity direction, in which $\mathbf{J}.\mathbf{v}=0$ must be satisfied. For most directions, the condition $\mathbf{J}.\mathbf{v}=0$ is never satisfied or satisfied by only few large $\mathbf{J}_\perp$. With this, the random stopping power $\langle S(\mathbf{v},\mathbf{b})\rangle$ is equal or well approximated by the contrain $\mathbf{J}_\perp=0$ in Eq. (5.39). For more details, see [20, 83]. With these general directions one simply obtain the random electronic stopping power $S(\mathbf{v})$, which is independent of $\mathbf{b}$,

$$S(\mathbf{v}) = \frac{i4\pi Z_1^2}{\Omega\ v}\sum_{\mathbf{q}}^{BZ}\sum_{\mathbf{G}}(\varepsilon^{-1}_{\mathbf{G},\mathbf{G}}(\mathbf{q},(\mathbf{q}+\mathbf{G}).\mathbf{v})-\delta_{\mathbf{G},\mathbf{G}})\frac{\mathbf{v}.(\mathbf{q}+\mathbf{G})}{|\mathbf{q}+\mathbf{G}|^2}. \tag{5.40}$$

It has been noted the calculated value of the random electronic stopping power can be replaced by the average over impact parameters of the position dependent stopping power alone any given channel [20].

However, let us follow now the complete derivation for the random electronic stopping power as obtained from its definition: "the average over impact

parameters of the position dependent stopping power":

$$
\begin{aligned}
S(\mathbf{v}) &= \frac{1}{A_b}\int d\mathbf{b}\; S(\mathbf{v},\mathbf{b}) \\
&= \frac{i4\pi Z_1^2}{\Omega\; v}\sum_{\mathbf{q}}^{BZ}\sum_{\mathbf{G}}\sum_{\mathbf{J}_\perp}(\varepsilon^{-1}_{\mathbf{G},\mathbf{G}+\mathbf{J}_\perp}(\mathbf{q},(\mathbf{q}+\mathbf{G}).\mathbf{v})-\delta_{\mathbf{G},\mathbf{G}+\mathbf{J}_\perp})\frac{1}{A_b}\int d\mathbf{b}e^{-i\mathbf{b}.\mathbf{J}_\perp} \\
&\times \frac{\mathbf{v}.(\mathbf{q}+\mathbf{G})}{|\mathbf{q}+\mathbf{G}+\mathbf{J}_\perp|^2} \\
&= \frac{i4\pi Z_1^2}{\Omega\; v}\sum_{\mathbf{q}}^{BZ}\sum_{\mathbf{G}}\sum_{\mathbf{J}_\perp}(\varepsilon^{-1}_{\mathbf{G},\mathbf{G}+\mathbf{J}_\perp}(\mathbf{q},(\mathbf{q}+\mathbf{G}).\mathbf{v})-\delta_{\mathbf{G},\mathbf{G}+\mathbf{J}_\perp})\;\delta_{\mathbf{J}_\perp,0}\frac{\mathbf{v}.(\mathbf{q}+\mathbf{G})}{|\mathbf{q}+\mathbf{G}+\mathbf{J}_\perp|^2} \\
&= \frac{i4\pi Z_1^2}{\Omega\; v}\sum_{\mathbf{q}}^{BZ}\sum_{\mathbf{G}}(\varepsilon^{-1}_{\mathbf{G},\mathbf{G}}(\mathbf{q},(\mathbf{q}+\mathbf{G}).\mathbf{v})-\delta_{\mathbf{G},\mathbf{G}})\frac{\mathbf{v}.(\mathbf{q}+\mathbf{G})}{|\mathbf{q}+\mathbf{G}|^2},
\end{aligned}
\tag{5.41}
$$

where A_b is the normalized area of the impact parameter $\mathbf{b}$.

This last result can be further refactored in order to highlight that the stopping power is indeed real-valued. Using the fact that the response function $\varepsilon^{-1}(\mathbf{r}t,\mathbf{r}'t')$ is real-valued, its Fourier transform has the following symmetry (see Appendix A of Ref. [76] for a derivation):

$$
\varepsilon^{-1}_{\mathbf{G}\mathbf{G}'}(\mathbf{q},\omega) = \left[\varepsilon^{-1}_{-\mathbf{G}-\mathbf{G}'}(-\mathbf{q},-\omega)\right]^*. \tag{5.42}
$$

Then, for each $\mathbf{q}+\mathbf{G}$ that appears in the summation in Eq. (5.41), the corresponding $-\mathbf{q}-\mathbf{G}$ will be part of the summation as well. As a consequence, only the imaginary part of ε^{-1} yields a contribution to the summation and the RESP can be finally recast into

$$
S(\mathbf{v}) = \frac{4\pi Z_1^2}{\Omega v}\sum_{\mathbf{q}}^{\mathrm{BZ}}\sum_{\mathbf{G}}\mathrm{Im}\left\{-\varepsilon^{-1}_{\mathbf{G},\mathbf{G}}[\mathbf{q},\mathbf{v}\cdot(\mathbf{q}+\mathbf{G})]\right\}\frac{\mathbf{v}\cdot(\mathbf{q}+\mathbf{G})}{|\mathbf{q}+\mathbf{G}|^2}. \tag{5.43}
$$

Both equations Eq. (5.43) and Eq. (5.39) that we have derived are different from the corresponding equations derived by Campillo and Pitarke [21, 64, 20]. In fact, they have used the so called the imaginary part of the projectile self energy in order to derive both equations the random and position dependent of the electronic stopping power.

Anyway we have recalculated the RESP results of both Si and Al using the same parameters used in Campillo and Pitarke articles; almost the same results have been found as will be explained in the results part of my thesis.

In the next section, we derive the electronic stopping power of the free electron gas equation "The Lindhard's formula" from the complete periodic solid of the electronic stopping power equation (5.43).

5.2.3 The Lindhard's formula as special case

A free electron gas is just a particular case of a periodic system. Then using the just-derived RESP equation (5.41) for the periodic system, the simpler case of a free electron gas target can be obtained.

First, one transforms the discrete summations into an integral. We use the following relation: $\sum_{\mathbf{q}\in BZ}\sum_{\mathbf{G}} f(\mathbf{q}+\mathbf{G}) \Rightarrow \frac{\Omega_0 N_{\mathbf{q}}}{(2\pi)^3}\int f(\mathbf{Q})d\mathbf{Q}$, in order to rewrite equation (5.41) into a 3-dimensional integral:

$$S(\mathbf{v}) = \frac{4\pi Z_1^2}{(2\pi)^3\ v}\int d\mathbf{Q}\ \mathrm{Im}[-\varepsilon^{-1}(Q,\mathbf{Q}.\mathbf{v})]\frac{\mathbf{Q}.\mathbf{v}}{Q^2}, \tag{5.44}$$

where $\mathbf{Q} = \mathbf{q} + \mathbf{G}$. We have also used the fact that the free electron gas is completely isotropic, i.e. $\varepsilon^{-1}_{\mathbf{GG}}(\mathbf{q},\omega) = \varepsilon^{-1}(Q,\omega)$.

Our Eq. (5.44) is precisely the one found in Refs. [83] and [66].

To recover the original Lindhard's formula of the free electron gas from Eq. (5.44), we now introduce the spherical coordinates transformation (Q,θ,ϕ) in Eq. (5.44). The z-axis is chosen so to align with $\mathbf{v}$. Thus the integrated functions is independent from ϕ, i.e. $\int d\mathbf{Q} \Rightarrow 2\pi\int_0^\infty Q^2dQ\int_0^\pi d\theta \mathrm{sin}\theta$:

$$S(\mathbf{v}) = \frac{Z_1^2}{\pi v}\int_0^\infty dQ\int_0^\pi d\theta\ \mathrm{sin}\theta\ Qv\mathrm{cos}\theta\ \mathrm{Im}[-\varepsilon^{-1}(Q,Qv\mathrm{cos}\theta)]. \tag{5.45}$$

To simplify this last equation, we apply a change of variable $\omega = Qv\mathrm{cos}\theta$ (and thus $d\omega = -Q\ v\ sin\theta d\theta$):

$$S(\mathbf{v}) = \frac{Z_1^2}{\pi v^2}\int_0^\infty \frac{dQ}{Q}\int_{-Qv}^{Qv} d\omega\ \omega\ \mathrm{Im}[-\varepsilon^{-1}(Q,\omega)]. \tag{5.46}$$

This is the Lindhard formula, as can be read in Ref. [40] for instance.

Sometimes, the parity with respect to ω of the causal function $\omega\mathrm{Im}[\varepsilon^{-1}(\omega)]$ is further used to limit the range of integration even further:

$$S(\mathbf{v}) = \frac{2Z_1^2}{\pi v^2}\int_0^\infty \frac{dQ}{Q}\int_0^{Qv} d\omega\ \omega\ \mathrm{Im}[-\varepsilon^{-1}(Q,\omega)]. \tag{5.47}$$

We have just shown that our Eq. (5.44) allows us to recover the well-known Lindhard formula. This further assesses our expression, which departs from the one of Campillo *et al.* [21] by a factor 2.

5.3 Conclusion

We have presented a brief history of the electronic stopping power based on the linear response theory starting from the simple case of the non interacting homogeneous electron gas for the solid state system. We have derived in details the position dependent and random electronic stopping power equations of periodic crystal, in which slightly different equations have been found from that in the literature. This thesis will specifically focus on the random electronic stopping power.

We have implemented the formula in an ab initio code ABINIT that can calculate the RESP of any material within the linear response dielectric formalism. This is explained in details in the next chapter.

Chapter 6

Development and computational details

In this Chapter, we present the main steps that have been done in order to implement the RESP equation within two approximations RPA and ALDA in the latest version of the ABINIT software. We study also the difficulties and challenges raised by the complex convergence of RESP calculations in details. Furthermore, we introduce a new method to evaluate the fully converged results of the RESP of any bulk targets. To illustrate the methods and its details, we will exemplify how to calculate the fully converged value of the RESP of the Si target using the valence electrons within RPA.

6.1 Practical implementation in a periodic plane-wave approach

In the previous chapter, we have obtained the so-called RESP S:

$$S(\mathbf{v}) = \frac{4\pi Z_1^2}{N_{\mathbf{q}}\Omega}\frac{1}{|\mathbf{v}|}\sum_{\mathbf{q}}^{\mathrm{BZ}}\sum_{\mathbf{G}}\mathrm{Im}\left\{-\varepsilon^{-1}_{\mathbf{G},\mathbf{G}}[\mathbf{q},\mathbf{v}(\mathbf{q}+\mathbf{G})]\right\}\frac{\mathbf{v}.(\mathbf{q}+\mathbf{G})}{|\mathbf{q}+\mathbf{G}|^2}. \tag{6.1}$$

It is clear from Eq. (6.1) that the imaginary dielectric matrix is the central quantity to characterize the slowing down of a charged particle in a condensed matter target within linear-response. Therefore, the first step which has to be done is to find a suitable ab initio code that could be used for the RESP implementation task.

Many modern ab initio codes for periodic systems are capable of calculating the inverse dielectric matrix $\varepsilon^{-1}_{\mathbf{G}\mathbf{G}'}(\mathbf{q},\omega)$ for finite frequencies ω. For instance, this quantity is requested in the GW framework [36, 39]. The present work for

instance relies on the *GW* subroutines available in the ABINIT software [34]. Figure 6.1 represents the flowchart of RESP code.

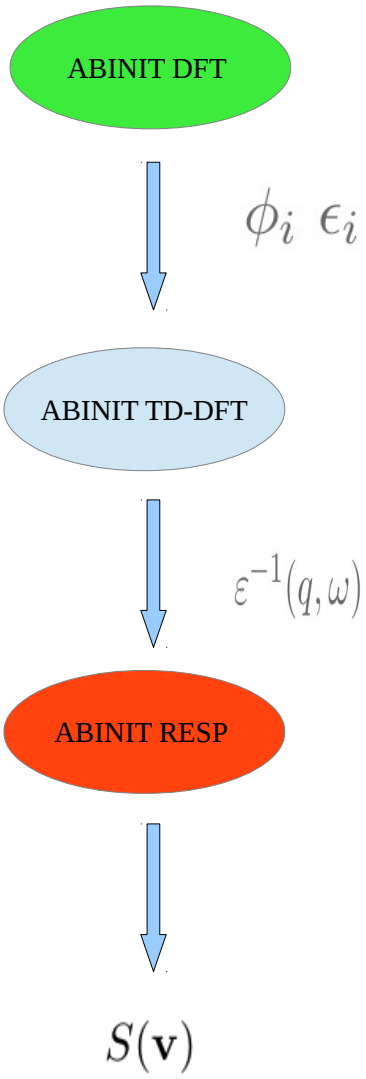


Figure 6.1: The flowchart of the RESP code.

6.1.1 Technicalities

As we will show in the following, the convergence of the stopping power with respect to the calculation parameters is strikingly slow even for small unit cell systems. This difficulty makes the use of symmetry operations absolutely crucial to perform calculations on an affordable time-scale.

Eq. (6.1) can be rewritten with the use of the symmetries $\mathcal{R}$ contained in the crystal space group that produces the star of $\mathbf{q}$ vectors. With this, Eq. (6.1) reads

$$S(\mathbf{v}) = \frac{4\pi Z^2}{N_{\mathbf{q}}\Omega}\frac{1}{|\mathbf{v}|}\sum_{\mathbf{q}}^{\text{IBZ}}\sum_{\mathcal{R}\in R_{\mathbf{q}}}\sum_{\mathbf{G}}\text{Im}\left\{-\varepsilon^{-1}_{\mathcal{R}^{-1}\mathbf{G},\mathcal{R}^{-1}\mathbf{G}}[\mathbf{q},\mathbf{v}.(\mathcal{R}\mathbf{q}+\mathbf{G})]\right\}\frac{\mathbf{v}.(\mathcal{R}\mathbf{q}+\mathbf{G})}{|\mathcal{R}\mathbf{q}+\mathbf{G}|^2}, \tag{6.2}$$

where the summation over $\mathbf{q}$ only runs over the irreducible wedge of the Brillouin Zone (IBZ). This equation is what we have implemented in the ABINIT software.

Then we have faced another difficulty during the implementation task. We found that the inverse dielectric matrix needs to be evaluated for many energies $\omega = \mathbf{q} + \mathbf{G}$. For sure it would be almost intractable to calculate and invert the dielectric matrix for each requested ω. We rather calculate and invert the dielectric matrix on a dense grid of frequency and then perform a cubic spline interpolation in order to evaluate its diagonal at the desired energy.

The imaginary part of the inverse dielectric matrix is a rather noisy function of the energy, which can be smoothed with an increase of the broadening η in Eq. (4.26).

Due to the spline interpolation, the number of sampling frequencies (ABINIT parameter `nfreqre`) becomes an extra-parameter to be converged.

The maximum frequency needed for $\varepsilon^{-1}(\omega)$ is set by the maximum velocity $\mathbf{v}$ and the dielectric matrix cutoff through $\omega_{\max} \approx \mathbf{G}.\mathbf{v}$. Figure 6.2 shows the accuracy of using the cubic spline interpolation as a function of `nfreqre` in predicting the energy loss value of any desired value ω. Our reference calculation (red line) is obtained using 6 points per Hartree. This density of frequency will be retained in the rest of the thesis.

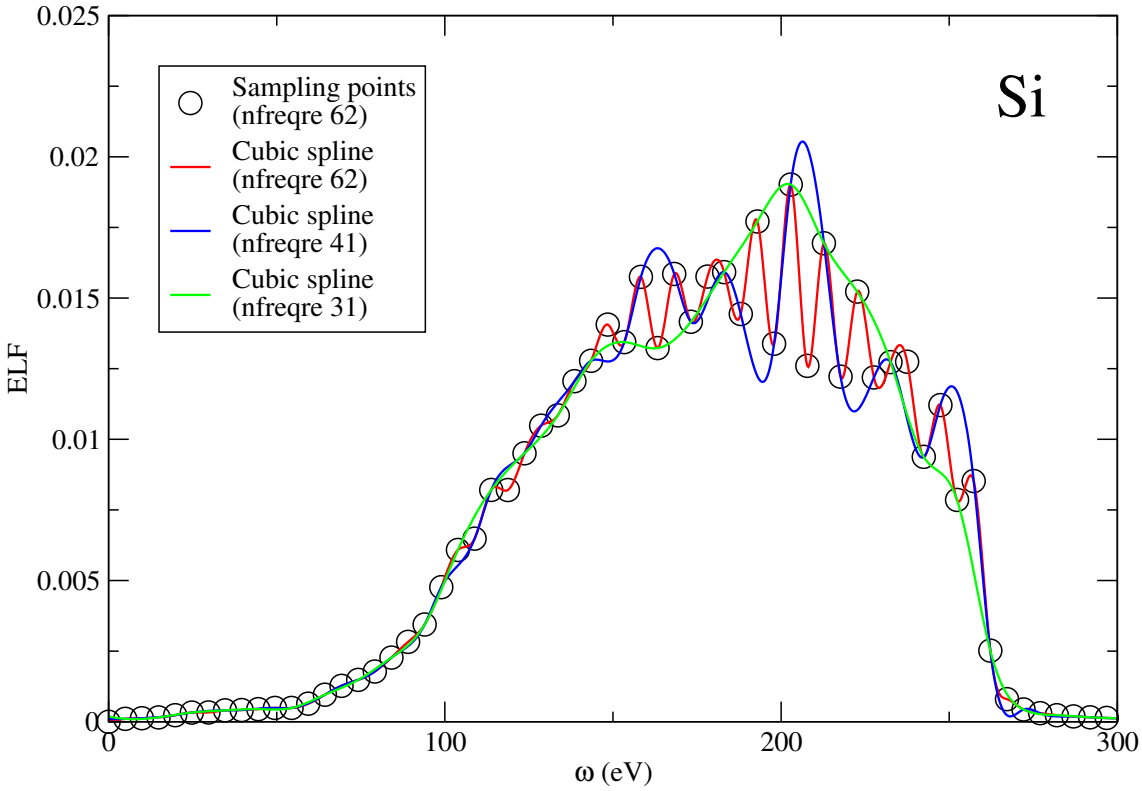


Figure 6.2: The accuracy of using the cubic spline interpolation with increasing the `nfreqre`. All the calculated values are obtained at $|\mathbf{q}+\mathbf{G}| = 3.71$ a.u. along [111]. This study have been done using the following parameters: $4\times4\times4$ with 4 shifts of $\mathbf{q}$ point mesh, 400 bands and the broadening η is 1.5 eV.

Next we are going to show the first test to assess the accuracy of our RESP code for the electronic stopping power of any bulk material.

6.1.2 Assessment against previous calculations

In order to assess our calculation method, we first tackled the task of reproducing the only series of articles [20, 21, 64] we are aware of that implemented the linear-response RESP from fully *ab initio* calculations. Using our norm-conserving pseudopotential implementation in ABINIT, we calculated the RESP for proton ($Z = 1$) in bulk silicon and bulk aluminum at their experimental lattice constant.

Following in particular Ref. [64], we used the same convergence parameters in order to offer a direct comparison in Fig. 6.3. These authors were admittedly aware that their parameters were too loosely converged to offer comparison

against experiment. In Fig. 6.3, we just aim at demonstrating the correctness of the implementation.

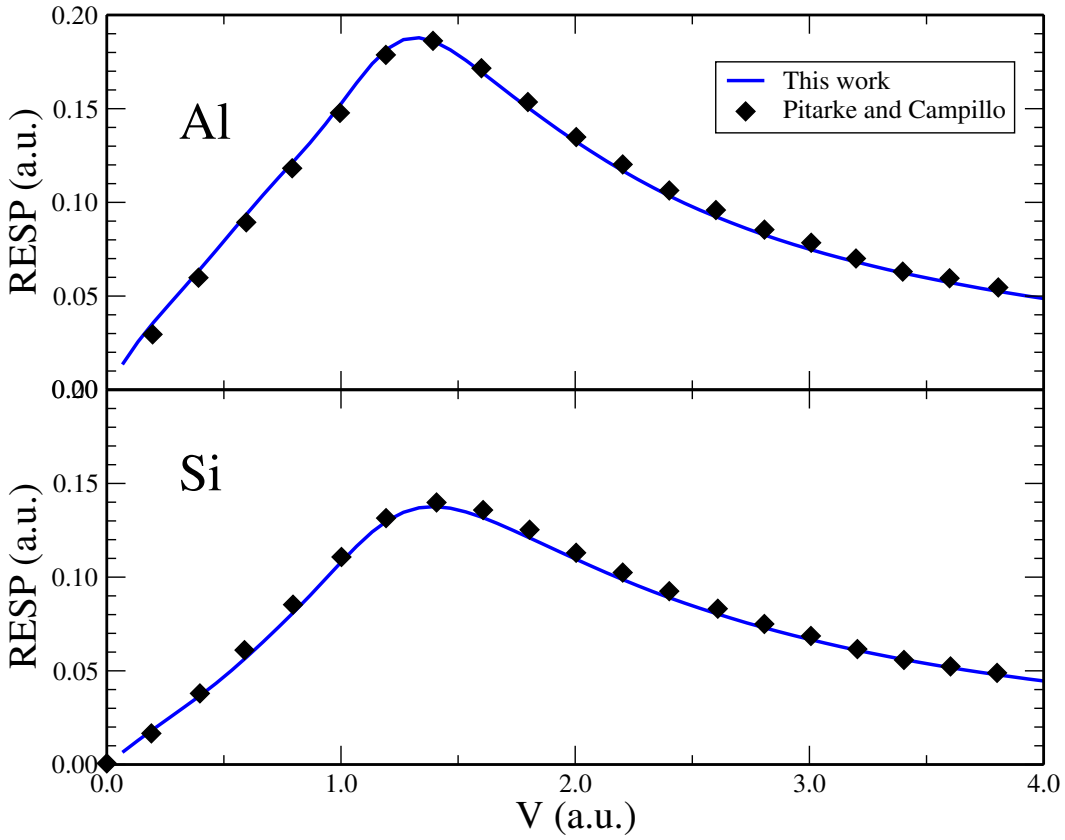


Figure 6.3: Comparison of the RESP as a function of the projectile velocity within RPA from our implementation (solid blue line) against previously published results from Ref. [64] (black diamond symbols). The calculations are converged with the same level of accuracy as prescribed in the previous work.

Silicon and aluminum are described by valence electron only norm-conserving pseudopotentials. The dielectric matrices have been limited to a 15×15 representation in plane-waves, corresponding to an energy cutoff of 0.75 Ha in silicon and of 1.35 Ha in aluminum. The number of bands is limited to 200 for silicon and to 60 in aluminum. The **k**-point mesh is 8×8×8 for Si and 10×10×10 for Al. Finally, whereas Ref. [64] employs an analytic continuation technique that extrapolates the inverse dielectric function from purely imaginary frequencies to purely real frequencies, our work relies on a direct evaluation of the response functions for real frequencies. However we have to use a finite value for the

broadening parameter η entering in Eq. (4.26). A value $\eta = 1.5$ eV was used to produce the the data reported in Fig. 6.3.

Despite the difference in the sampling of the inverse dielectric matrix, the agreement between our calculations and the previously published results is strikingly good. It appears that the data published in Ref. [64] are consistent with our Eq. (6.1) rather than their own expression which is doubled compared to us. As a consequence, the RESP code is ready to be used in understanding the electronic stopping power phenomena in a series of target materials.

6.1.3 Convergence issues

As already alluded to in the previous paragraph, the calculation of RESP requires extremely large convergence parameters that were not accessible 15 years ago and that are still challenging nowadays.

In Fig. 6.5 and in Fig. 6.4, we show the convergence behavior of the RESP as a function of the other convergence parameters. The parameters can be grouped into two independent sets: the number of bands and the dielectric matrix cutoff on one side in Fig. 6.5 and the **k**-point and **q**-point sampling on the other side in Fig. 6.4.

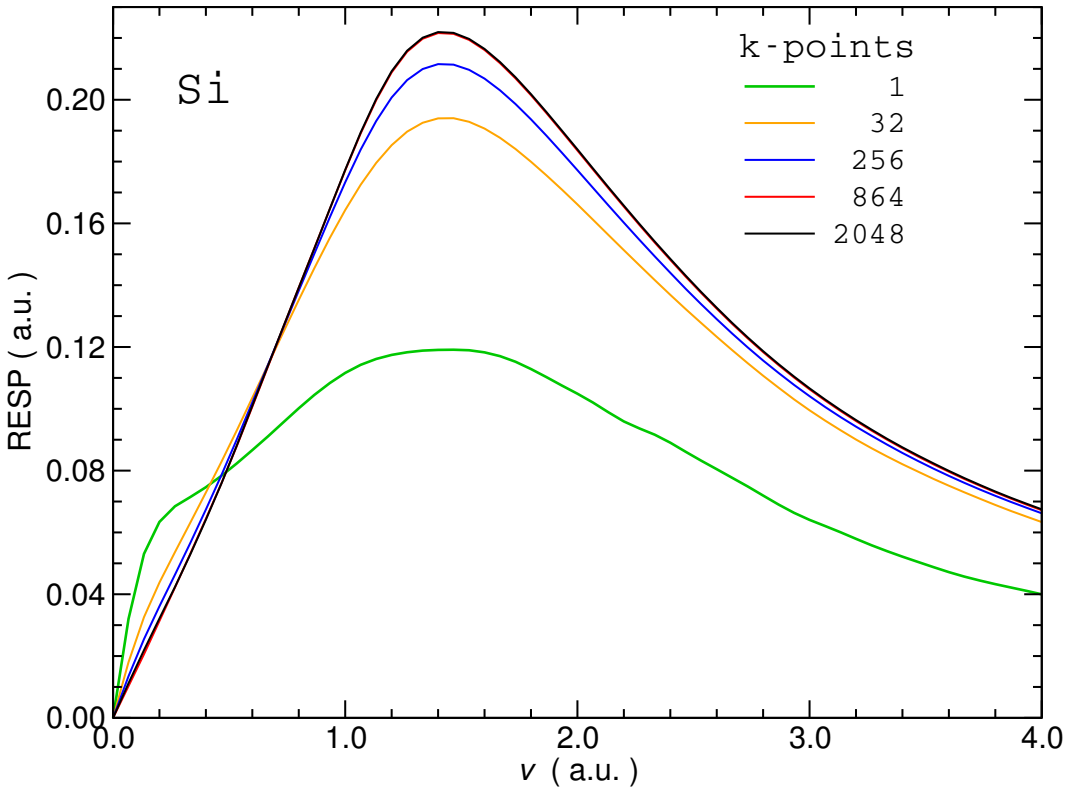


Figure 6.4: Convergence of the RESP of silicon within RPA as a function of **k**-points. The convergence with respect to the **k**-point grid was evaluated for a fixed number of bands (400) and a fixed dielectric matrix cutoff (8 Ha).

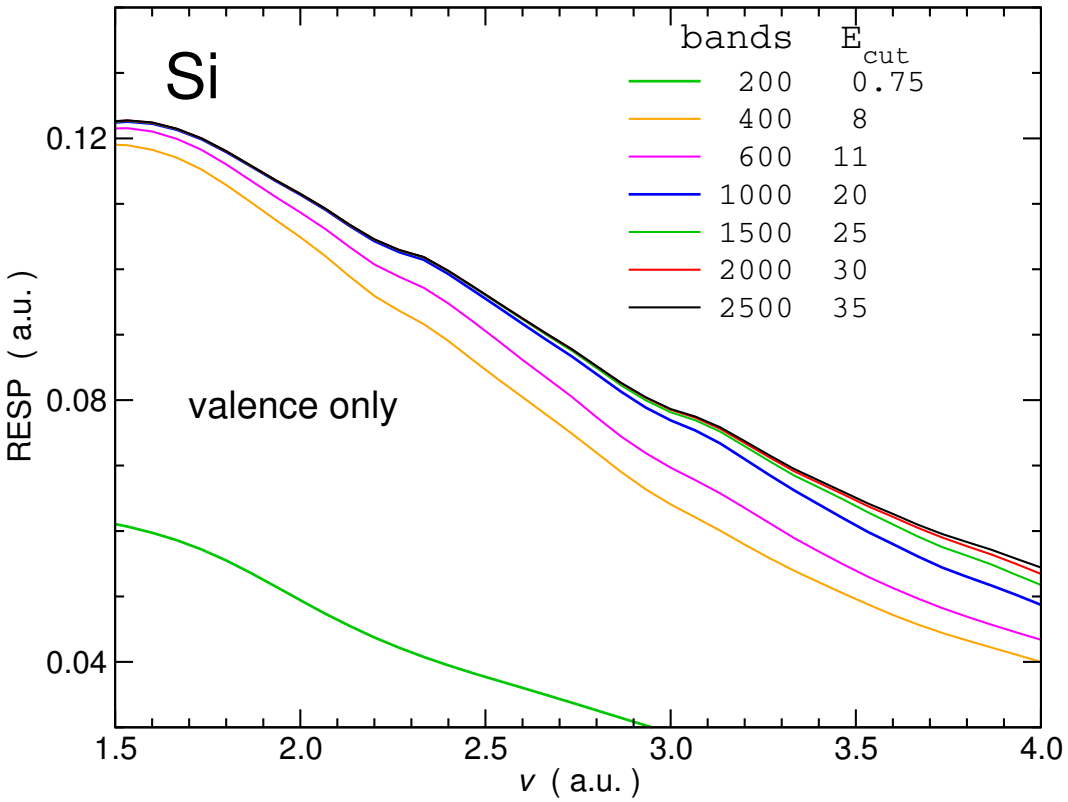


Figure 6.5: Convergence of the RESP of silicon within RPA as a function of the number of bands and of the dielectric matrix cutoff. The convergence with respect to the number of bands and dielectric matrix cutoff was obtained a fixed Γ-point sampling.

First of all, as a general comment, the convergence of RESP appears as extremely slow compared to the convergence parameters required in ground-state DFT or even in standard excited state calculations within TD-DFT. The number of bands necessary to converge the RESP up to velocity $v = 4.$ a.u. (which corresponds to a proton at 0.4 MeV) is around 1500, to be compared to the 4 occupied bands of silicon. The converged dielectric matrix cutoff energy is 25 Ha, to be compared to the cutoff energy for wave functions in norm-conserving pseudo-potential of about 10 Ha. The RESP peak necessitates at least 864 **k**-points in the BZ, which corresponds to a 6×6×6 Monkhorst-Pack grid with 4 different origins, whereas standard calculations usually require only 256 **k**-points in the BZ (4×4×4 grid with 4 shifts).

The extremely slow convergence with respect to these parameters has two different origins in the equations presented in the two previous chapters. That is why we grouped the convergence parameters into two sets.

Firstly, the dielectric matrix cutoff and the number of bands are tightly related as can be inferred from the matrix element $M_{\mathbf{k}ij}(\mathbf{q}+\mathbf{G})$. The $M_{\mathbf{k}ij}(\mathbf{q}+\mathbf{G})$ is defined in the Kohn-Sham polarizability χ^{KS}, which is given as:

$$M_{\mathbf{k}ij}(\mathbf{q}+\mathbf{G}) = \langle \mathbf{k}-\mathbf{q}i|e^{-i(\mathbf{q}+\mathbf{G}).\mathbf{r}}|\mathbf{k}j\rangle. \tag{6.3}$$

If high energy empty bands are included in the sum of states formula of χ^{KS}, the representation of these states in plane-wave involves high energy plane-waves. These high plane-waves are coupled with the occupied states through large reciprocal lattice vectors $\mathbf{G}$ in Eq. (6.3). This observation justifies why the convergence with respect to bands and to the dielectric matrix cutoff cannot be evaluated independently. In Fig. 6.5, we have shown the RESP curves for the converged dielectric matrix cutoff associated with a given number of bands. For instance, for 400 bands, a dielectric matrix cutoff of 8 Ha is sufficient. However, for 1500 bands, it should rather be set to 25 Ha.

Secondly, the BZ sampling appears through the $\mathbf{k}$-points in Eq. (4.26) and through the $\mathbf{q}$-points in Eq. (6.1). Whereas the $\mathbf{q}$-points are only constrained to be differences of $\mathbf{k}$-points due to the evaluation of the matrix elements in Eq. (6.3), we have limited ourselves to the very same grids for both $\mathbf{k}$- and $\mathbf{q}$-points since a down-sampling analogous to Ref. [57] would have induced marginal computational gains only. The convergence with respect to $\mathbf{k}$-points in Eq. (4.26) is made smoother thanks to a well adapted value of the broadening parameter η. For instance, in Fig. 6.4, the curve with Γ-point was obtained $\eta = 12$ eV, while the result with 2048 points used $\eta = 1$ eV.

As a consequence of the presented convergence study, the task of understanding the RESP of proton in any target material at the fully converged level will not be an easy task. This difficulty enforced us to look for a new method or strategy that can be used to evaluate the fully converged parameters, or at least to help us in saving the requested computer memory or reducing the computational effort.

6.2 A method to achieve convergence at a lower cost

Since the RESP calculations require very strict convergence of the parameters, we had to introduce a new strategy to perform the RESP calculation that we named **extrapolation scheme**. The RESP value mostly depends on three important parameters: the number of bands, k-points sampling and the number of plane-waves used for ε^{-1}. As the absolute convergence is difficult to obtain and as the convergence factors have different origins, it is legitimate

to evaluate the possibility to reach the global convergence by adding up the different contributions.

The idea of the extrapolation scheme is to perform the RESP value in three separated steps as following:

- The valence electrons contribution: the fully converged RESP can be estimated by converging separately the number of plane-waves and bands using the Gamma point only on the one hand and the number of k-points with low number of bands and plane-waves on the other hand.
- The core electrons contribution: the RESP of the core electrons contribution can be estimated by using only one k-point since the bands of the inner shell electrons are highly localized, i.e. they are not dispersive in **k**-space.
- Finally, the fully converged value of the RESP is simply estimated by adding the two contributions of the valence and the core electrons to each others.

In other words, we mean to extrapolate the RESP of the valence electrons contribution thanks to the formula:

$$\begin{aligned} S_e(\text{extrap.}, \text{high})_{val} = S_e((\text{bands}, \text{E}_{\text{cut}}) = \text{low}, \mathbf{k} = \text{high}) \\ + S_e((\text{bands}, \text{E}_{\text{cut}}) = \text{high}, \mathbf{k} = \text{low}) \\ - S_e((\text{bands}, \text{E}_{\text{cut}}) = \text{low}, \mathbf{k} = \text{low}). \end{aligned} \quad (6.4)$$

Also, the RESP of the core electrons contribution can be estimated by using the following formula:

$$\begin{aligned} S_e(\text{extrap.}, \text{high})_{core} = S_e((\text{bands}, \text{E}_{\text{cut}}) = \text{low}, \mathbf{k} = \text{high})_{val} \\ + S_e((\text{bands}, \text{E}_{\text{cut}}) = \text{high}, \mathbf{k} = \text{low})_{core+val} \\ - S_e((\text{bands}, \text{E}_{\text{cut}}) = \text{low}, \mathbf{k} = \text{low})_{val}, \end{aligned} \quad (6.5)$$

where low/high characterizes the convergence level respectively for the number of bands and dielectric matrix cutoff and for the **k**-point grid.

With these techniques at hand, we are now ready to calculate RESP that are converged in absolute.

In Fig. 6.6, we demonstrate that the extrapolation is indeed justified, in which Eq. (6.4) is numerically demonstrated. The difference between the more converged curve (600 bands and $E_{\text{cut}} = 11$ Ha) and the least converged curve (400 bands and $E_{\text{cut}} = 8$ Ha) is almost the same when evaluated with a Γ

point sampling (red line) as when evaluated with a dense grid of 864 **k**-points in the BZ.

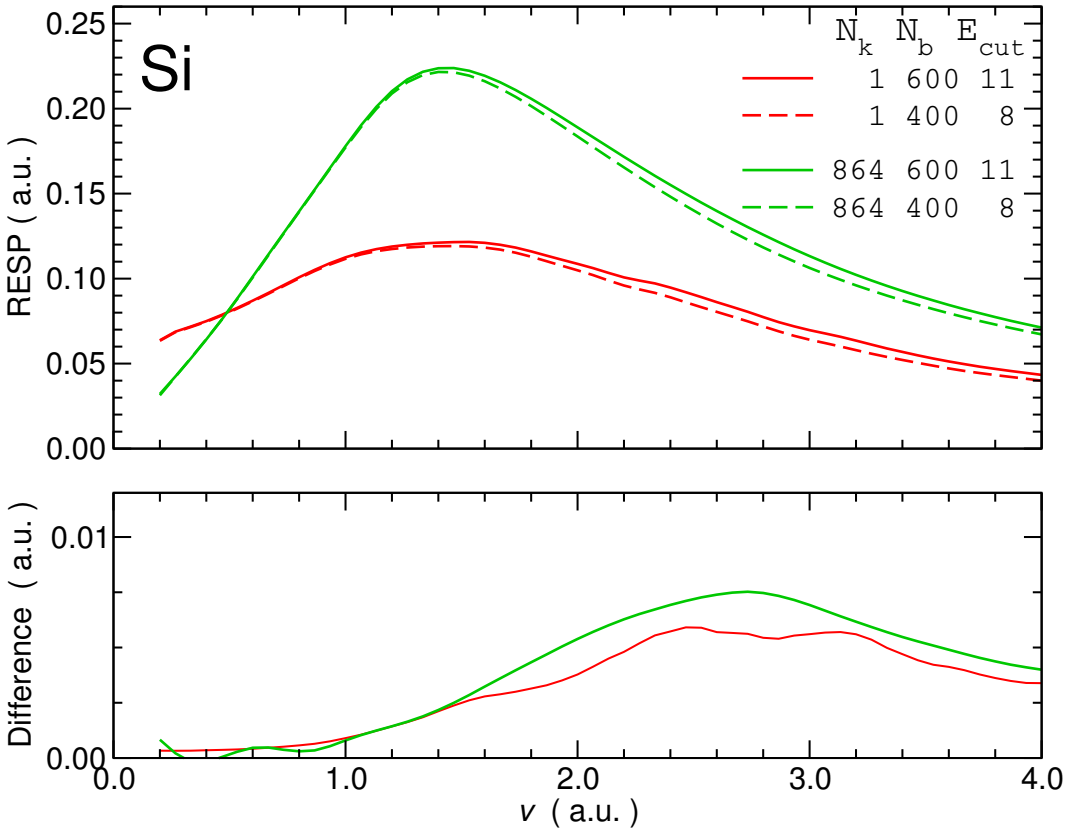


Figure 6.6: Comparison of the convergence rate for 2 **k**-point meshes: Γ (red lines) and 864 BZ points (green lines). The upper panel shows the RESP for two levels of convergence, whereas the lower panel shows their difference.

Moreover, the core extrapolation of Eq. (6.5) can be nicely understood as shown in Fig. 6.7. Fig. 6.7 shows the comparisons between the calculated RESP value of the core electrons at the level of (2s2p electrons) using three **k**-point meshes: 256 BZ points, 8 BZ points and Γ point. The results shows almost the same RESP core contribution can be estimated only with using Γ point. Right now, the contribution of the (1s electron) is not taken to the account. This is because of the probability of exciting an electron in this state is extremely low.

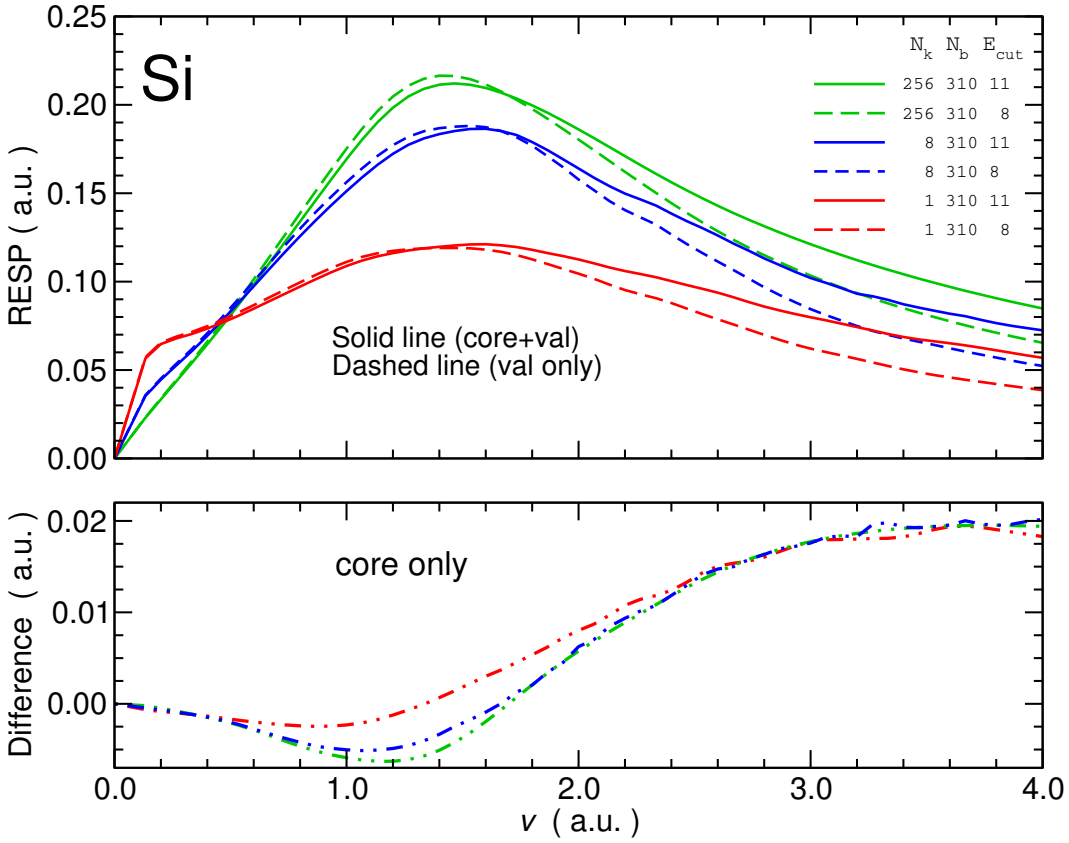


Figure 6.7: Comparison of the RESP core contribution calculated using 3 **k**-point meshes: 256 BZ points (green lines), 8 BZ points (blue lines) and Γ (red lines). The upper panel shows the RESP for two levels of electrons contribution, i.e., the 2s2p3s3p electrons and 3s3p electrons only whereas the lower panel shows their difference, i.e., the 2s2p electrons only).

6.2.1 Application to silicon

In this part, we only present the first attempt to evaluate the fully converged RESP of proton in Si target by using the extrapolation scheme. The results will be obtained for both the valence electrons and core electrons (excluded the 1s state) contribution within only RPA.

- **The valence contribution:**

  The fully converged value has been calculated as follows. First, using Γ point only to find the most converged result with respect to the number of bands and plane-waves. As shown in Fig. 6.5, the 2000 bands and E_{cut} equal to 25 Ha are converged parameters. Then, finding the con-

verged q point mesh by using low parameters values (E_{cut}=8 Ha and 400 bands). As shown in Fig. 6.4, the 864 BZ points is the converged value corresponding to η=1.0 eV. Finally, using the extrapolation scheme in Eq. (6.4) one can find the fully RESP converged value. The converged RESP value is corresponding to the following parameters: 2000 bands, 25 Ha of E_{cut} and 864 BZ points. The final results can be seen in Fig. 6.8.

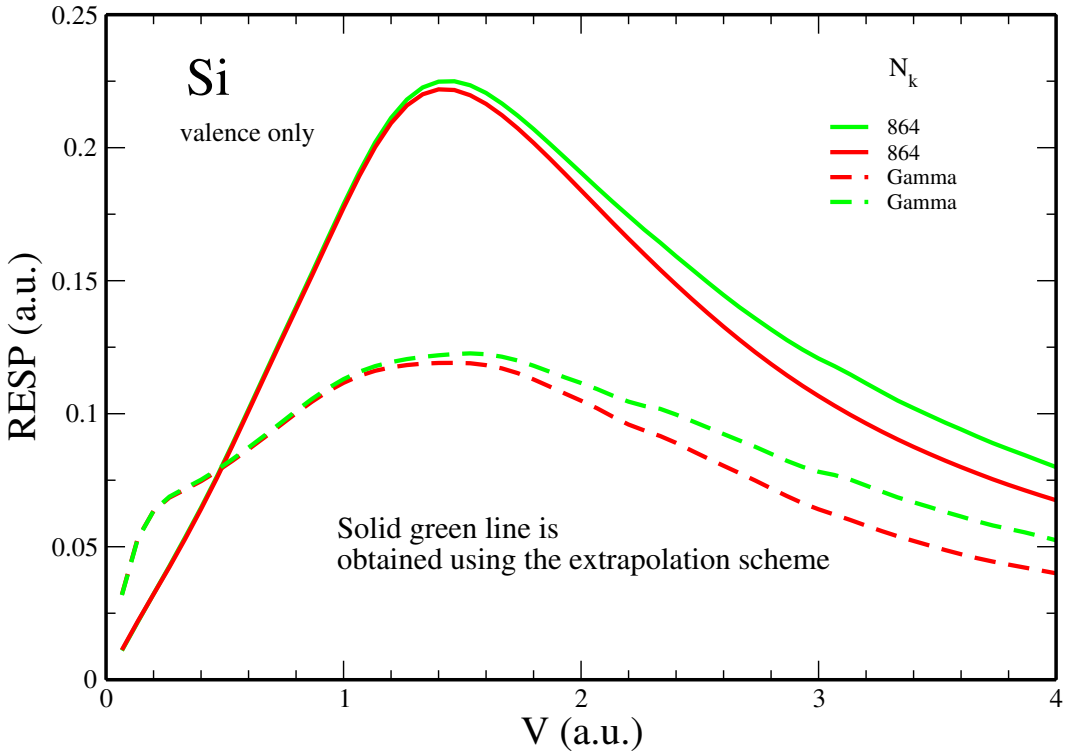


Figure 6.8: The fully Converged RESP of valence electrons in Si target for proton (Z_1=1) within the linear response of RPA calculated by extrapolation scheme in Eq. (6.4). The green line obtained for highly converged parameters (2000 bands and E_{cut} = 25 Ha), the red line obtained for low converged parameters (400 bands and E_{cut} = 8 Ha).

- **The core contribution:**

  In this example, we need to find the converged values as follows. First, using Γ point only to find the most converged result with respect to the number of bands and plane-waves. As shown in Fig. 6.9, the 2500 bands and E_{cut} equal to 35 Ha are converged parameters. Then, finding the

converged q point mesh by using low parameters values (E_{cut}=8 Ha and 400 bands). As shown in Fig. 6.4, the 864 BZ points is the converged value corresponding to η=1.0 eV. Finally, using the extrapolation scheme in Eq. (6.5) one can find the fully RESP converged value. The converged RESP value is corresponding to the following parameters: 2500 bands, 35 Ha of E_{cut} and 864 BZ points. The final results can be seen in Fig. 6.10.

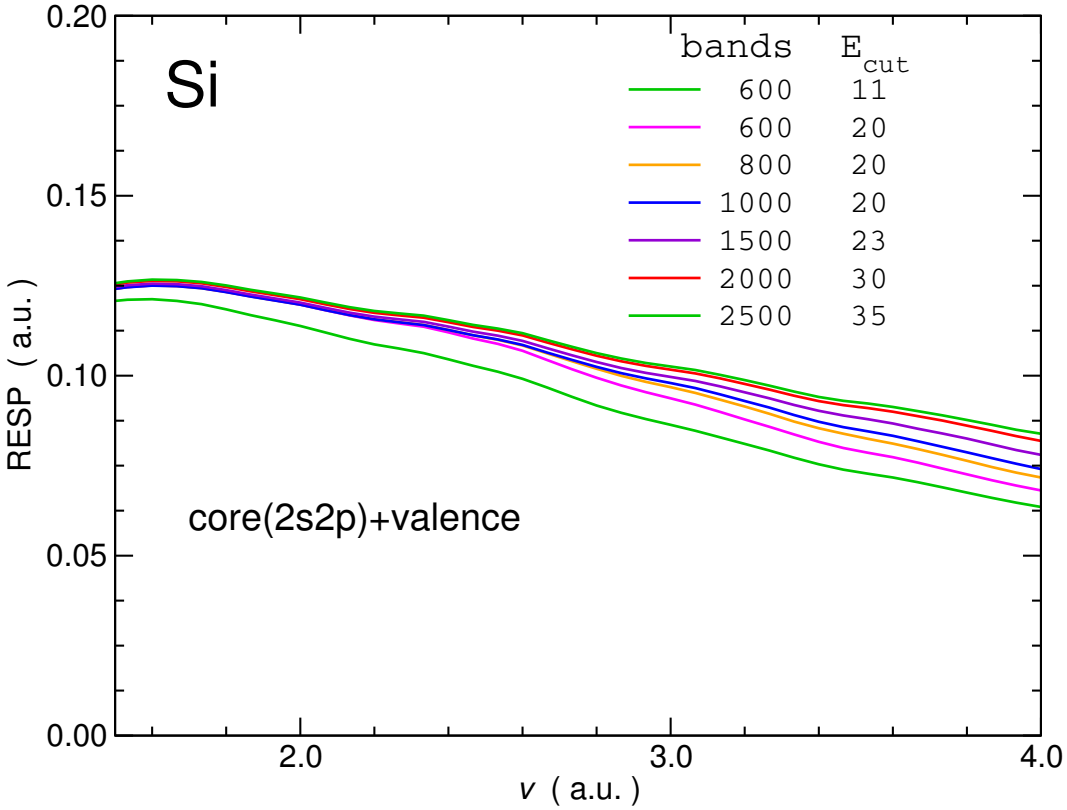


Figure 6.9: Convergence of the RESP of silicon within RPA as a function of the number of bands and of the dielectric matrix cutoff. The convergence with respect to the number of bands and dielectric matrix cutoff was obtained for a fixed Γ-point sampling. The convergence study is obtained for the (2s2p3s3p) electrons.

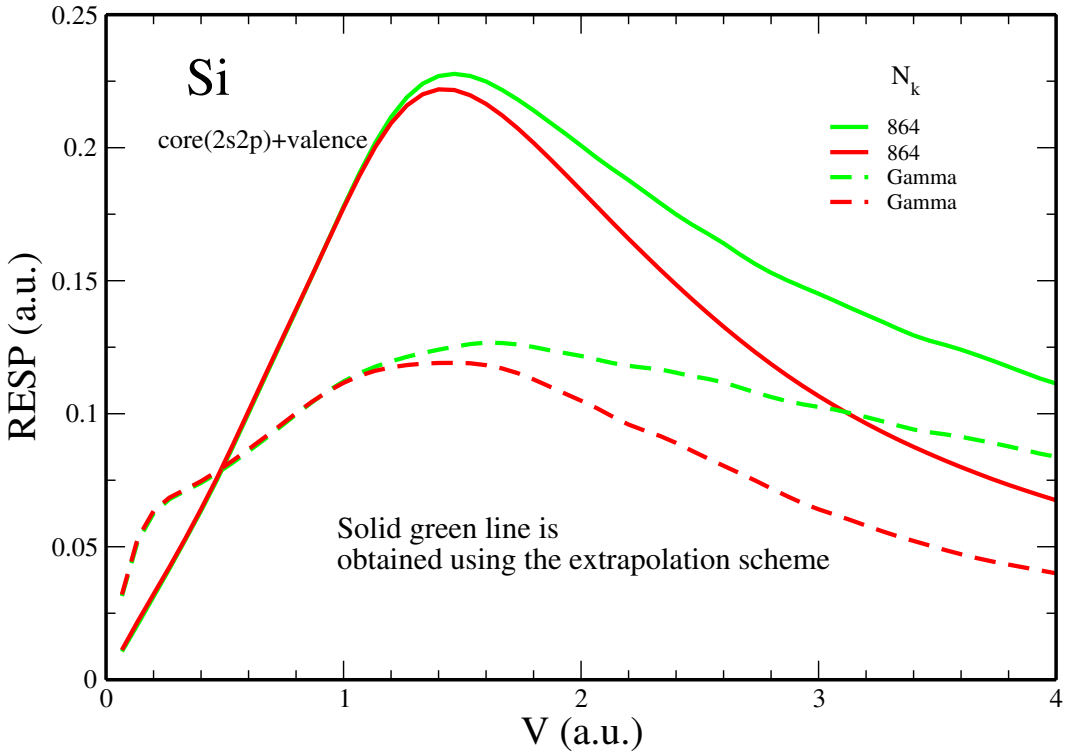


Figure 6.10: The fully Converged RESP of (2s2p3s3p) electrons in Si target for proton (Z_1=1) within the linear response of RPA calculated by extrapolation scheme in Eq. (6.5). The green line obtained for highly converged parameters (2500 bands and E_{cut} = 35 Ha) for the all electrons (without 1s), the red line obtained for low converged parameters (400 bands and E_{cut} = 8 Ha) for valence only.

6.3 Conclusion

In this chapter, we have developed a computer program to calculate the RESP of periodic solids, within the linear-response approach to TDDFT. Furthermore, the convergence issues of the RESP calculations have been shown in details. Also, we have presented an extrapolation scheme that can be used to overcome the convergence problems of the RESP calculations.

Next chapter, we will present the RESP for solid materials in details.

Chapter 7

Stopping power of bulk materials

In this chapter, we present a comprehensive study on the RESP of the solid materials. First of all, we evaluate the validity of using the LDA of the Lindhard theory, sometimes called the Local Plasma Density Approximation (LPDA). In order to predict the best results compared to the available experimental data, we will answer the following two questions: The first one is what is the best approximation RPA or ALDA? The second one is should we go beyond the valence electrons contribution? Finally, with the formalism described in the previous chapters, we check the validity of some commonly stated rules of thumbs concerning the RESP of solid materials.

7.1 First principle against models based on the free-electrons gas

In the previous chapter, we have seen that the convergence issues are dramatic. Thus, the task of understanding the electronic stopping power in real material is still a very challenging job. This fact is true for the calculations within a simple approximation like RPA even when taking into account the valence electrons only. Now that we have a working implementation of the *ab initio* RESP, We would like to seize the opportunity to evaluate the validity of the simpler models that are often used for real targets. According to the literature, models based on the free-electron gas (FEG) have been developed and used with a relative success in the previous fifty years.

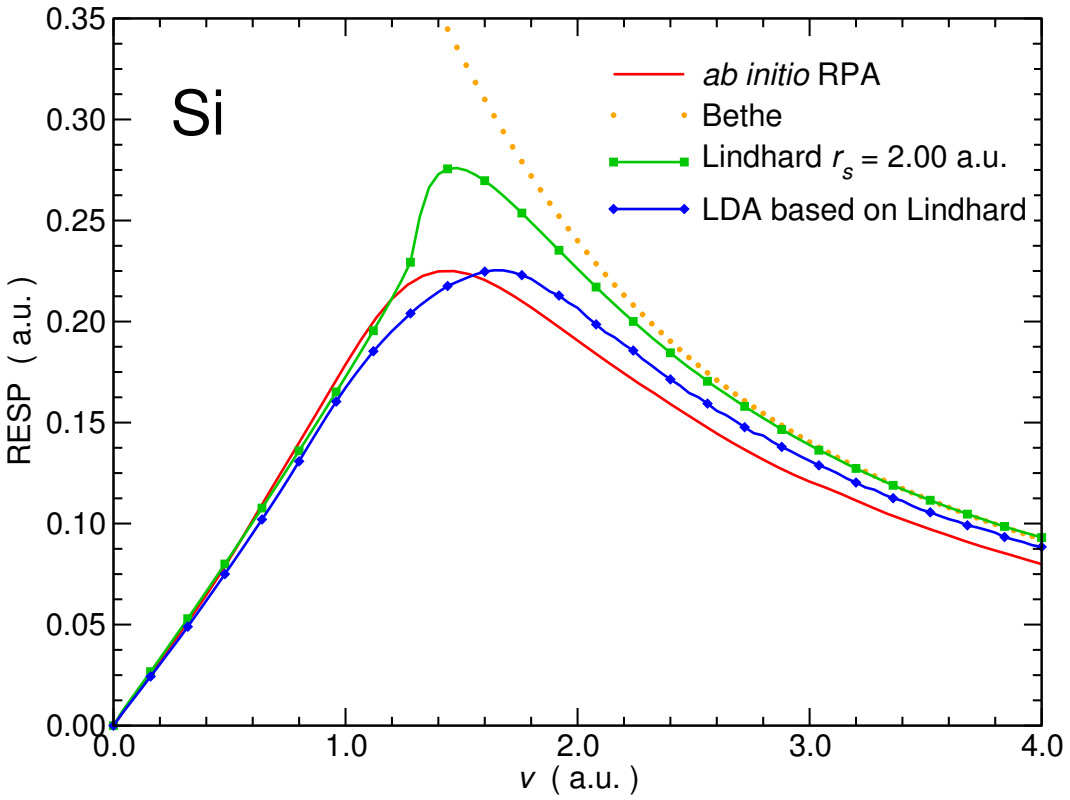


Figure 7.1: FEG-based modeling of the RESP against the reference *ab initio* RPA calculation.

In this section, we propose to examine the validity of these models against the calculated *ab initio* RPA for silicon, as shown in Fig. 7.1. We will focus only on the most used models like the Bethe's formula and Lindhard's formula with and with out LDA.

The crudest modeling we consider here is the analytic formula from Bethe:

$$S_e = \frac{Z_1^2 \omega_p^2}{v^2} \ln\left(\frac{2v^2}{\omega_p}\right), \tag{7.1}$$

where $\omega_p = \sqrt{4\pi\rho_0}$ is the classical plasma frequency and ρ_0 is the average electronic density. In Fig. 7.1, the Bethe formula is not evaluated for $v <$ 1. a.u., since the formula shows a divergence there. However the Bethe formula is effective to capture the large v behavior, since it was derived based on considering a moving projectile with high but non relativistic velocity. More details can be found in chapter 2.

Then a huge improvement is due to Lindhard [47] , who derived the RPA RESP formula for a FEG at a given homogeneous electron density ρ_0. The

Lindhard RESP still requires a numerical evaluation of a double integral [40], for more details see chapter 5. Fig. 7.1 shows the Lindhard RESP evaluated at the same average density as the valence electrons of bulk silicon, (r_s = 2.00 a.u.). The Lindhard RESP deviates noticeably from the *ab initio* RPA, especially around the peak at $v = 1.4$ a.u..

A route to improve the description of real inhomogeneous solids is the local density approximation (LDA) to RESP [45, 40]. This approximation assumes that the RESP of a solid can be obtained as the spatial average over Lindhard RESP evaluated at the local density, however more discussion about this theory is given in chapter 5.

In this work, the LDA-Lindhard theory have been applied for the Si target as following: First, within the *ab initio* DFT framework the valence density was obtained. Then, we have applied Eq. (5.11) to produce the electronic stopping power as a function of ion's velocity for this given valence density.

Fig. 7.1 shows that the LDA based on Lindhard produces a rather meaningful evaluation of the RESP of Si. As we will see next, LDA based on Lindhard is not adequate when including the tightly bound core electrons.

As a consequence, the earliest stopping theories which are based on the FEG system show advantages and disadvantages in practice, for example: The Bethe's formula can be used to study swift projectile, but it can not be used in the case of for low velocity projectile. In addition, Lindhard's theory may be considered as the first choice if we are only interested in predicting the stopping power peak position. Furthermore, Lindhard's formula is found to be a acceptable method if the target medium does not contain the core electrons, or if we are not looking for finding high accuracy results.

7.2 Physical approximations relevant for bulk materials

Before going further in understanding the electronic stopping of solid, we must introduce a more deep study in order to find the best way to predict the available experimental data. Therefore, this section will be devoted to test the following: First, we will look for more efficient approximations for the exchange-correlation beyond RPA, since the calculated RESP within RPA shows a largely underestimated value comparing to the experiment. Second, we will investigate the core electrons contribution on the RESP value using the presented *ab initio* formalism. Also, we try also to calculate the core electrons RESP contribution using a simple approximation like LPDA (LDA based on Lindhard) and we test this method. Finally, we check the linear response lim-

itations of the RESP, especially at low energy, in comparison to the higher order perturbation consideration.

7.2.1 RPA vs ALDA

In earlier works [87, 88], it has been shown that the quality of the structure factor S is much improved when switching on the exchange-correlation contribution from RPA to ALDA. As the structure factor is closely related to the stopping power, one can anticipate that the stopping power will be affected and hopefully improved by the inclusion of the ALDA kernel in TDDDFT.

In terms of the inverse dielectric function, the dynamic structure factor can be written as [78]:

$$\mathrm{S}(\mathbf{Q},\omega) = -\frac{\mathbf{Q}^2}{4\pi^2\rho}\mathrm{Im}\left[\varepsilon^{-1}(\mathbf{Q},\omega)\right], \tag{7.2}$$

where, the ρ is the electron density.

The structure factor $S(\mathbf{Q},\omega)$ can be linked to several experimental measurements: electron energy loss spectroscopy (EELS) and to the inelastic X-ray scattering (IXSS). By analyzing the $S(\mathbf{Q},\omega)$ results, one can extract some useful information which can be used to understand the RESP results. For instance, in Fig. 7.2, we present the accuracy of the calculated $S(\mathbf{Q},\omega)$ using both RPA and ALDA comparing to the experimental data.

Fig. 7.2 shows that the agreement between the experiment and the calculated $S(\mathbf{Q},\omega)$ by using ALDA is very good, while a much worse agreement between the calculated $S(\mathbf{Q},\omega)$ value using RPA and the experiment can be noted.

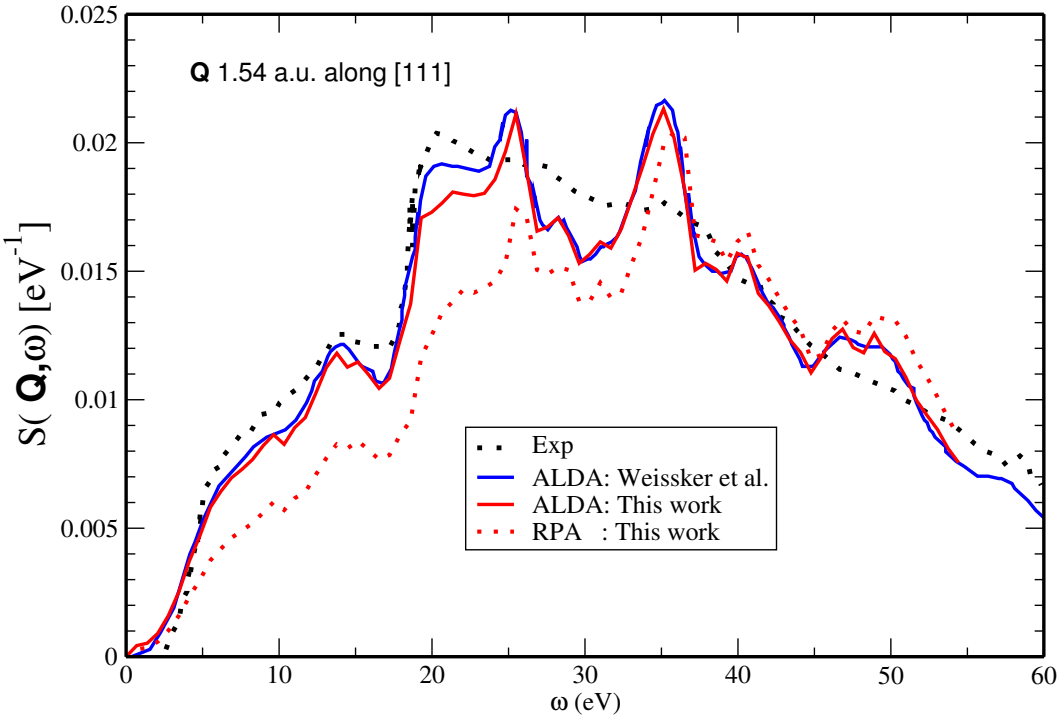


Figure 7.2: Comparison of the calculated dynamic structure factor using both RPA and ALDA with the available theoretical and experimental data for silicon. Both the experimental and theoretical data have been taken from Ref. [87]. The present results have been obtained using the same convergence parameters as found in Ref.[87].

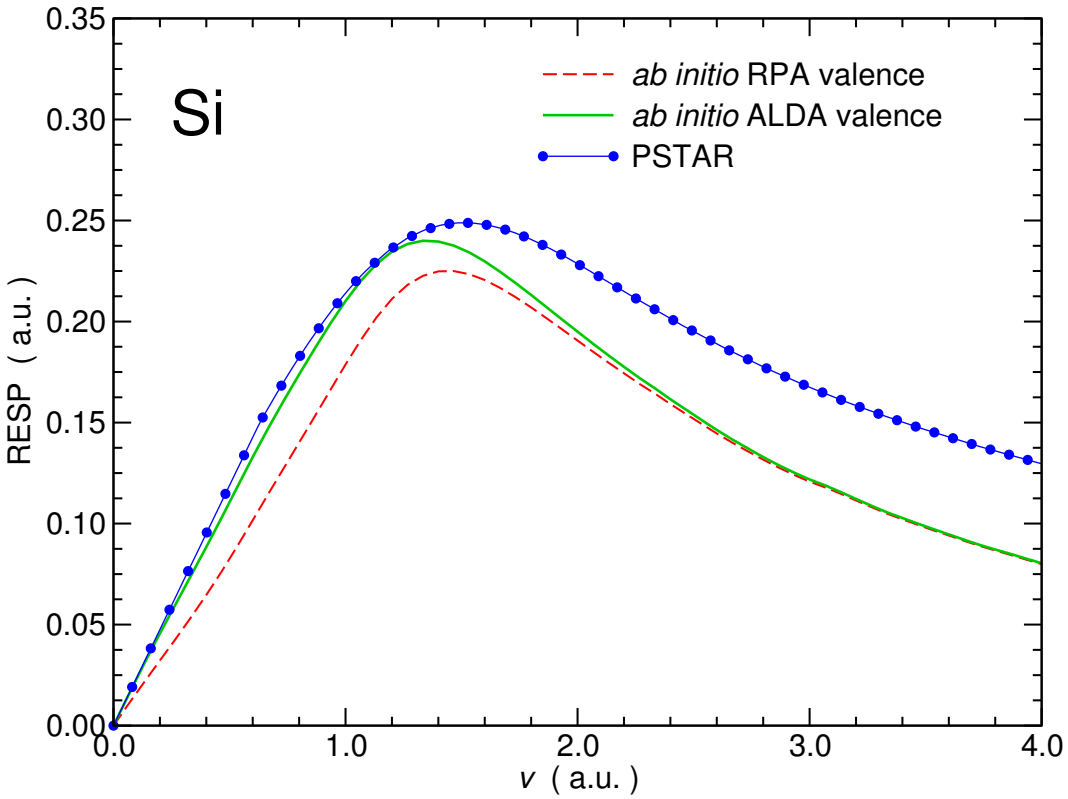


Figure 7.3: RESP of Si using different approximations for the TDDFT kernel: RPA (dashed red line) and ALDA (solid green line). Silicon is described by its valence electrons only. Experiment from the PSTAR database[7] (blue circle symbols) is given as a reference.

Turning back to the RESP, the results are expected to change much when using ALDA instead of RPA. Figure 7.3 demonstrates how the inclusion of the ALDA kernel increase much the RESP in the low velocity regime. However, for the larger velocities $v > 2$ a.u., the RESP is completely insensitive to the TDDFT kernel. Thanks to ALDA, the agreement with respect to experiment is excellent for low velocities up to the peak, but still remains largely underestimated for higher velocities.

7.2.2 Core states contribution

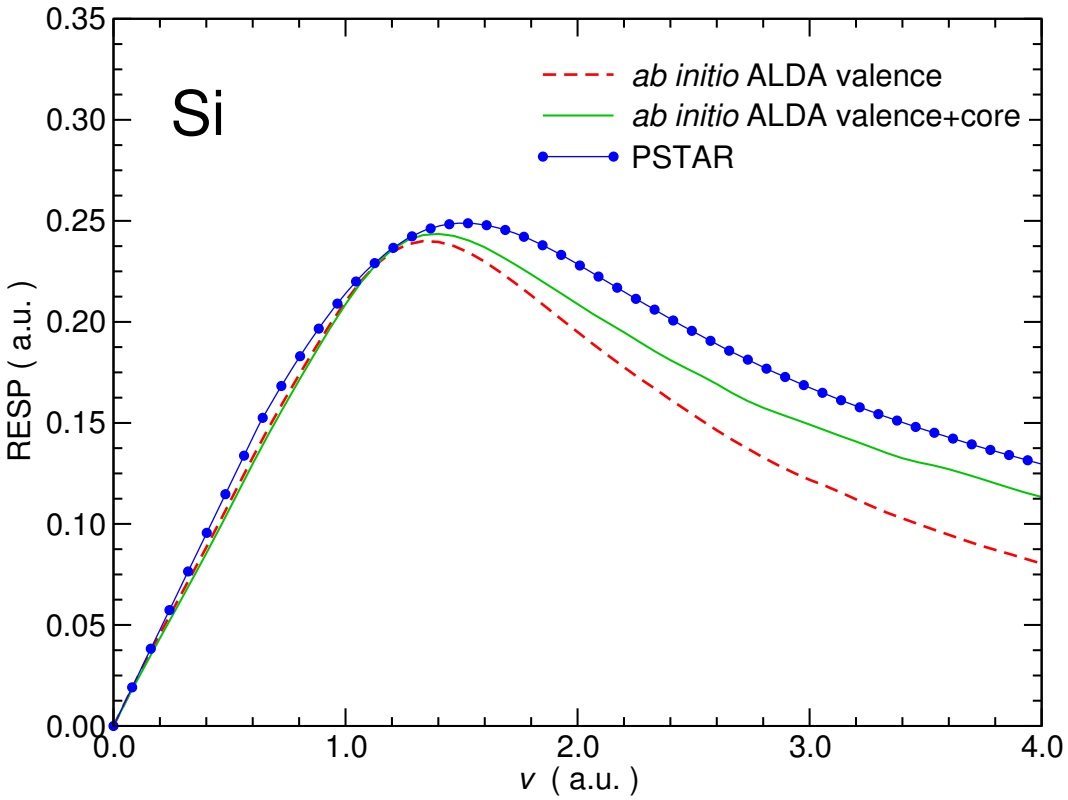


Figure 7.4: RESP of Si within ALDA including (solid green line) or not (dashed red line) the contribution from the core $2s$ and $2p$ electrons. Experiment from the PSTAR database[7] (blue circle symbols) is given as a reference.

***ab initio* inclusion of the core contribution** To address the underestimation of the RESP for large velocities, the natural step is to include the description of the core states. Indeed, we have shown in Chapter 6 that the RESP is much sensitive to the high-energy transitions included in the response χ^{KS} and that a huge number of empty bands is necessary to achieve convergence. In an analogous manner, the RESP can be expected to be much affected by core electrons. For instance, in silicon, the $2s$ and $2p$ electrons are located about 100 eV below the valence and can contribute to the loss processes for moderate values of the velocity v. The $1s$ electrons which lie 1700 eV below the valence can be safely disregarded.

The effect of the $2s2p$ electrons of Si on the RESP can be appreciated from Fig. 7.4, where the calculation with two pseudopotentials with or without $2s$ and $2p$ have been carried out. The $2s2p$ electrons yield a significant additional

contribution to the RESP for velocities beyond 1.5 a.u., whereas they have no effect below. However, even when introducing the core electrons, the RESP for high velocity is underestimated by about 10-15% with respect to experiment.

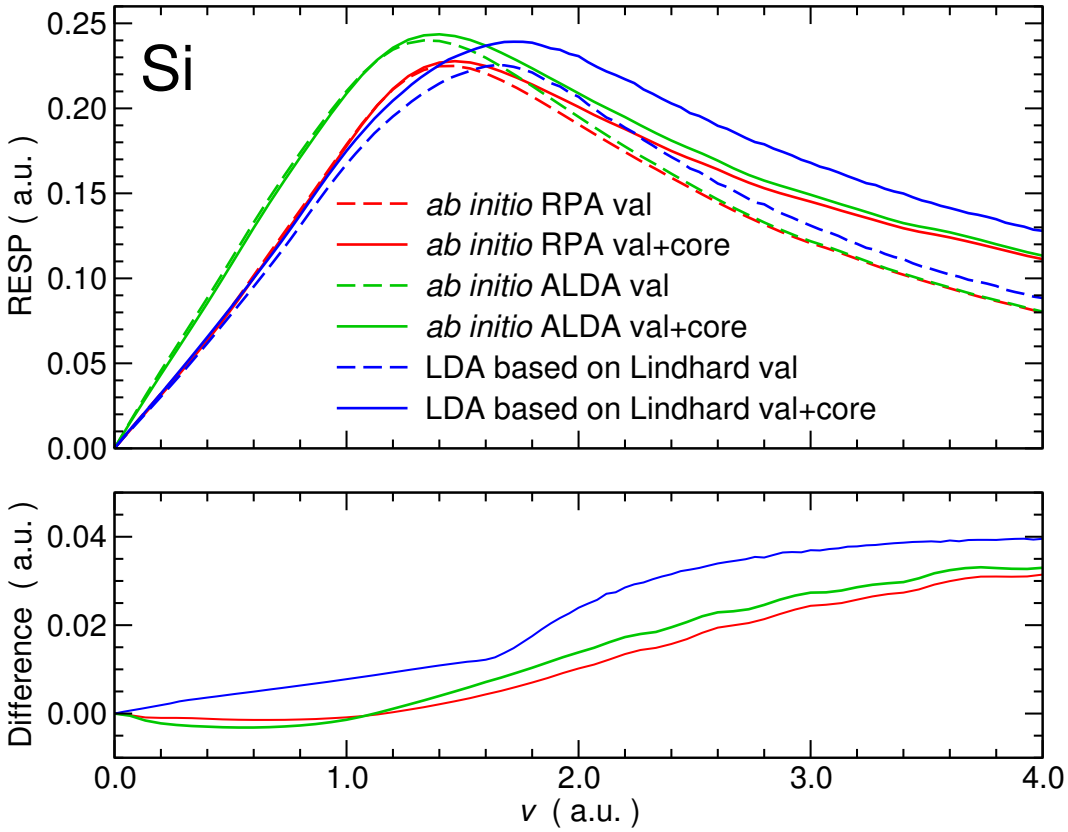


Figure 7.5: Upper panel: RESP of Si within RPA (red lines), ALDA (green lines), and LDA based on Lindhard (blue lines) including (solid lines) or not (dashed lines) the contribution from the core $2s$ and $2p$ electrons. Lower panel: Core-only contribution to the RESP of Si as obtained through the difference between the calculations with and without $2s$ and $2p$ within RPA, ALDA, or LDA based on Lindhard.

Unfortunately, the calculations with explicit core states not only have more occupied states in the summation of Eq. (4.26), but also have a much harder pseudo-potential, that in turn induces a higher dielectric matrix cutoff. Silicon now requires $E_{\rm cut} = 35$ Ha instead of 25 Ha. With such a high computational burden, it would be then desirable to have an approximate scheme to handle the core states. Thanks to the extrapolation scheme as introduced in Eq. (6.5) in the previous Chapter which help to overcome the core convergence problem.

Let us analyze further here the contribution from the core electrons alone. In the lower panel of Fig. 7.5, we evaluate the contribution of the core electrons to the RESP of Si for different approximations as the difference between the RESP curves obtained in the upper panel. In contrast with the statement issued for valence electrons, the effect of the ALDA kernel is negligible: the ALDA and the RPA core RESP are almost identical.

What is still missing in the core contribution? Hence, even when including the core states properly in silicon, the calculated RESP still underestimates slightly the experimental RESP for the large velocities. We then wonder if this underestimation is a problem due to the bad description of the core states or of the valence states. To try to answer that question, we have performed calculations for a bulk systems that does not have really bound core electrons, namely the body-centered cubic lithium. Indeed, Li is a metal with a $2s^1$ valence electron, but the $1s^2$ electrons below are very loosely bound. Their binding energy is around 60 eV to be compared to the 300 eV of the $1s$ electron of carbon.

Figure 7.6 shows that the calculated RESP value using ALDA in Li target for high proton velocity ($v > 2$ $a.u.$) are almost the same as the available experimental data from Refs. [28, 42]. This almost perfect result points to the fact that the ALDA is not the most suitable approach to evaluate the core electrons RESP contribution. This could be the subject of further investigations in the future.

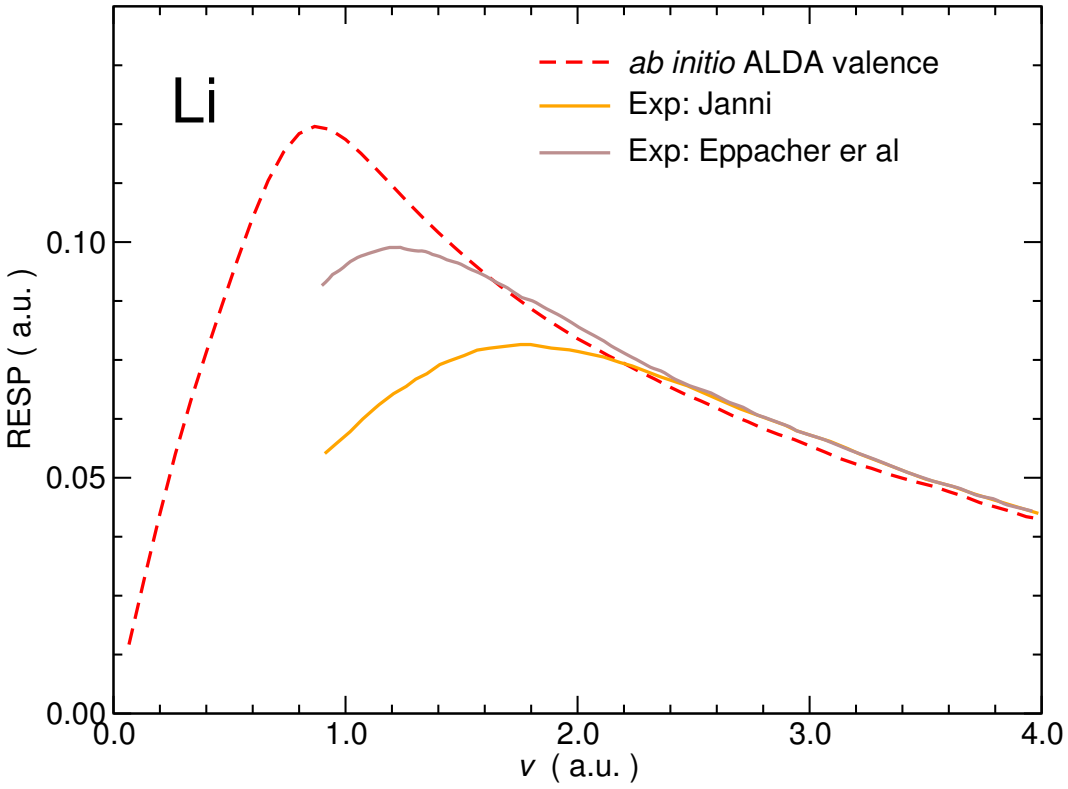


Figure 7.6: The electrons RESP of Li within ALDA in linear-response (dashed red line) compared to the available experimental data. Experiments (probably bcc crystal) by Janni [42] (orange line) and Eppacher et al. [28] (brown line).

Is LDA RESP a valid alternative to the full evaluation of core electrons? We also considered the opportunity to have a cheap evaluation of the core contribution using the LDA based on the Lindhard stopping power. In the upper panel of Fig. 7.5, the LDA RESP is calculated for both the valence electronic density and the valence plus core electronic density. The difference between the two can be compared with the full *ab initio* calculation in the lower panel. The LDA technique is not perfectly adequate to describe the core contribution. Indeed, the stopping power continuously increases starting from the lowest velocities. In other words, the LDA core misses the shell effect: the core contribution should be zero up to the minimum velocity that allows the core electrons to be excited.

Even though the LDA technique could describe the core contribution with a reasonable accuracy, we rather use an explicit introduction of the core electrons through adequate pseudo-potentials in all the following RESP results of the

study.

7.2.3 Effect of the higher order terms

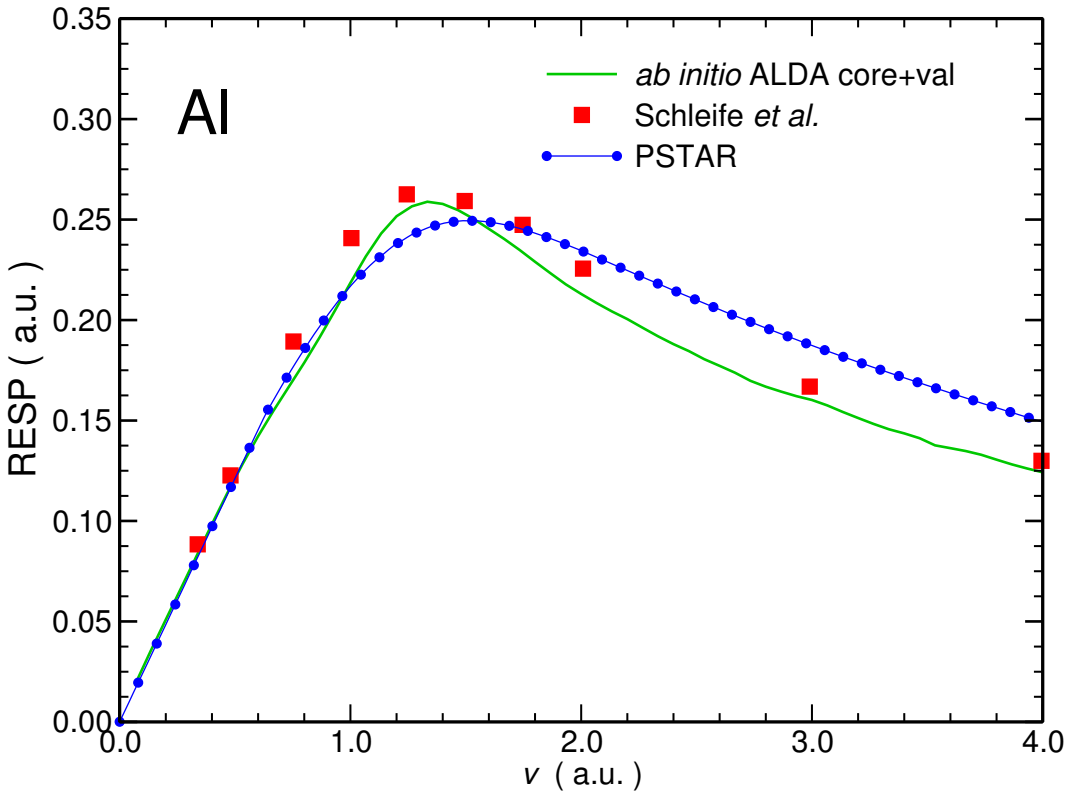


Figure 7.7: RESP of Al within ALDA in linear-response (solid green line) compared to the time-propatation results of Scheifle and coauthors.[77] Experiment from the PSTAR database[7] (blue circle symbols) is given as a reference.

In a recent study, Schleife and coworkers [77] produced a high quality ALDA stopping power calculation for aluminum using the time-propagation approach to TDDFT. Their calculations readily include the perturbation to all orders, whereas ours are limited to the linear response by construction. Hence, the comparison can allow us to evaluate the magnitude of the higher-order terms.

In Fig. 7.7, one can compare our linear-response results to the time-propagation data of Ref. [77] for the traveling of an off-channeled proton in Al. The differences are indeed rather small, around 5 % for the worse data points. Considering the conceptual differences in the two approaches and their own convergence issues, we consider this close match as an impressive success of the linear-response theory. Surprisingly, the error due to the linear-response

approximation does not vary much with the proton velocity. This comparison validates the linear-response approach, at least for protons with velocities larger than 0.5 a.u..

7.3 RESP for bulk materials

With the formalism described in the previous Chapter, we check the validity of some commonly stated rules of thumbs concerning the RESP.

7.3.1 How weak is the RESP anisotropy of anisotropic materials?

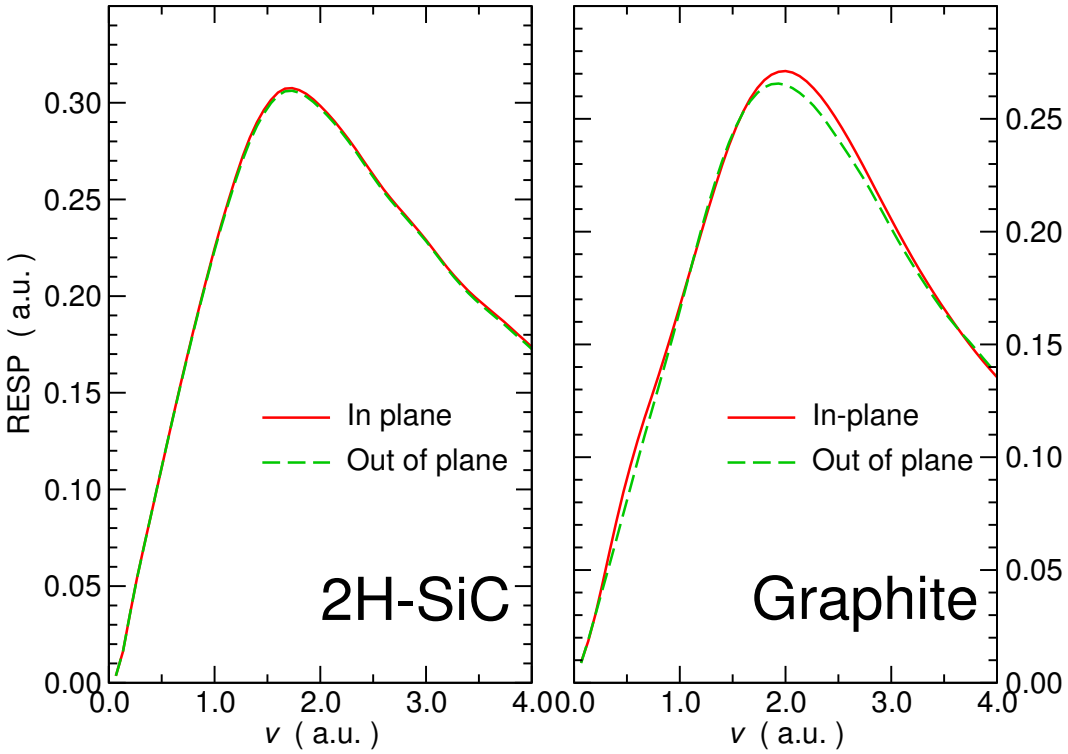


Figure 7.8: Anisotropy of the RESP of 2H-SiC (left-hand panel) and of graphite (right-hand panel) within ALDA including the $2s2p$ electrons of Si.

In an anisotropic material, the RESP not only depends on the magnitude of the velocity, but also on its direction. This anisotropy is usually completely disregarded in the interpretation of the experimental data, either because the

anisotropy is expected to be small, or because the experimental samples are poly-crystalline (and the anisotropy is then averaged out).

We analyze in Fig. 7.8 the anisotropy of the RESP of two prototypical crystals, 2H-SiC (silicon carbide in wurzite structure) and graphite. Fig. 7.8 shows the RESP along a direction in the plane against the RESP along the out of plane axis. The dense structure of wurzite SiC is weakly anisotropic and, as expected, the RESP is almost insensitive to the direction of $\mathbf{v}$. The layered structure of graphite, which consists in hexagonal planes of carbon separated by a large spacing, may give rise to a larger anisotropy. However, the RESP in right-hand panel of Fig. 7.8 has a very small direction dependence, which amounts to at most 3 % in the peak region.

As a conclusion, the anisotropy of the RESP is always very weak, even for crystal structures which are much anisotropic.

7.3.2 Is the Bragg's additivity rule valid?

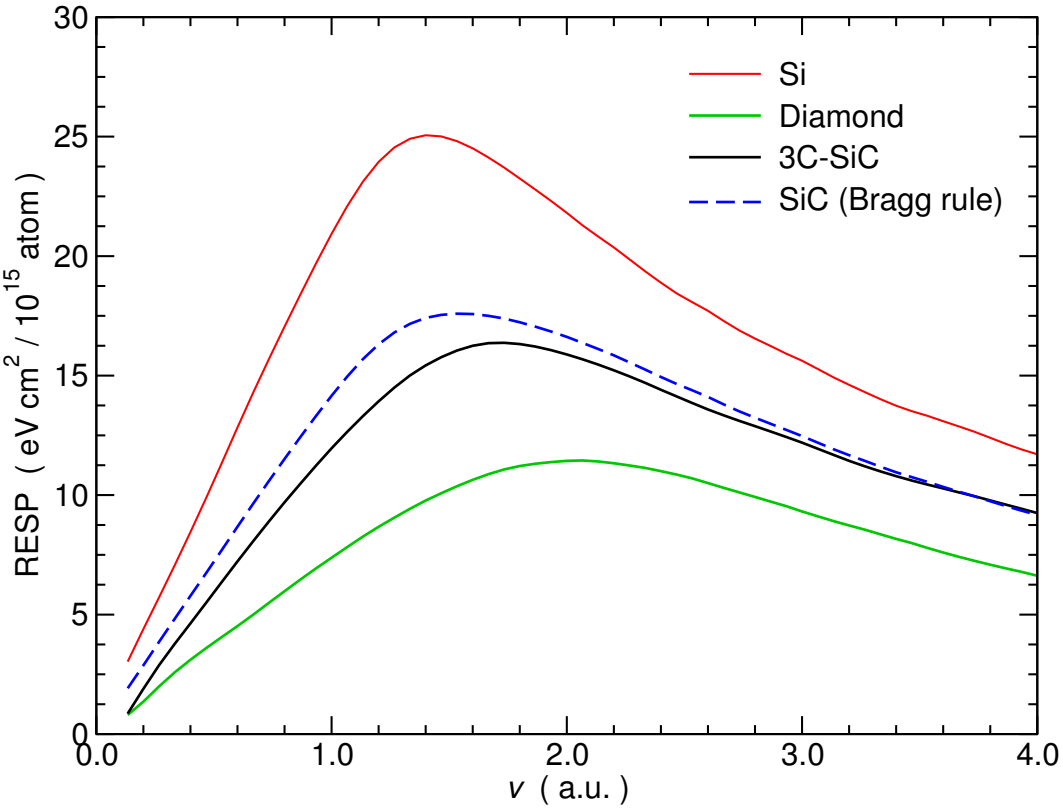


Figure 7.9: RESP of Si, diamond, 3C-SiC within ALDA including the $2s2p$ electrons of Si. The Bragg's rule SiC (dashed blue line) was obtained using Eq. (7.3).

It has been observed since the early times of the particle irradiation[18] that the electronic stopping power is mainly proportional to the average density of electrons, so that the stopping power of compounds could be obtained as a weighted average of the stopping power of its constituents. Exemplifying this statement, known as the Bragg's additivity rule, for silicon carbide would read

$$\frac{S_e(\mathrm{SiC})}{\rho_{at}(\mathrm{SiC})} = \frac{S_e(\mathrm{Si})}{\rho_{at}(\mathrm{Si})} + \frac{S_e(\mathrm{C})}{\rho_{at}(\mathrm{C})}, \tag{7.3}$$

where ρ_{at} is the atomic density. From experimental databases, some deviations for this rule are well documented.[93, 82] However, the deviations mainly occur for light elements, such as organic polymers.

In Fig. 7.9, we test the adequacy of Eq. (7.3) for 3C-SiC (zinc blende structure). This case should be the simplest case for the Bragg's rule, due to the

similarity between the crystals considered here. All three crystals, Si, diamond, and 3C-SiC, have a similar crystal structure (diamond or zinc blende), have the same local environment, and have the same electronic configuration. The Bragg's rule indeed shows its efficacy for the large velocity regime, $\mathbf{v} > 2$ a.u.. However, for low to moderate velocities, the deviation between the Bragg's rule RESP of SiC and the *ab initio* RESP of SiC is as large as 15 %.

Considering a very simple test case, we shed light on a significant violation of the Bragg's rule. This statement casts doubts about the application of this rule of thumbs for more complex cases, for instance, when the formal charge varies (oxides), or when the bonding changes (single or double bonds).

7.3.3 Is the structural phase effect vanishing?

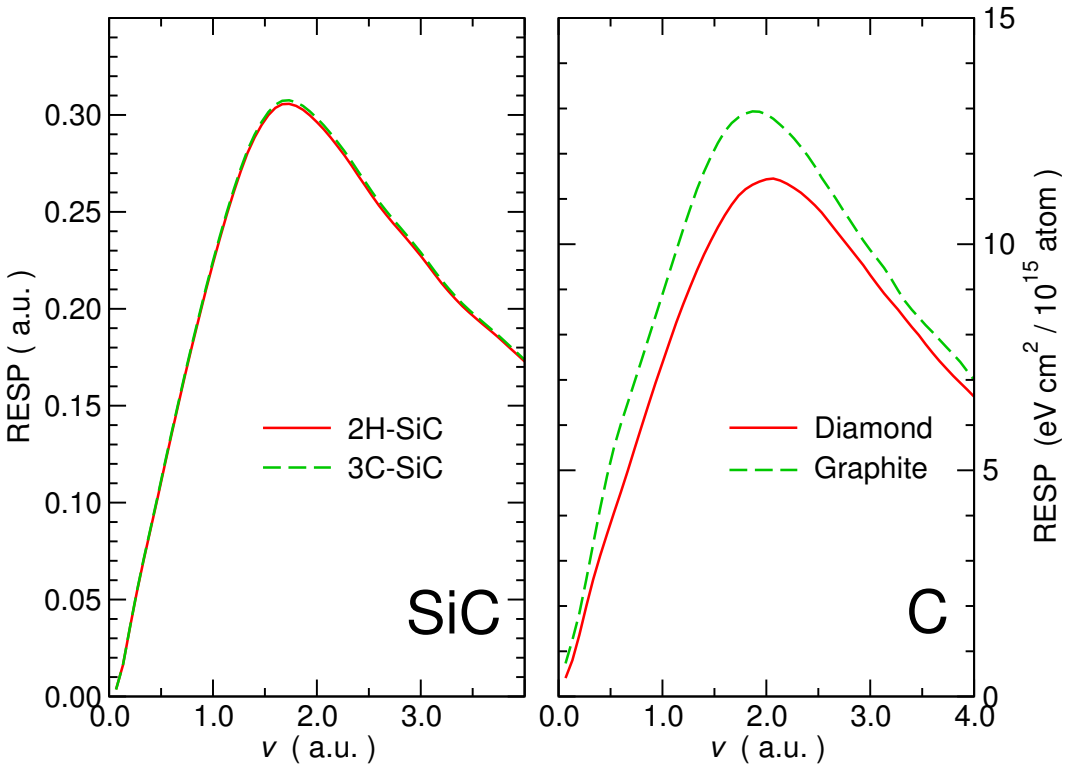


Figure 7.10: RESP of SiC (left-hand panel) and of carbon (right-hand panel) within ALDA including the $2s2p$ electrons of Si. 3C-SiC and 2H-SiC phases are shown for silicon carbide, whereas graphite and diamond phases are shown for carbon.

The empirical Bragg's rule also implies that the details of the crystalline structure does not influence much the RESP. We propose to check that assumption

for two prototypical examples.

Silicon carbide can crystallize in many different phases, named polytypes. The left-hand panel of Fig. 7.10 shows the RESP for the 2H-SiC (wurzite) and 3C-SiC (zinc blende). These two phases only differ through the stacking of the planes in the (111) direction. The local environment is exactly the same in the two structures. In order to ease the comparison between the two, we have used an ideal wurzite structure instead of the experimental structure and we have used an hexagonal supercell of the cubic polytype with 6 atoms. Finally, the difference in the RESP for the two phases appears as negligible in the left-hand panel of Fig. 7.10.

The phases of carbon are a more challenging example. Indeed the diamond phase of carbon involves tetrahedrically coordinated atoms with sp^3 hybridized electrons, whereas the graphite phase is a layered crystal with sp^2 hybridized electrons. In these two structures, the nature of the bonding is affected and the consequences on the RESP are huge as shown in the right-hand panel of Fig. 7.10. The increase in stopping power of graphite follows the empirical trends highlighted in Ref. [75], which is named the bond effect.

The RESP appears as sensitive to the details of the bonds, however the long-range structure is clearly not a relevant parameter, as demonstrated by the different stacking patterns in SiC.

7.4 Conclusion

In this Chapter, we have produced high quality stopping power curves with the assistance of an extrapolation technique. Also, we have shown that the necessity of a proper description of the core electrons and of the exchange-correlation within ALDA. With the comparison with the time-propagation results of Ref. [77], we have evaluated an upper limit for the non-linear effects of 5 % in aluminum.

With the *ab initio* RESP, we have checked some empirical rules of thumbs that are commonly employed for the experimental interpretation or for the prediction with empirical codes, such as SRIM [93]. Whereas the anisotropy of the RESP in anisotropic materials can be safely ignored, the Bragg's additivity rule and the phase insensitivity cannot be taken for granted.

Next chapter, we show the validity of using the *ab-initio* for complex materials such as the Ice, water in the gas phase and polymer materials.

Chapter 8

Stopping power in organic systems

Very intriguing phenomena occur for the stopping power of organic systems. It has been noted [75] for long that the nature of the chemical bonds affects much the electronic stopping power especially for light atoms. Indeed, carbon is very versatile and can take part to multiple types of bonds (simple, double, triple). We just have seen in the previous chapter how graphite and diamond noticeably differ. Along the same lines, it is well known experimentally that the different water phases (vapour, liquid, ice) show rather different stopping powers.

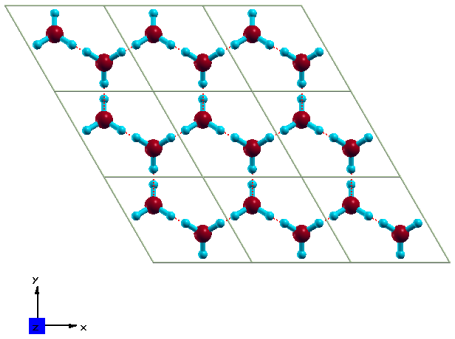
In this chapter, we sketch the first steps towards the evaluation of the RESP from *ab initio* calculations. We present the calculations that have been possible to carry out, but also show how difficult it would be to obtain converged results for isolated systems. The end of the chapter is meant to pave the way for a future study.

This chapter first focuses on the RESP of water H_2O since its value strongly depends on the phase (gas or solid phases). Then, this chapter studies the RESP of polymers so to check the contribution of the bond effect.

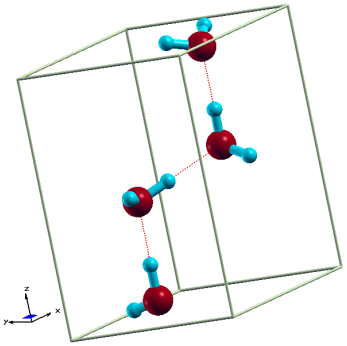
8.1 RESP of the H_2O molecule in two phases: The solid and gas phases

The first step is to choose the crystal structure of the solid water, since the ice can be found in many different forms. We have considered the H_2O ice in a Hexagonal crystal (ice Ih) which has the symmetry $P6_3/mmc$, since it is the natural form of the ice on Earth. The hexagonal crystal has unit cell dimensions a=8.5379 bohr and c=13.9 bohr at 250 K, with 4 molecules per unit cell as found in Ref. [71]. Fig. 8.1 shows the unit cell of the ice Ih and the periodic ice Ih crystal with a view along the c-axis. As shown in Fig. 8.1, between two

adjacent oxygen atoms lies exactly one hydrogen atom, closer to one of the oxygen atoms. This bond is then called hydrogen bond. Furthermore, to each oxygen atom belong exactly two hydrogen atoms, which are closest to it.



(a) View of Ice structure along the c-axis.



(b) The hexagonal unit cell of ice Ih.

Figure 8.1: Structure of water in the ice Ih phase

Even with the more complex structure (ice Ih) than the bulk materials (Si, diamond, Graphite, Al, Li,..etc) studied in the previous chapter, we managed to use our extrapolation method to find the converged RESP value of proton projectile in ice Ih. As shown in Fig. 8.2, the calculated ALDA RESP converged value of ice Ih target is almost acceptable result in comparison with the available experimental data.

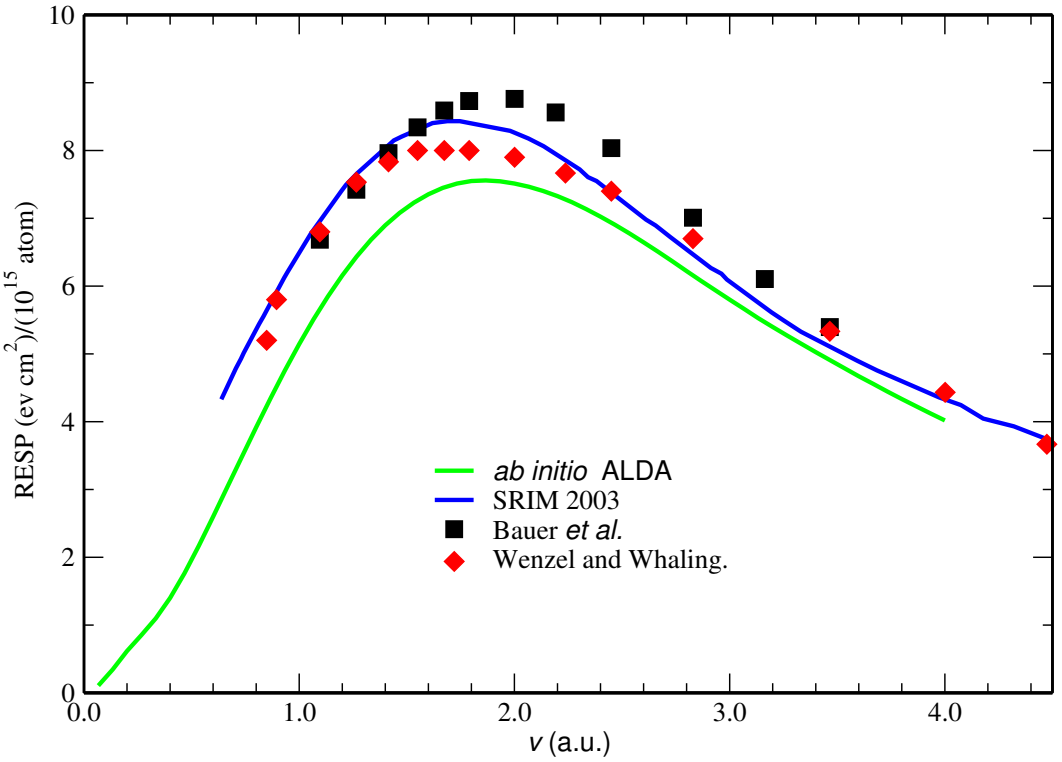


Figure 8.2: The validity of RESP of plane wave framework in evaluating of ice-Ih target within ALDA in linear-response (solid green line) compared to the available experimental data. Experiments by Bauer *et al.* [5] (black square points) and Wenzel and Whaling [89] (red diamond points). The SRIM 2003 [93] is semi empirical code (solid blue line).

Unfortunately, the success of the plane wave framework in calculating the RESP of ice cannot be transposed to the H_2O in gas phase. Indeed for an isolated system like H_2O in gas phase, another convergence parameter has to be taken to the account. This convergence parameter is the box volume which is used to make the H_2O molecule isolated. The purpose is to make the inter-molecular interactions almost negligible at the large box volume, so that a gas phase is well mimiced.

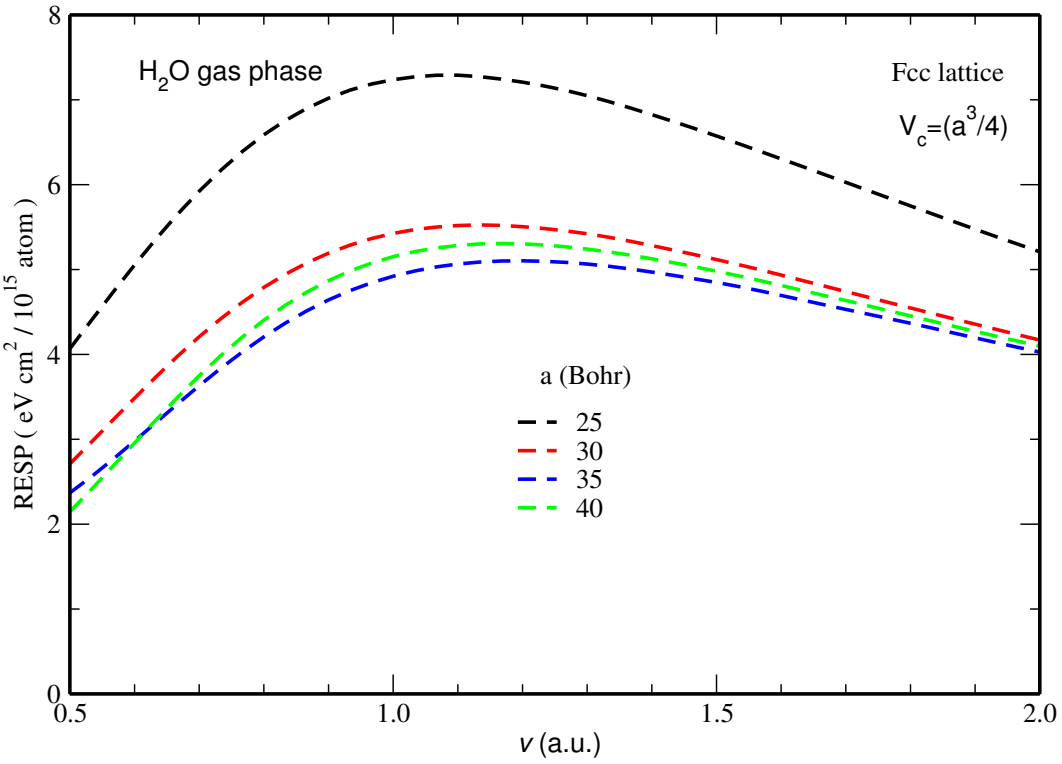


Figure 8.3: RESP of proton in the H_2O gas phase target as a function of the cell volume V_c. For all V_c the following parameters have been used: $N_k = 8$, $E_{cut} = 4$ Ha for $\varepsilon^{-1}_{\mathbf{GG'}}(\mathbf{q}, \omega)$, $\eta = 1.5$ eV and using a number of bands so that the highest transition is $\Delta E_{band} = 42$ eV. Thus, the same excitation density will be used for all the volume V_c. Note that the low velocity part below 0.5 a.u. is very unstable and is not shown here.

First, we would like to have an evaluation of the cell volume V_c necessary to obtain the stopping power of the isolated system. It is not feasible to converge all the paramters at once. Therefore we choose to evaluate V_c with loosely converged values for the other parameters. We use a low value $E_{cut} = 4$ Ha. Then we choose the number of empty states not fixing it, but rather fixing the energy of the highest empty states. Here we select the number of states so that the highest transition is $\Delta E_{band} = 42$ eV. The k-point grid is $2 \times 2 \times 2$. As shown in the Fig. 8.3, the volume for a face-centered cubic cell necessary to obtain an isolated molecule appears to be obtain for a lattice constant equal to 35 bohr. In fact, this volume is very large comparing with what is usually used for the ground state study. Therefore, the absolute convergence will be extremely hard to be achieved. Even for a low value of E_{cut} for $\varepsilon^{-1}_{\mathbf{GG'}}(\mathbf{q}, \omega)$,

the required number of bands to account all the possible electronic excitations will be an incredible quantity.

Let us try to evaluate this number. Fig. 8.4 shows the convergence behavior of the RESP as a function of dielectric matrix cutoff and the number of bands using only the gamma point. For small box (FCC cell with $a = 20$ Bohr), the number of bands necessary to converge the RESP up to velocity $v = 4.$ a.u. is around 2500 using $E_{cut} = 15$ Ha. Thus, the number of bands at $E_{cut} = 15Ha$ extrapolated to the converged box size (FCC cell with $a = 35$ bohr) is about 13000! This is far beyond our capabilities as of today.

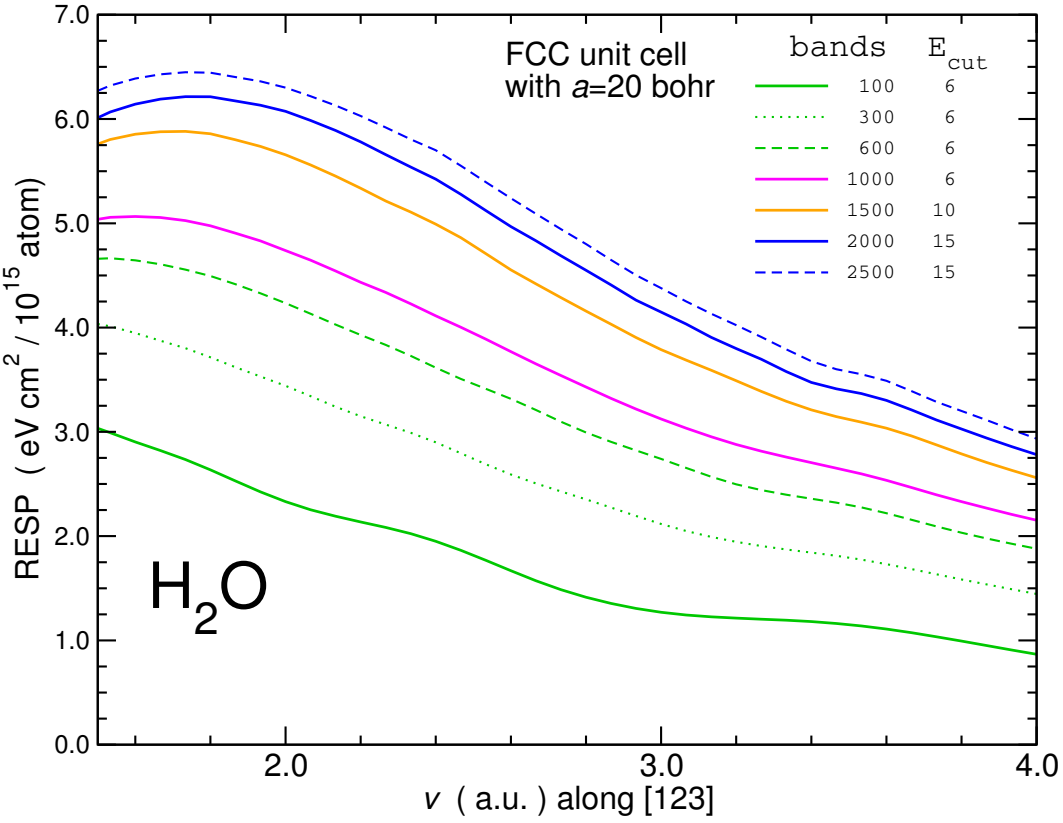


Figure 8.4: Convergence of the RESP of H_2O gas target within ALDA as a function of the number of bands and of the dielectric matrix cutoff. The convergence with respect to the number of bands and dielectric matrix cutoff was obtained for a fixed Γ-point sampling with $\eta = 4$ eV. The convergence study is obtained for the all electrons (without 1s state of the oxygen atom).

As a consequence, a different approach from the linear response RESP within the plane wave framework should be used to investigate the isolated

systems, such as the H_2O vapor. It could be a good idea to write and develop the RESP equation within localized orbitals instead of plane-waves. Of course, localized orbitals have their own limitations such as the difficult fulfilment of the Bethe sum-rule [52]. Next we test the RESP in another isolated system: the single chain polymers in particular polyethylene (PE) and polyacetylene (PA).

8.2 RESP for polymers

Without debate the polymers material are very important in the industrial life. For instance, the polyethylene (PE) is formed into tubing, and is used in building services pipework systems, heating and cooling systems and domestic water piping. Furthermore, it is used to produce the plastic insulated wire and cable which is used for conveying electricity (for example, in the home, in automobiles and in the Synchrotron). Since the emission of synchrotron radiation can produce a damage in this insulated cable, we are going to study the stopping of the proton ions in a polymer targets. Thus, in the future this study can help to find the most suitable polymer in resisting the synchrotron radiations.

In this part, we investigate the volume necessary to have an isolated polymer chain using our RESP plane-wave code for two polymers: PE and Polyacetylene (PA). We chose these polymers target since the carbon (C) atoms can form different type of bonds. PE is a series a single bonds, whereas PA is an alternating sequence of single and double bonds. Thus, the RESP contribution of the bonds type can be examined.

We have been focusing on the solid materials all the time, but for H_2O. From the results of H_2O gas phase, we expected to face the same complexity in calculating the converged RESP for isolated polymer.

Fig. 8.5 shows the view of the single isolated chain of PA. PE (the most common plastic) usually refers to an organic polymer with the repeating unit $(C_2H_2)_n$. In PA the carbon atoms have an alternating single and double bonds, each carbon bound to one hydrogen atom.

Fig. 8.6 shows the view of the single isolated chain of PE. PE usually refers to an organic polymer with the repeating unit $(C_2H_4)_n$. Unlike PA, the carbon atoms in PE have single bonds only, each carbon bound to two hydrogen atoms.

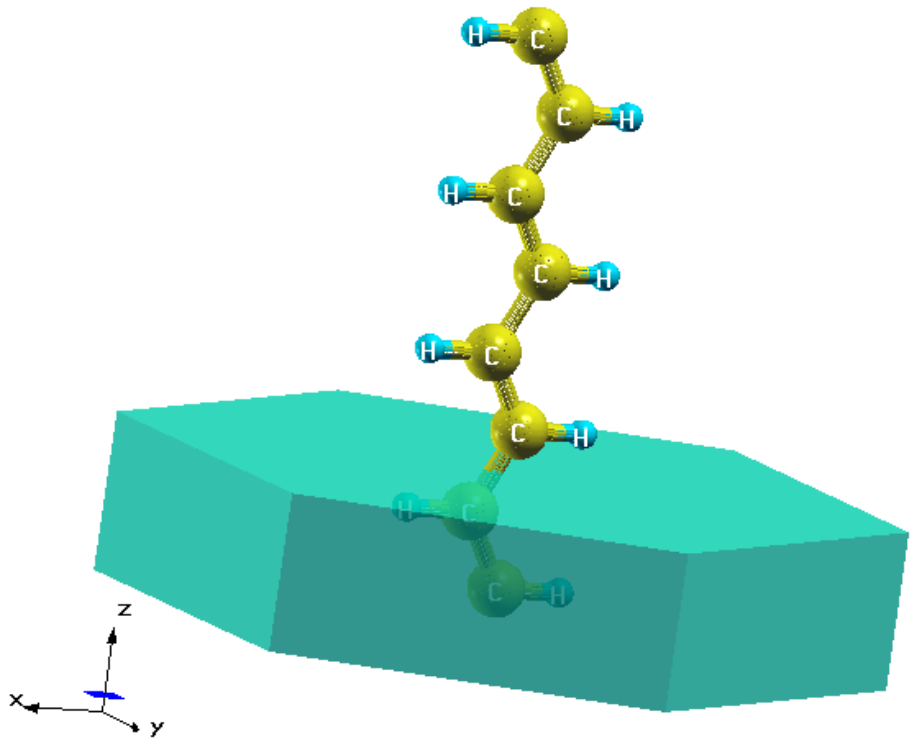


Figure 8.5: View of single isolated PA chain along the z-axis. The length of C=C bond is 1.34 Å which is found in each unit C2H2, and the C-C bond length is 1.451 Å.

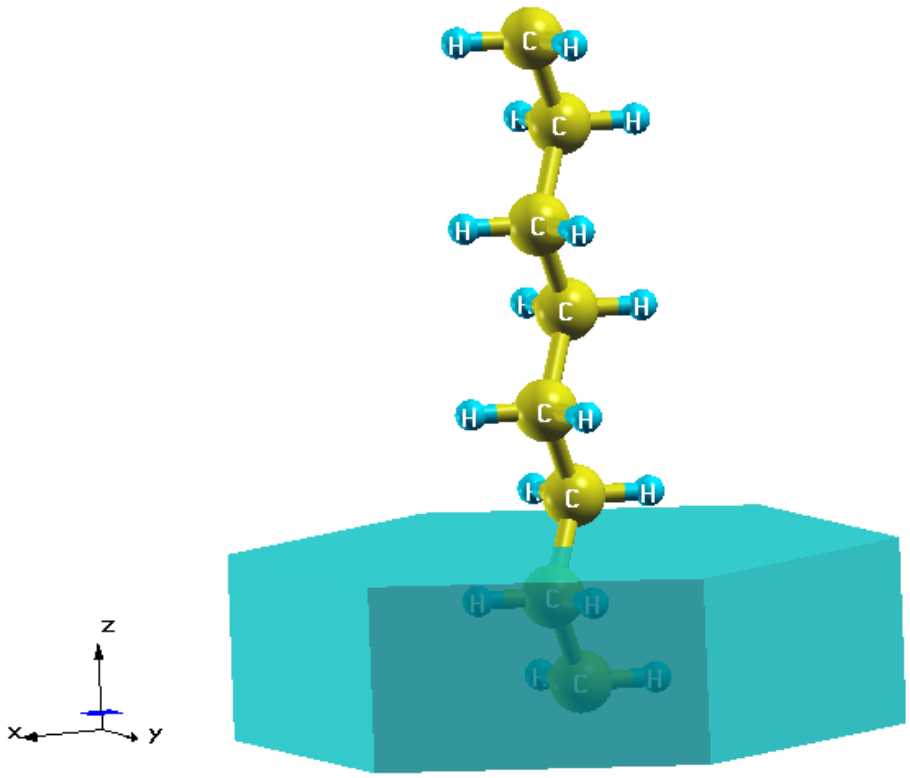


Figure 8.6: View of single isolated PA chain along the z-axis. The length of single bond (c-c) is 1.535 Å.

As shown in the Fig. 8.7 and in Fig 8.8, the volume V_c for isolated polymers in an orthorhombic cell with the lattice constants a, b, c is respectively $a, b = 35$ and $c = 4.66$ Bohr for PA and $a, b = 35$ and $c = 4.812$ Bohr for PE. Again, this volume is very large comparing with what is usually used for the ground state study. Therefore, the convergence task will be so hard that it is impossible with the current status of the code.

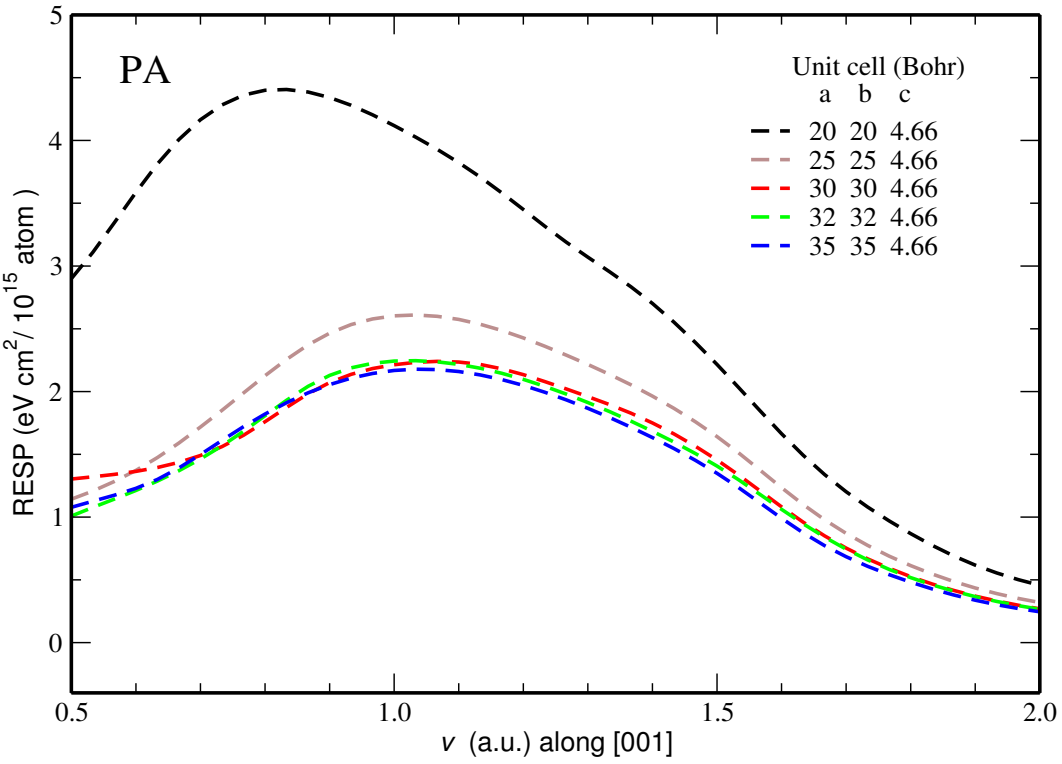


Figure 8.7: Volume convergence test of PA. RESP of proton in the PA target as a function of the cell volume V_c (The cell is orthorhombic P type). For all V_c the following parameters have been used: $N_k = 1$ the gamma point, $E_{cut} = 8$ Ha for $\varepsilon^{-1}_{\mathbf{G}\mathbf{G}'}(\mathbf{q}, \omega)$, $\eta = 6$ eV and using $\Delta E_{band} = 68$ eV energy band. The same excitation density is used for the all V_c.

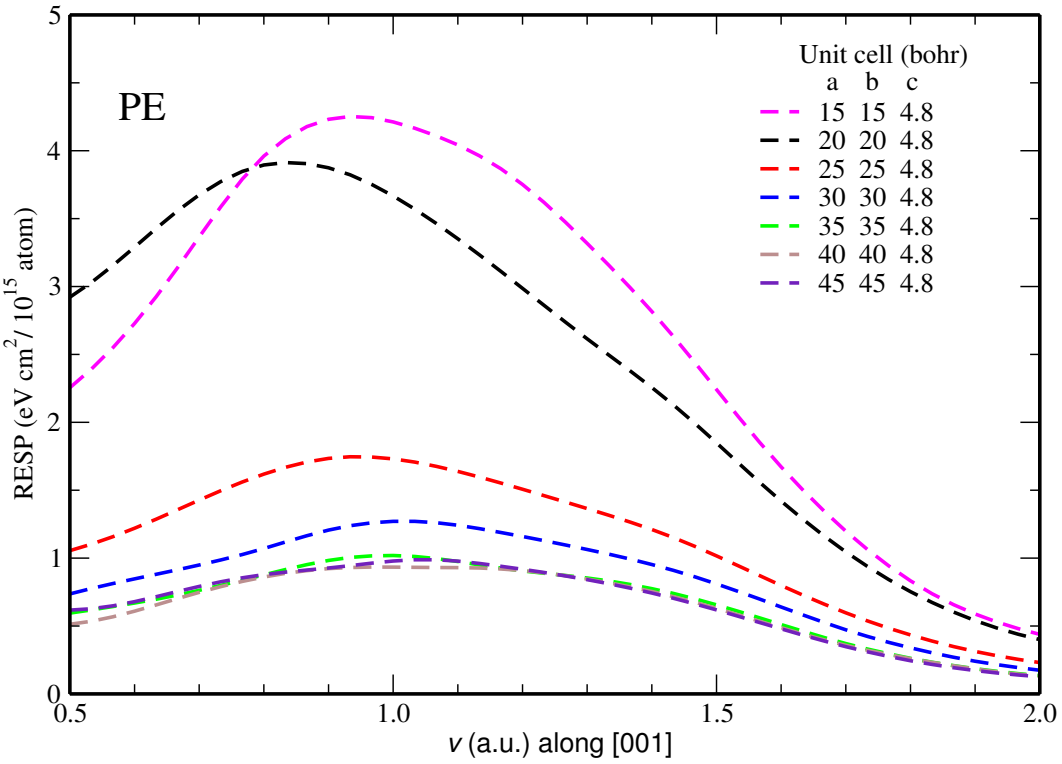


Figure 8.8: Volume convergence test of PE. RESP of proton in the PE target as a function of the cell volume V_c (The cell is orthorhombic P type). For all V_c the following parameters have been used: $N_k = 1$ the gamma point, $E_{cut} = 8$ Ha for $\varepsilon^{-1}_{\mathbf{GG'}}(\mathbf{q}, \omega)$, $\eta = 6$ eV and using $\Delta E_{band} = 68$ eV energy band. The same excitation density is used for the all V_c.

According to this study, we decided to study the RESP contribution of bond types in solid polymers instead the isolated one. This task is one of our perspectives.

8.3 Conclusion

In this chapter, the validity of using the linear response RESP within the plane wave framework has been examined for organic systems in solid and gas phases. We found that the plane-wave framework can only be used to study the RESP of H_2O in ice phase. We managed to calculate the fully converged RESP value of this target. Also, the obtained converged results show a nice agreement with the available experimental data.

Unlike the H_2O ice phase, we realized that the plane wave framework is very hard to be used for H_2O vapor. We demonstrated the impossibility of the convergence task with the current status of ABINIT. Furthermore, we found that the polymers have the same convergence problems as found in H_2O the gas phase.

Finally, one has to use alternative frame work or formalism which can reduce the required computational efforts in studying the RESP of such materials. This is one of our future scientific tasks.

Chapter 9

Conclusions and perspectives

Summary

In this thesis, we have derived in details the position dependent and random electronic stopping power equations of periodic crystals, in which slightly different equations have been found from those in the literature. The Lindhard's free-electron gas formula could be obtained as a particular case of the periodic crystal equations.

Then, we have developed a computer program to calculate the RESP of periodic solids, within the linear-response approach to TDDFT. Also, we have shown in details the convergence issues of the RESP calculations. In order to overcome the convergence problems, we have presented and devised an extrapolation scheme. As an example, we have shown how to calculate the RPA RESP value of proton in Si target (with $2s2p3s3p$ electrons and with valence only) using the extrapolation method. However, we have managed to produce high quality converged stopping power curves using this extrapolation technique. In the beginning of this work, we have focused on testing the RESP in simple solid materials such as: Si, diamond, Al, 3C-SiC, 2H-SiC, graphite and Li.

Moreover, we have shown the importance of using a suitable description of the core electrons. For instance, we have seen that the ALDA formalism is very good in calculating the RESP value in the valence electrons target (like Li) at high proton velocity ($\mathbf{v}>2$ a.u.), but is not giving the same high quality results for the core electrons of the target (like Si, Al, etc.). These observations are pointing to the shortcoming of the ALDA in treating the core electrons. However, these small discrepancy at high velocity may be due to not a counting the even deeper core states like the $1s$ of Si, C, O, etc. Furthermore, we have shown that the accuracy of using the LDA based on the Lindhard's stopping

power in evaluating the RESP core contributions is quite reasonable, in spite of the shell effect is not well accounted within the LDA as shown in the thesis.

In addition, we have tested the importance of including the exchange-correlation within ALDA in producing more accurate results at low proton velocity. In fact, we have shown that the successful of calculating the dynamical structure factor and the valence RESP in Si target using ALDA at low velocity is better than using RPA, where the results have been compared to the experiments. These results indicated the necessity of describing the exchange-correlation within ALDA.

Also, we have checked the the limitations of the linear response theory. In fact, the obtained results are more accurate than what we had expected. For example, with the comparison with the time-propagation results of Ref. [77], we have evaluated an upper limit for the non-linear effects of 5 % in aluminum.

We have investigated the Bragg's additivity rule which is failing even for 3C-SiC, so it cannot be taken for granted for more complex compounds. Also, we have checked the RESP phase effect in SiC and in C targets. The phase insensitivity cannot be taken for granted. Since the obtained RESP results shows different phase sensitivity behavior: it is almost negligible in SiC target, while it is very important in the C target. We have shown that the anisotropy of the RESP in anisotropic materials can be safely ignored, since we have shown that the calculated RESP results are almost the same in 2H-SiC and graphite along two different velocity directions.

In the final part of this thesis, we have focused on testing the RESP in more complex targets such as: H_2O in two phases (the solid and gas) and in two type polymers (PE and PA). We have shown an acceptable result of the RESP in H_2O solid phase compared to the available experimental data with our plane-wave linear-response RESP code. Then, we have tested the possibility of using the RESP code within the PW framework for an isolated organic systems by analyzing the results of the convergence study. As we have found in the convergence test, the volume necessary to isolate the images is very large in PE, PA and also in H_2O gas phase. Therefore, we expect to face an incredible computational task to find the converged RESP in such the isolated materials. For instance, we have shown in the case of the H_2O gas phase that the required number of bands needed to accounting for all the possible electronic excitations is about 13000 at the isolation volume. As a consequence, we think the linear response RESP within the PW framework is only suitable to be applied for crystal systems.

Perspectives

In the future, we aim to continue developing the RESP code, for example we will implemented the position dependent electronic stopping power formula in an *ab initio* code ABINIT. Then, we could use this code to study the channelling effect of electronic stopping power in a series of periodic materials. The chanelling is the easy propagation of ions along the crystalline directions that do not cross the region of large electronic density.

At the same time, we will continue studying the RESP in more complex materials. For instance, we will investigate the Bragg law for more complex compounds (for which the valence changes a lot) such as III-V semiconductors or oxides. Imagine the change in valence between the titanium atom in the metal, or in TiO_2, or in Ti_2O_3.

Regarding the task of understanding the RESP phase effect in water target (solid and gas phase) which was not possible to be done using PW RESP code. Therefore, we are now evaluating the opportunity to write RESP formula in localized orbitals instead the PW framework. Historically, the localized orbitals calculations of the RESP were the first to be carried out (beyond the FEG) [74, 52]. Lots of developpments have already been done in that particular direction. Comparing the PW and the localized orbitals could be much insightful.

Appendix A

Calculation parameters

This appendix provides the details of the parameters used to calculate the converged results in this thesis, as given in tables A.1 and A.2. Also, this appendix provides the lattice parameters of all crystal solids that have been investigated in this work, as given in table A.3.

Table A.1: A list of the low convergence parameters that used in this manuscript.

Target	E_{cut} (Ha)	N_b	$N_{\mathbf{k}}$	η (eV)
Si (valence)	8	400	1	12
Si (core)	8	400	1	12
Diamond	4	200	8	6
Li	6	200	16	4
AL (valence)	4	200	8	7
AL (core)	4	200	8	7
3C-SiC	4	200	8	6
2H-SiC	4	200	8	6
Graphite	4	200	4	9.5
Ice Ih	11	1000	4	2

Table A.2: A list of the high convergence parameters that used in this manuscript.

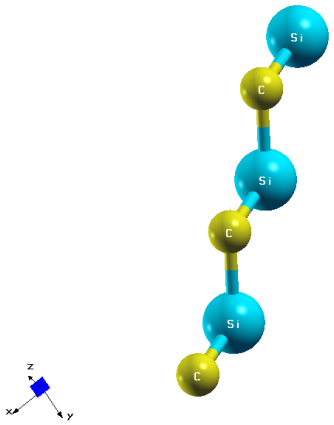
Target	E_{cut} (Ha)	N_b	$N_{\mathbf{k}}$	η (eV)
Si (valence)	25	2000	864	1
Si (core)	35	2500	864	1
Diamond	26	600	2048	1.5
Li	25	1200	2000	0.75
AL (valence)	25	1000	2048	1
AL (core)	30	2000	2048	1
3C-SiC	35	2000	2048	0.75
2H-SiC	35	2000	2048	0.75
Graphite	35	2000	484	1
Ice Ih	20	2500	48	1

Table A.3: A list of the structural parameters used in this manuscript.

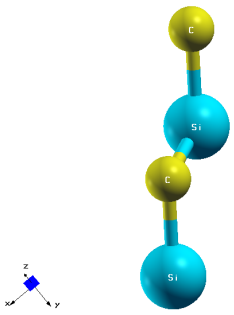
Target	The lattice parameters (Bohr)
Si	a=10.26
Diamond	a=6.7405
Li	a=3.51
AL	a=7.653
3C-SiC	a=8.2384
Graphite	a, b=4.65 and c=12.6763
Ice Ih	a, b=8.5379 and c=13.9
PA	a, b=35 and c=4.66
PE	a, b=35 and c=4.812

Figure A.1 shows the SiC crystal structure build in two phases the 2H-SiC crystal and the 3C-SiC crystal (has hexagonal super cell contains 6 atoms). For both 2H-SiC and 3C-SiC solids, we have used the same real space primitive translations vectors (rprim): rprim(i,1)(0.5, 0.0, 0.5), rprim(i,2)=(0.0, 0.5, 0.5) and rprim(i,3)=(-1, -1, 1). Furthermore, the atoms position in the reduced coordinates (xred) are given as following for 2H-SiC crystal: Two Si atoms are

located at [1/3, 1/3, -1/2] and [2/3, 2/3, -1]. Also, two C atoms are placed at [1/3, 1/3, -1/8] and [2/3, 2/3, -5/8]. While, the xred of atoms position of the 3C-SiC crystal are given as: Three Si atoms are located at [0, 0, 0], [1/3, 1/3, -1/3] and [2/3, 2/3, -2/3] and three C atoms are placed at [1/3, 1/3, -1/12], [1/3, 1/3, -5/12] and [1, 1, -9/12]. In addition, the lattice parameters are given as following: a=8.154 Bohr for 3C-SiC and a=8.154 with a/c=2/3 ratio.



(a) The 3C-SiC (6 atoms super cell) crystal
.



(b) The 2H-SiC crystal.

Figure A.1: A view of SiC structure in two phases 2H-SiC and 3C-SiC.

Table A.4 shows the atoms position in Cartesian coordinates (xcart) for the isolated PA chain.

Table A.4: A list of the atoms position of the isolated PA-chain used in this manuscript.

Atom type	The xcart (Bohr)
C	[0.000, 0.000,-1.107]
C	[1.225, 0.000, 1.107]
H	[-2.035, 0.000,-1.115]
H	[3.260, 0.000, 1.115]

Table A.5 shows the atoms position (xcart) for the isolated PE chain.

Table A.5: A list of the atoms position of the isolated PE-chain used in this manuscript.

Atom type	The xcart (Bohr)
C	[0.594, 0.548, 1.203]
C	[-0.594,-0.548,-1.203]
H	[2.507, 0.105, 1.203]
H	[-2.507,-0.105,-1.203]
H	[0.364, 2.545, 1.203]
H	[-0.364,-2.545,-1.203]

Table A.6 shows the atoms position (xred) for the ice Ih crystal.

Table A.6: A list of the atoms position of the ice Ih crystal used in this manuscript.

Atom type	The xred (Bohr)
O	[0.333, 0.666, 0.060]
O	[0.666, 0.332, 0.936]
O	[0.333, 0.667, 0.436]
O	[0.667, 0.334, 0.560]
H	[0.335, 0.670, 0.195]
H	[0.454, 0.908, 0.020]
H	[0.664, 0.329, 0.695]
H	[0.546, 0.091, 0.521]
H	[0.446, 0.542, 0.482]
H	[0.095, 0.542, 0.482]
H	[0.904, 0.458, 0.982]
H	[0.553, 0.458, 0.982]

List of Publications

1. Ab initio electronic stopping power of protons in bulk materials, Abdullah A. Shukri, Fabien Bruneval, and Lucia Reining, Physical Review B **93**, 035128 (2016).

2. Recent developments of the ABINIT software package, X. Gonze, B. Amadon, J.-M. Beuken, A. Bokhanchuk, F. Bruneval, G. Geneste, M. Giantomassi, Y. Gillet, F. Jollet, J. Laflamme, A. Lherbier, A. Martin, S. Poncé, Y. Pouillon, G.-M. Rignanese, A. A. Shukri, M. Torrent, B. Van Troeye, M. Verstraete, and J. Zwanziger, submitted to Computer Physics Communications (2015).

Bibliography

[1] I. Abril, R. Garcia-Molina, C. D. Denton, F. J. Pérez-Pérez, and N. R. Arista. Dielectric description of wakes and stopping powers in solids. *Phys. Rev. A*, 58:357–366, Jul 1998.

[2] N. R. Arista and W. Brandt. Energy loss and straggling of charged particles in plasmas of all degeneracies. *Phys. Rev. A*, 23:1898–1905, Apr 1981.

[3] Nestor R Arista. Low-velocity stopping power of semidegenerate quantum plasmas. *Journal of Physics C: Solid State Physics*, 18(26):5127, 1985.

[4] Manuel D. Barriga-Carrasco. Proton stopping using a full conserving dielectric function in plasmas at any degeneracy. *Phys. Rev. E*, 82:046403, Oct 2010.

[5] P. Bauer, W. Käferböck, and V. Nečas. Investigation of the electronic energy loss of hydrogen ions in h 2 o: influence of the state of aggregation. *Nuclear Instruments and Methods in Physics Research Section B: Beam Interactions with Materials and Atoms*, 93(2):132–136, 1994.

[6] A. Baurichter, P. Sigmund, and A. H. Sørensen. Panel discussion on stopping of heavy ions. *Nuclear Instruments and Methods in Physics Research Section B: Beam Interactions with Materials and Atoms*, 195(1):224–231, 2002.

[7] M.J. Berger, J.S. Coursey, M.A. Zucker, and J. Chang. Estar, pstar, and astar: Computer programs for calculating stopping-power and range tables for electrons, protons, and helium ions (version 1.2.3), 2005.

[8] H. Bethe. Zur theorie des durchgangs schneller korpuskularstrahlen durch materie. *Ann. Phys., Lpz.*, 397:325–400, 1930.

[9] H. A. Bethe. *Z. Phys.*, 76:293, 1932.

[10] F. Bloch. *Ann. Physik*, 16:285, 1933.

[11] F. Bloch. Stopping power of atoms with several electrons. *Z. Phys*, 81:363, 1933.

[12] N. Bohr. On the theory of the decrease of velocity of moving electrified particles on passing through matter. *Phil. Mag*, 23(2):10–31, 1912.

[13] N. Bohr. Lx. on the decrease of velocity of swiftly moving electrified particles in passing through matter. *The London, Edinburgh, and Dublin Philosophical Magazine and Journal of Science*, 30(178):581–612, 1915.

[14] Niels Bohr. Ii. on the theory of the decrease of velocity of moving electrified particles on passing through matter. *The London, Edinburgh, and Dublin Philosophical Magazine and Journal of Science*, 25(145):10–31, 1913.

[15] E. Bonderup. *Mat. Fys. Medd. Dan. Vid. Selsk*, 35(1), 1967.

[16] F. Bonsignori and A. Desalvo. A dielectric approach to electronic energy loss in real solids under channeling conditions. *Lettere al Nuovo Cimento*, 1(12):589–591, 1969.

[17] F. Bonsignori and A. Desalvo. A dielectric calculation of energy loss to valence electrons under channeling conditions. *Journal of Physics and Chemistry of Solids*, 31(10):2191 – 2198, 1970.

[18] W. H. Bragg and R. Kleeman. Xxxix. on the α particles of radium, and their loss of range in passing through various atoms and molecules. *Philosophical Magazine Series 6*, 10(57):318–340, 1905.

[19] A. F. Burenkov, F. F. Komarov, and M. A. Kumakhov. Energy loss of charged particles in crystals. *physica status solidi (b)*, 99(1):417–428, 1980.

[20] I Campillo, J.M Pitarke, and A.G Eguiluz. Electronic stopping power of aluminum crystal. *Phys. Rev. B*, 58:10307 – 10314, 1998.

[21] I Campillo, J.M Pitarke, A.G Eguiluz, and Alberto García. Electronic stopping power of periodic crystals. *Nuclear Instruments and Methods in Physics Research Section B: Beam Interactions with Materials and Atoms*, 135(1-4):103 – 106, 1998.

[22] M. Corradini, R. Del Sole, G. Onida, and M. Palummo. Analytical expressions for the local-field factor $g(q)$ and the exchange-correlation kernel $k_{xc}(r)$ of the homogeneous electron gas. *Phys. Rev. B*, 57:14569–14571, Jun 1998.

[23] C. G. Darwin. A theory of the absorption and scattering of the α rays. *Phil. Mag*, 13:901–20, 1912.

[24] C. D. Denton, I. Abril, R. Garcia-Molina, J. C. Moreno-Marín, and S. Heredia-Avalos. Influence of the description of the target energy-loss function on the energy loss of swift projectiles. *Surface and Interface Analysis*, 40(11):1481–1487, 2008.

[25] A Desalvo and R Rosa. A dielectric calculation of energy loss to valence electrons of channelled protons in silicon. *J. Phys. C*, 10(10):1595, 1977.

[26] J. J. Dorado and F. Flores. Molecular-orbital theory for the stopping power of atoms in the low-velocity regime: The case of helium in alkali metals. *Phys. Rev. A*, 47:3062–3072, Apr 1993.

[27] D. M. Duffy and A. M. Rutherford. Including the effects of electronic stopping and electron-ion interactions in radiation damage simulations. *J. Phys.: Condens. Matter*, 19(1):016207, 2007.

[28] Ch. Eppacher, R. D. Mui no, D. Semrad, and A. Arnau. Stopping power of lithium for hydrogen projectiles. *Nuclear Instruments and Methods in Physics Research Section B: Beam Interactions with Materials and Atoms*, 96(3-4):639–642, 1995. The Interaction of Swift Particles and Electromagnetic Fields with Matter.

[29] E. Fermi. Un metodo statistico per la determinazione di alcune priorieta dell'atome. *Rend. Accad. Naz. Lincei*, 6:602–607, 1927.

[30] E. Fermi and E. Teller. The capture of negative mesotrons in matter. *Phys. Rev.*, 72:399–408, Sep 1947.

[31] A. L. Fetter and J D. Walecka. *Quantum Theory of Many-Particle Systems*. McGraw-Hill, 1971.

[32] G. Garcia, C. Elsässer, S. Louie, and M. Cohen. *Phys. Rev. B*, 46:9829, 1992.

[33] JA Gaunt. The stopping power of hydrogen atoms for α-particles according to the new quantum theory. In *Mathematical Proceedings of the Cambridge Philosophical Society*, volume 23, pages 732–754. Cambridge Univ Press, 1927.

[34] X. Gonze, B. Amadon, P. M. Anglade, J. M. Beuken, F. Bottin, P. Boulanger, F. Bruneval, D. Caliste, R. Caracas, M. Côté, T. Deutsch,

L. Genovese, Ph. Ghosez, M. Giantomassi, S. Goedecker, D. R. Hamann, P. Hermet, F. Jollet, G. Jomard, S. Leroux, M. Mancini, S. Mazevet, M. J. T. Oliveira, G. Onida, Y. Pouillon, T. Rangel, G. M. Rignanese, D. Sangalli, R. Shaltaf, M. Torrent, M. J. Verstraete, G. Zerah, and J. W. Zwanziger. Abinit: First-principles approach to material and nanosystem properties. *Comput. Phys. Commun.*, 180:2582, 2009.

[35] E. K. U. Gross and W. Kohn. Local density-functional theory of frequency-dependent linear response. *Phys. Rev. Lett.*, 55:2850–2852, Dec 1985.

[36] L. Hedin. New method for calculating the one-particle green's function with application to the electron-gas problem. *Phys. Rev.*, 139:A796–A823, Aug 1965.

[37] G. H. Henderson. Lix. the decrease of energy of α particles on passing through matter. *Philosophical Magazine Series 6*, 44(262):680–688, 1922.

[38] P. Hohenberg and W. Kohn. Inhomogeneous electron gas. *Phys. Rev.*, 136:B864–B871, Nov 1964.

[39] M. S. Hybertsen and S. G. Louie. Electron correlation in semiconductors and insulators: Band gaps and quasiparticle energies. *Phys. Rev. B*, 34:5390–5413, Oct 1986.

[40] G. J. Iafrate and J. F. Ziegler. Numerical evaluation of lindhard's theory of stopping power for a charged particle in a free electron gas. *Journal of Applied Physics*, 50(9):5579–5581, 1979.

[41] G. J. Iafrate, J. F. Ziegler, and M. J. Nass. Application of lindhard's dielectric theory to the stopping of ions in solids. *Journal of Applied Physics*, 51(2):984–987, 1980.

[42] F. J. Janni. Proton range-energy tables, 1 kev-10 gev, energy loss, range, path length, time-of-flight, straggling, multiple scattering, and nuclear interaction probability. part ii. for 92 elements. *Atomic Data and Nuclear Data Tables*, 27:341, 1982.

[43] R. O. Jones and O. Gunnarsson. *Rev. of Modern Physics*, 61:689, 1989.

[44] A. A. Kugler. Theory of the local field correction in an electron gas. *Journal of Statistical Physics*, 12(1):35–87, 1975.

[45] J. Lindhard and M. Scharff. Energy loss in matter by fast particles of low charge. *Mat. Fys. Medd. Dan. Vid. Selsk*, 27:1–31, 1953.

[46] J. Lindhard and A. Winther. Stopping power of electron gasand equipartition rule. *Mat. Fys. Medd. Dan. Vid. Selsk*, 34(1), 1964.

[47] Jens Lindhard. On the properties of a gas of charged particles. *Mat. Fys. Medd. Dan. Vid. Selsk*, 28(8):1, 1954.

[48] M.A.L. Marques, C.A. Ullrich, F. Nogueira, A. Rubio, K. Burke, and E.K.U. Gross (Eds.). *Time-Dependent Density Functional Theory*, volume 706 of *Lecture Notes in Physics*. Springer, 2006.

[49] C. P. Martin and J. Schwinger. Theory of many-particle systems. i. *Phys. Rev.*, 115:1342–1373, Sep 1959.

[50] G. Maynard and C. Deutsch. Energy loss and straggling of ions with any velocity in dense plasmas at any temperature. *Physical Review A*, 26(1):665, 1982.

[51] C. Møller. Passage of hard beta rays through matter. *Ann. Physik*, 14:531, 1932.

[52] Erik Holm Mortensen, Jens Oddershede, and John R. Sabin. Polarization propagator calculations of generalized oscillator strengths and stopping cross sections of he. *Nuclear Instruments and Methods in Physics Research Section B: Beam Interactions with Materials and Atoms*, 69(1):24 – 32, 1992.

[53] L. C. Northcliffe. Passage of heavy ions through matter. *Annual Review of Nuclear Science*, 13(1):67–102, 1963.

[54] Ari Ojanperä, Arkady V. Krasheninnikov, and Martti Puska. Electronic stopping power from first-principles calculations with account for core electron excitations and projectile ionization. *Phys. Rev. B*, 89:035120, Jan 2014.

[55] Giovanni Onida, Lucia Reining, and Angel Rubio. Electronic excitations: density-functional versus many-body green's-function approaches. *Rev. Mod. Phys.*, 74:601–659, Jun 2002.

[56] J. Ortner and I. M. Tkachenko. Stopping power of strongly coupled electronic plasmas: Sum rules and asymptotic forms. *Phys. Rev. E*, 63:026403, Jan 2001.

[57] J. Paier, M. Marsman, K. Hummer, G. Kresse, I. C. Gerber, and J. G. Ángyán. Screened hybrid density functionals applied to solids. *J. Chem. Phys.*, 124(15):–, 2006.

[58] H. Paul. Stopping power for light ions.

[59] H. Paul and A. Schinner. An empirical approach to the stopping power of solids and gases for ions from 3li to 18ar. *Nuclear Instruments and Methods in Physics Research B*, 179:299–315, aug 2001.

[60] H. Paul and A. Schinner. Judging the reliability of stopping power tables and programs for protons and alpha particles using statistical methods. *Nuclear Instruments and Methods in Physics Research Section B: Beam Interactions with Materials and Atoms*, 227(4):461–470, 2005.

[61] Helmut Paul and Andreas Schinner. An empirical approach to the stopping power of solids and gases for ions from 3li to 18ar - part ii. *Nuclear Instruments and Methods in Physics Research Section B: Beam Interactions with Materials and Atoms*, 195(1-2):166–174, 2002.

[62] D. R. Penn. Electron mean-free-path calculations using a model dielectric function. *Physical Review B*, 35(2):482, 1987.

[63] M. Petersilka, U. J. Gossmann, and E. K. U. Gross. Excitation energies from time-dependent density-functional theory. *Phys. Rev. Lett.*, 76:1212–1215, Feb 1996.

[64] J.M. Pitarke and I. Campillo. Band structure effects on the interaction of charged particles with solids. *Nuclear Instruments and Methods in Physics Research Section B: Beam Interactions with Materials and Atoms*, 164-165(0):147 – 160, 2000.

[65] J. M. Pruneda, D. Sánchez-Portal, A. Arnau, J. I. Juaristi, and E Artacho. Electronic stopping power in lif from first principles. *Physical review letters*, 99(23):235501, 2007.

[66] J.M. Pruneda, D. Sánchez-Portal, A. Arnau, J.I. Juaristi, and E. Artacho. Heating electrons with ion irradiation: A first-principles approach. *Nuclear Instruments and Methods in Physics Research Section B: Beam Interactions with Materials and Atoms*, 267(4):590 – 593, 2009. Proceedings of the 17th International Workshop on Inelastic Ion-Surface Collisions.

[67] M. Quijada, A. G. Borisov, I. Nagy, R. P. D. Mui no, and P. M. Echenique. Time-dependent density-functional calculation of the stopping power for protons and antiprotons in metals. *Phys. Rev. A*, 75:042902, Apr 2007.

[68] C. P. Race, D. R. Mason, M. W. Finnis, W. M. C. Foulkes, A. P. Horsfield, and A. P. Sutton. The treatment of electronic excitations in atomistic

models of radiation damage in metals. *Reports on Progress in Physics*, 73(11):116501, 2010.

[69] Lucia Reining, V. Olevano, A. Rubio, and g. Onida. Excitonic effects in solids described by time-dependent density-functional theory. *Phys. Rev. Lett.*, 88:066404, Jan 2002.

[70] R. H. Ritchie and A. Howie. Electron excitation and the optical potential in electron microscopy. *Philosophical Magazine*, 36(2):463–481, 1977.

[71] K. Röttger, A. Endriss, J. Ihringer, S. Doyle, and WF. Kuhs. Lattice constants and thermal expansion of h2o and d2o ice ih between 10 and 265 k. *Acta Crystallographica Section B: Structural Science*, 50(6):644–648, 1994.

[72] C. C. Rousseau, W. K. Chu, and D. Powers. Calculations of stopping cross sections for 0.8-to 2.0-mev alpha particles. *Physical Review A*, 4(3):1066, 1971.

[73] E. Runge and E. K. U. Gross. Density-functional theory for time-dependent systems. *Phys. Rev. Lett.*, 52:997–1000, Mar 1984.

[74] John R. Sabin and Jens Oddershede. Shell corrections to electronic stopping powers from orbital mean excitation energies. *Phys. Rev. A*, 26:3209–3219, Dec 1982.

[75] John R. Sabin and Jens Oddershede. Theoretical stopping cross sections of c-h, c-c and c=c bonds for swift protons. *Nucl. Instrum. Meth. B*, 27(2):280 – 286, 1987.

[76] W.M. Saslow and G.F. Reiter. Plasmons and characteristic energy loss in periodic solids. *Phys. Rev. B*, 7:2995–3003, Apr 1973.

[77] A. Schleife, Y. Kanai, and A. A. Correa. Accurate atomistic first-principles calculations of electronic stopping. *Phys. Rev. B*, 91:014306, Jan 2015.

[78] W. Schülke. *Electron dynamics by inelastic X-ray scattering*. OUP Oxford, 2007.

[79] P. Sigmund. *Particle Penetration and Radiation Effects-General Aspects and Stopping of Swift Point Charges*. Berlin: Springer, 2006.

[80] L. H. Thomas. The calculation of atomic fields. *Proc. Camp. Philos. Soc*, 23:542–548, 1927.

[81] J. J. Thomson. Ionization by moving electrified particles. *Phil. Mag*, 23:449–57, 1912.

[82] D. I. Thwaites. Bragg's rule of stopping power additivity: A compilation and summary of results. *Radiation Research*, 95(3):pp. 495–518, 1983.

[83] T. M. H. E. Tielens, G. E. W. Bauer, and T. H. Stoof. Dielectric theory of the electronic stopping power of fast ions in crystals. *Phys. Rev. B*, 49:5741–5744, Feb 1994.

[84] I. V. Tokatly and O. Pankratov. Many-body diagrammatic expansion in a kohn-sham basis: Implications for time-dependent density functional theory of excited states. *Phys. Rev. Lett.*, 86:2078–2081, Mar 2001.

[85] C.A. Ullrich. *Time-Dependent Density-Functional Theory: Concepts and Applications*. Oxford Graduate Press, 2012.

[86] G. S. Was. *Fundamentals of Radiation Materials Science*. Springer-Verlag, Berlin, Heidelberg, 2007.

[87] HC. Weissker, J. Serrano, S. Huotari, F. Bruneval, F. Sottile, G. Monaco, M. Krisch, V. Olevano, and L. Reining. Signatures of short-range many-body effects in the dielectric function of silicon for finite momentum transfer. *Phys. Rev. Lett.*, 97:237602, Dec 2006.

[88] HC. Weissker, J. Serrano, S. Huotari, E. Luppi, M. Cazzaniga, F. Bruneval, F. Sottile, G. Monaco, V. Olevano, and L. Reining. Dynamic structure factor and dielectric function of silicon for finite momentum transfer: Inelastic x-ray scattering experiments and *ab initio* calculations. *Phys. Rev. B*, 81:085104, Feb 2010.

[89] W. A. Wenzel and W. Whaling. The stopping cross section of d_2o ice. *Phys. Rev.*, 87:499–503, Aug 1952.

[90] J. A. White and D. M. Bird. Implementation of gradient-corrected exchange-correlation potentials in carparrinello total-energy calculations. *Phys. Rev. B*, 50:4954–4957, Aug 1994.

[91] J. F. Ziegler. Srim-the stopping and range of ions in matter.

[92] J. F. Ziegler. Stopping of energetic light ions in elemental matter. *Journal of Applied Physics*, 85(3):1249–1272, 1999.

[93] J. F. Ziegler, J. P. Biersack, and U. Littmark. *The stopping and ranges of ions in matter*. Pergamon, New York, 1985.

[94] A. Zupan, P. Blaha, K. Schwartz, and J. P. Perdew. *Phys. Rev. B*, 58:11266, 1998.